

# Contents

<b>Contents</b>	<b>i</b>
<b>1 Surface Second-Harmonic Generation Yield</b>	<b>1</b>
1.1 The three layer model for the SSHG yield . . . . .	2
1.1.1 Multiple SHG reflections . . . . .	5
1.1.2 Multiple reflections for the linear field . . . . .	6
1.1.3 Deriving the SSHG yield . . . . .	7
1.2 $\mathcal{R}_{\text{IF}}$ for different polarization cases . . . . .	9
1.2.1 $\mathcal{R}_{pP}$ ( <i>p</i> -in, <i>P</i> -out) . . . . .	11
1.2.2 $\mathcal{R}_{sP}$ ( <i>s</i> -in, <i>P</i> -out) . . . . .	12
1.2.3 $\mathcal{R}_{pS}$ ( <i>p</i> -in, <i>S</i> -out) . . . . .	12
1.2.4 $\mathcal{R}_{sS}$ ( <i>s</i> -in, <i>S</i> -out) . . . . .	13
1.3 Some scenarios of interest . . . . .	14
1.3.1 The 3-layer model without multiple reflections . . . . .	14
1.3.2 The two layer, or Fresnel (2-layer-fresnel) model . . . . .	15
1.3.3 The 2-layer-bulk model: evaluating $\mathcal{P}(2\omega)$ and $\mathbf{E}(\omega)$ in the bulk . . . . .	15
1.3.4 The 2-layer-vacuum model: evaluating $\mathcal{P}(2\omega)$ and $\mathbf{E}(\omega)$ in the vacuum . . . . .	15
1.3.5 The 3-layer-hybrid model: evaluating $\mathcal{P}(2\omega)$ in $\ell$ and $\mathbf{E}(\omega)$ in the bulk . . . . .	16
1.4 About coding the SSHG yield . . . . .	16
<b>2 Results</b>	<b>18</b>
2.1 Results for the Si(001)(2×1) surface . . . . .	19
2.1.1 Calculating $\chi^{xxx}$ . . . . .	20
2.1.2 Overview of the calculated $\mathcal{R}$ spectra . . . . .	25
2.2 Results for the Si(111)(1×1):H surface . . . . .	26
2.2.1 Calculating $\chi^{xxx}$ . . . . .	28
2.2.2 Comparing the theoretical $\mathcal{R}$ to experiment . . . . .	30
<b>3 Final Remarks</b>	<b>41</b>
3.1 Conclusions . . . . .	41
3.2 Future Work . . . . .	42
<b>A Derived expressions for the SHG yield</b>	<b>43</b>
A.1 Some useful expressions . . . . .	43
A.1.1 $2\omega$ terms . . . . .	44
A.1.2 $1\omega$ terms . . . . .	45

A.1.3	Nonzero components of $\chi(-2\omega; \omega, \omega)$	46
A.2	$\mathcal{R}_{pP}$	47
A.2.1	For the (111) surface	48
A.2.2	For the (110) surface	51
A.2.3	For the (001) surface	52
A.3	$\mathcal{R}_{pS}$	53
A.3.1	For the (111) surface	54
A.3.2	For the (110) surface	54
A.3.3	For the (001) surface	55
A.4	$\mathcal{R}_{sP}$	55
A.4.1	For the (111) surface	56
A.4.2	For the (110) surface	57
A.4.3	For the (001) surface	57
A.5	$\mathcal{R}_{ss}$	58
A.5.1	For the (111) surface	58
A.5.2	For the (110) surface	59
A.5.3	For the (001) surface	59
<b>B</b>	<b>Deriving the SSHG yield without multiple reflections</b>	<b>60</b>
B.1	Three layer model for SSHG radiation	60
B.1.1	SSHG Yield	63
<b>C</b>	<b>Some limiting cases of interest</b>	<b>66</b>
C.1	The two layer model	66
C.2	Taking $\mathcal{P}(2\omega)$ and the fundamental fields in the bulk	67
C.3	Taking $\mathcal{P}(2\omega)$ and the fundamental fields in the vacuum	69
C.4	Taking $\mathcal{P}(2\omega)$ in $\ell$ and the fundamental fields in the bulk	71
<b>D</b>	<b>The two layer model for SHG radiation from Sipe, Moss, and van Driel</b>	<b>74</b>
D.1	$\mathcal{R}_{pP}$	75
D.2	$\mathcal{R}_{pS}$	77
D.3	$\mathcal{R}_{sP}$	78
D.4	Summary	79
<b>Bibliography</b>		<b>80</b>

# Chapter 1

# Surface Second-Harmonic Generation Yield

## Outline

---

1.1	The three layer model for the SSHG yield . . . . .	2
1.1.1	Multiple SHG reflections . . . . .	5
1.1.2	Multiple reflections for the linear field . . . . .	6
1.1.3	Deriving the SSHG yield . . . . .	7
1.2	$\mathcal{R}_{\text{iF}}$ for different polarization cases . . . . .	9
1.2.1	$\mathcal{R}_{pP}$ ( <i>p</i> -in, <i>P</i> -out) . . . . .	11
1.2.2	$\mathcal{R}_{sP}$ ( <i>s</i> -in, <i>P</i> -out) . . . . .	12
1.2.3	$\mathcal{R}_{pS}$ ( <i>p</i> -in, <i>S</i> -out) . . . . .	12
1.2.4	$\mathcal{R}_{sS}$ ( <i>s</i> -in, <i>S</i> -out) . . . . .	13
1.3	Some scenarios of interest . . . . .	14
1.3.1	The 3-layer model without multiple reflections . . . . .	14
1.3.2	The two layer, or Fresnel (2-layer-fresnel) model . . . . .	15
1.3.3	The 2-layer-bulk model: evaluating $\mathcal{P}(2\omega)$ and $\mathbf{E}(\omega)$ in the bulk . . . . .	15
1.3.4	The 2-layer-vacuum model: evaluating $\mathcal{P}(2\omega)$ and $\mathbf{E}(\omega)$ in the vacuum . . . . .	15
1.3.5	The 3-layer-hybrid model: evaluating $\mathcal{P}(2\omega)$ in $\ell$ and $\mathbf{E}(\omega)$ in the bulk . . . . .	16
1.4	About coding the SSHG yield . . . . .	16

---

In this chapter, I will walk the reader through the considerations for developing the three layer (3-layer) model for the SSHG yield. We will then derive explicit expressions for each of the four polarization configurations for the incoming and outgoing fields. These expressions will be simplified by taking into account the symmetry relations for the (111), (110), and (001) surfaces. I have also included Appendices A, B, C, and D that contain a wealth of supplementary derivations for all the work contained in this chapter.

## 1.1 The three layer model for the SSHG yield

In this section, we will derive the formulas required for the calculation of the SSHG yield, defined by

$$\mathcal{R}(\omega) = \frac{I(2\omega)}{I^2(\omega)}, \quad (1.1)$$

with the intensity given by [1, 2]

$$I(\omega) = \begin{cases} \frac{c}{2\pi} n(\omega) |E(\omega)|^2 & (\text{CGS units}) \\ 2\epsilon_0 c n(\omega) |E(\omega)|^2 & (\text{MKS units}) \end{cases}, \quad (1.2)$$

where  $n(\omega) = \sqrt{\epsilon(\omega)}$  is the index of refraction with  $\epsilon(\omega)$  as the dielectric function,  $\epsilon_0$  is the vacuum permittivity, and  $c$  the speed of light in vacuum.

There are several ways to calculate  $R$ , one of which is the procedure followed by Cini [3]. This approach calculates the nonlinear susceptibility and at the same time the radiated fields. However, I present an alternative derivation based on the work of Mizrahi and Sipe [4], since the derivation of the 3-layer model is straightforward. In this scheme, the surface is represented by three regions or layers. The first layer is the vacuum region (denoted by  $v$ ) with a dielectric function  $\epsilon_v(\omega) = 1$  from where the fundamental electric field  $\mathbf{E}_v(\omega)$  impinges on the material. The second layer is a thin layer (denoted by  $\ell$ ) of thickness  $d$  characterized by a dielectric function  $\epsilon_\ell(\omega)$ . It is in this layer where the SHG takes place. The third layer is the bulk region denoted by  $b$  and characterized by  $\epsilon_b(\omega)$ . Both the vacuum and bulk layers are semi-infinite (see Fig. 1.1).

To model the electromagnetic response of the 3-layer model, we follow Ref. [4] and assume a polarization sheet of the form

$$\mathbf{P}(\mathbf{r}, t) = \mathcal{P} e^{i\kappa \cdot \mathbf{R}} e^{-i\omega t} \delta(z - z_\beta) + \text{c.c.}, \quad (1.3)$$

where  $\mathbf{R} = (x, y)$ ,  $\kappa$  is the component of the wave vector  $\nu_\beta$  parallel to the surface, and  $z_\beta$  is the position of the sheet within medium  $\beta$ . Ref. [5] demonstrates that the solution of the Maxwell equations for the radiated fields  $E_{\beta,p\pm}$ , and  $E_{\beta,s}$  with  $\mathbf{P}(\mathbf{r}, t)$  as a source at points  $z \neq 0$ , can be written as

$$(E_{\beta,p\pm}, E_{\beta,s}) = \left( \frac{\gamma i \tilde{\omega}^2}{\tilde{w}_\beta} \hat{\mathbf{p}}_{\beta\pm} \cdot \mathcal{P}, \frac{\gamma i \tilde{\omega}^2}{\tilde{w}_\beta} \hat{\mathbf{s}} \cdot \mathcal{P} \right), \quad (1.4)$$

where  $\gamma = 2\pi$  in CGS units or  $\gamma = 1/2\epsilon_0$  in MKS units, and  $\tilde{\omega} = \omega/c$ . Also,  $\hat{\mathbf{s}}$  and  $\hat{\mathbf{p}}_{\beta\pm}$  are the unitary vectors for the  $s$  and  $p$  polarizations of the radiated field, respectively. The  $\pm$  refers to upward (+) or downward (-) direction of propagation within medium  $\beta$ , as shown in Fig. 1.1. Also,  $\tilde{w}_\beta(\omega) = \tilde{\omega} w_\beta$ , where

$$\hat{\mathbf{p}}_{\beta\pm}(\omega) = \frac{\kappa(\omega) \hat{\mathbf{z}} \mp \tilde{w}_\beta(\omega) \hat{\boldsymbol{\kappa}}}{\tilde{w}_\beta n_\beta(\omega)} = \frac{\sin \theta_0 \hat{\mathbf{z}} \mp w_\beta(\omega) \hat{\boldsymbol{\kappa}}}{n_\beta(\omega)}, \quad (1.5)$$

with

$$w_\beta(\omega) = (\epsilon_\beta(\omega) - \sin^2 \theta_0)^{1/2}, \quad (1.6)$$

$\theta_0$  is the angle of incidence of  $\mathbf{E}_v(\omega)$ ,  $\kappa(\omega) = |\kappa| = \tilde{\omega} \sin \theta_0$ ,  $n_\beta(\omega) = \sqrt{\epsilon_\beta(\omega)}$  is the index of refraction of medium  $\beta$ , and  $z$  is the direction perpendicular to the surface that points towards the

vacuum. If we consider the plane of incidence along the  $\kappa z$  plane, then

$$\hat{\kappa} = \cos \phi \hat{\mathbf{x}} + \sin \phi \hat{\mathbf{y}}, \quad (1.7)$$

and

$$\hat{\mathbf{s}} = -\sin \phi \hat{\mathbf{x}} + \cos \phi \hat{\mathbf{y}}, \quad (1.8)$$

where  $\phi$  is the azimuthal angle with respect to the  $x$  axis.

It is important to mention that we must also calculate the bulk and surface dielectric functions,  $\epsilon_b(\omega)$  and  $\epsilon_\ell(\omega)$ . For this, we follow the method presented in Ref. [6]. For the bulk, the tensor components are equal in all three directions due to the cubic symmetry,

$$\varepsilon_b(\omega) = \epsilon_b^{xx}(\omega) = \epsilon_b^{yy}(\omega) = \epsilon_b^{zz}(\omega).$$

For the purpose of this calculation, we introduce the average value for the surface dielectric function,  $\varepsilon_\ell(\omega)$ . This entails that  $\epsilon_\ell^{xx}(\omega) = \epsilon_\ell^{yy}(\omega) \approx \epsilon_\ell^{zz}(\omega)$ , since symmetry is broken in the  $zz$  direction because of the surface. We find the average in the conventional way,

$$\varepsilon_\ell(\omega) = \frac{\epsilon_\ell^{xx}(\omega) + \epsilon_\ell^{yy}(\omega) + \epsilon_\ell^{zz}(\omega)}{3},$$

and use that quantity in the equations for the SSHG yield. In order to obtain a result which does not depend on the size of the vacuum region [7], we have normalized the surface dielectric function to the volume of the slab, instead of the volume of the super-cell. We remark that we could calculate  $\epsilon_{\text{half-slab}}^{\text{ab}}(\omega)$  using  $\mathcal{C}(z) = 1$  for the upper half of our slab and normalize to the volume of the half-slab. Nevertheless,  $\epsilon_\ell^{\text{ab}}(\omega)$  and  $\epsilon_{\text{half-slab}}^{\text{ab}}(\omega)$  give the same result [8, 9, 7].

In the 3-layer model the nonlinear polarization responsible for the SHG is immersed in the thin layer ( $\beta = \ell$ ), and is given by

$$\mathcal{P}_{\ell,i}(2\omega) = \begin{cases} \chi^{ijk}(-2\omega; \omega, \omega) E_j(\omega) E_k(\omega) & (\text{CGS units}) \\ \epsilon_0 \chi^{ijk}(-2\omega; \omega, \omega) E_j(\omega) E_k(\omega) & (\text{MKS units}) \end{cases}, \quad (1.9)$$

where  $\chi(-2\omega; \omega, \omega)$  is the dipolar surface nonlinear susceptibility tensor, and the Cartesian indices  $i, j, k$  are summed over if repeated.  $\chi^{ijk}(-2\omega; \omega, \omega) = \chi^{ikj}(-2\omega; \omega, \omega)$  is the intrinsic permutation symmetry due to the fact that SHG is degenerate in  $E_j(\omega)$  and  $E_k(\omega)$ . As in Ref. [4], we consider the polarization sheet (Eq. (1.3)) to be oscillating at some frequency  $\omega$  in order to properly express Eqs. (1.4)-(1.8). However, in the following we find it convenient to use  $\omega$  exclusively to denote the fundamental frequency and  $\kappa$  to denote the component of the incident wave vector parallel to the surface. The generated nonlinear polarization is oscillating at  $\Omega = 2\omega$  and will be characterized by a wave vector parallel to the surface  $\mathbf{K} = 2\kappa$ . We can carry over Eqs. (1.3)-(1.8) simply by replacing the lowercase symbols  $(\omega, \tilde{\omega}, \kappa, n_\beta, \tilde{w}_\beta, w_\beta, \hat{\mathbf{p}}_{\beta\pm}, \hat{\mathbf{s}})$  with uppercase symbols  $(\Omega, \tilde{\Omega}, \mathbf{K}, N_\beta, \tilde{W}_\beta, W_\beta, \hat{\mathbf{P}}_{\beta\pm}, \hat{\mathbf{S}})$ , all evaluated at  $2\omega$ . Of course, we always have that  $\hat{\mathbf{S}} = \hat{\mathbf{s}}$ .

From Fig. 1.1, we observe the propagation of the SH field as it is refracted at the layer-vacuum interface ( $\ell v$ ), and reflected multiple times from the layer-bulk ( $\ell b$ ) and layer-vacuum ( $\ell v$ ) interfaces. Thus, we can define

$$\mathbf{T}^{\ell v} = \hat{\mathbf{s}} T_s^{\ell v} \hat{\mathbf{s}} + \hat{\mathbf{P}}_{v+} T_p^{\ell v} \hat{\mathbf{P}}_{\ell+}, \quad (1.10)$$

as the transmission tensor for the  $\ell v$  interface,

$$\mathbf{R}^{\ell b} = \hat{\mathbf{s}} R_s^{\ell b} \hat{\mathbf{s}} + \hat{\mathbf{P}}_{\ell+} R_p^{\ell b} \hat{\mathbf{P}}_{\ell-}, \quad (1.11)$$

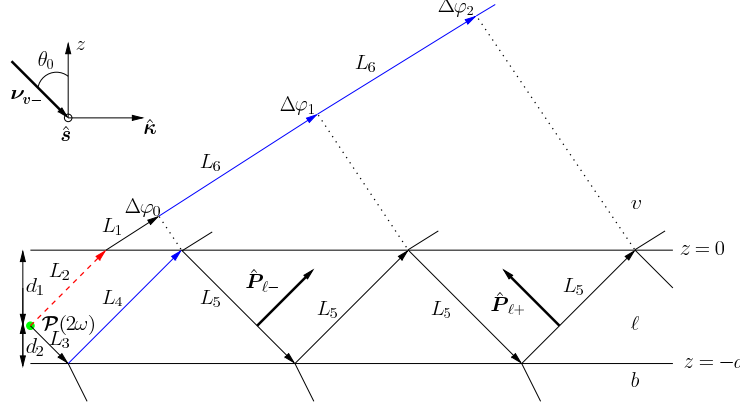


Figure 1.1: Sketch of the three layer model for SHG. The vacuum region ( $v$ ) is on top with  $\epsilon_v = 1$ ; the layer  $\ell$  of thickness  $d = d_1 + d_2$ , is characterized with  $\epsilon_\ell(\omega)$ , and it is where the SH polarization sheet  $\mathcal{P}_\ell(2\omega)$  is located at  $z_\ell = d_1$ . The bulk  $b$  is described with  $\epsilon_b(\omega)$ . The arrows point along the direction of propagation, and the  $p$ -polarization unit vector,  $\hat{\mathbf{P}}_{\ell- (+)}$ , along the downward (upward) direction is denoted with a thick arrow. The  $s$ -polarization unit vector  $\hat{\mathbf{s}}$ , points out of the page. The fundamental field  $\mathbf{E}(\omega)$  is incident from the vacuum side along the  $\kappa z$ -plane, with  $\theta_0$  its angle of incidence and  $\nu_{v-}$  its wave vector.  $\Delta\varphi_i$  denote the phase difference of the multiple reflected beams with respect to the first vacuum transmitted beam (dashed-red arrow), where the dotted lines are perpendicular to this beam.

as the reflection tensor for the  $\ell b$  interface, and

$$\mathbf{R}^{\ell v} = \hat{\mathbf{s}} R_s^{\ell v} \hat{\mathbf{s}} + \hat{\mathbf{P}}_{\ell-} R_p^{\ell v} \hat{\mathbf{P}}_{\ell+}, \quad (1.12)$$

as the reflection tensor for the  $\ell v$  interface. The Fresnel factors in uppercase letters,  $T_{s,p}^{ij}$  and  $R_{s,p}^{ij}$ , are evaluated at  $2\omega$  from the following well known formulas

$$\begin{aligned} t_s^{ij}(\omega) &= \frac{2w_i(\omega)}{w_i(\omega) + w_j(\omega)}, & t_p^{ij}(\omega) &= \frac{2w_i(\omega)\sqrt{\epsilon_i(\omega)\epsilon_j(\omega)}}{w_i(\omega)\epsilon_j(\omega) + w_j(\omega)\epsilon_i(\omega)}, \\ r_s^{ij}(\omega) &= \frac{w_i(\omega) - w_j(\omega)}{w_i(\omega) + w_j(\omega)}, & r_p^{ij}(\omega) &= \frac{w_i(\omega)\epsilon_j(\omega) - w_j\epsilon_i(\omega)}{w_i(\omega)\epsilon_j(\omega) + w_j(\omega)\epsilon_i(\omega)}. \end{aligned} \quad (1.13)$$

With these expressions we easily derive the following useful relations,

$$\begin{aligned} 1 + r_s^{\ell b} &= t_s^{\ell b}, \\ 1 + r_p^{\ell b} &= \frac{n_b}{n_\ell} t_p^{\ell b}, \\ 1 - r_p^{\ell b} &= \frac{n_\ell}{n_b} \frac{w_b}{w_\ell} t_p^{\ell b}, \\ t_p^{\ell v} &= \frac{w_\ell}{w_v} t_p^{v\ell}, \\ t_s^{\ell v} &= \frac{w_\ell}{w_v} t_s^{v\ell}. \end{aligned} \quad (1.14)$$

### 1.1.1 Multiple SHG reflections

The SH field  $\mathbf{E}(2\omega)$  radiated by the SH polarization  $\mathcal{P}_\ell(2\omega)$  will radiate directly into the vacuum and the bulk, where it will be reflected back at the layer-bulk interface into the thin layer. This beam will be transmitted and reflected multiple times, as shown in Fig. 1.1. As the two beams propagate, a phase difference will develop between them according to

$$\begin{aligned}\Delta\varphi_m &= \tilde{\Omega} \left( (L_3 + L_4 + 2mL_5)N_\ell - (L_2N_\ell + (L_1 + mL_6)N_v) \right) \\ &= \delta_0 + m\delta \quad m = 0, 1, 2, \dots,\end{aligned}\tag{1.15}$$

where

$$\delta_0 = 8\pi \left( \frac{d_2}{\lambda_0} \right) W_\ell,\tag{1.16}$$

and

$$\delta = 8\pi \left( \frac{d}{\lambda_0} \right) W_\ell,\tag{1.17}$$

where  $\lambda_0$  is the wavelength of the fundamental field in the vacuum,  $d$  is the thickness of layer  $\ell$ , and  $d_2$  is the distance of  $\mathcal{P}_\ell(2\omega)$  from the  $\ell b$  interface (see Fig. 1.1). We see that  $\delta_0$  is the phase difference of the first and second transmitted beams, and  $m\delta$  that of the first and third ( $m = 1$ ), first and fourth ( $m = 2$ ), and so on. Note that the thickness  $d$  of the layer  $\ell$  enters through the phase  $\delta$ , and the position  $d_2$  of the nonlinear polarization sheet  $\mathbf{P}(\mathbf{r}, t)$  (Eq. (1.3)) enters through  $\delta_0$ . In particular,  $d_2$  could be used as a variable to study the effects of multiple reflections on the SHG yield  $\mathcal{R}(2\omega)$ .

To take into account the multiple reflections of the generated SH field in the layer  $\ell$ , we proceed as follows. I include the algebra for the  $p$ -polarized SH field, and the  $s$ -polarized field could be worked out along the same steps. The  $p$ -polarized  $\mathbf{E}_{\ell,p}(2\omega)$  field reflected multiple times is given by

$$\begin{aligned}\mathbf{E}_{\ell,p}(2\omega) &= E_{\ell,p+}(2\omega) \mathbf{T}^{\ell v} \cdot \hat{\mathbf{P}}_{\ell+} + E_{\ell,p-}(2\omega) \mathbf{T}^{\ell v} \cdot \mathbf{R}^{\ell b} \cdot \hat{\mathbf{P}}_{\ell-} e^{i\Delta\varphi_0} \\ &\quad + E_{\ell,p-}(2\omega) \mathbf{T}^{\ell v} \cdot \mathbf{R}^{\ell b} \cdot \mathbf{R}^{\ell v} \cdot \mathbf{R}^{\ell b} \cdot \hat{\mathbf{P}}_{\ell-} e^{i\Delta\varphi_1} \\ &\quad + E_{\ell,p-}(2\omega) \mathbf{T}^{\ell v} \cdot \mathbf{R}^{\ell b} \cdot \mathbf{R}^{\ell v} \cdot \mathbf{R}^{\ell b} \cdot \mathbf{R}^{\ell v} \cdot \mathbf{R}^{\ell b} \cdot \hat{\mathbf{P}}_{\ell-} e^{i\Delta\varphi_2} + \dots \\ &= E_{\ell,p+}(2\omega) \mathbf{T}^{\ell v} \cdot \hat{\mathbf{P}}_{\ell+} + E_{\ell,p-}(2\omega) \mathbf{T}^{\ell v} \cdot \sum_{m=0}^{\infty} (\mathbf{R}^{\ell b} \cdot \mathbf{R}^{\ell v} e^{i\delta})^m \cdot \mathbf{R}^{\ell b} \cdot \hat{\mathbf{P}}_{\ell-} e^{i\delta_0}.\end{aligned}\tag{1.18}$$

From Eqs. (1.10) - (1.12) it is easy to show that

$$\mathbf{T}^{\ell v} \cdot (\mathbf{R}^{\ell b} \cdot \mathbf{R}^{\ell v})^n \cdot \mathbf{R}^{\ell b} = \hat{\mathbf{s}} T_s^{\ell v} (R_s^{\ell b} R_s^{\ell v})^n R_s^{\ell b} \hat{\mathbf{s}} + \hat{\mathbf{P}}_{v+} T_p^{\ell v} (R_p^{\ell b} R_p^{\ell v})^n R_p^{\ell b} \hat{\mathbf{P}}_{\ell-},$$

then,

$$\mathbf{E}_{\ell,p}(2\omega) = \hat{\mathbf{P}}_{\ell+} T_p^{\ell v} \left( E_{\ell,p+}(2\omega) + \frac{R_p^{\ell b} e^{i\delta_0}}{1 + R_p^{\ell b} R_p^{\ell v} e^{i\delta}} E_{\ell,p-}(2\omega) \right),\tag{1.19}$$

where we used  $R_{s,p}^{ij} = -R_{s,p}^{ji}$ . Using Eq. (1.4) and (1.14), we can readily write

$$\mathbf{E}_{\ell,p}(2\omega) = \frac{\gamma i \tilde{\Omega}}{W_\ell} \mathbf{H}_\ell \cdot \mathcal{P}_\ell(2\omega),\tag{1.20}$$

where

$$\mathbf{H}_\ell = \frac{W_\ell}{W_v} \left[ \hat{\mathbf{s}} T_s^{v\ell} (1 + R_s^M) \hat{\mathbf{s}} + \hat{\mathbf{P}}_{v+} T_p^{v\ell} (\hat{\mathbf{P}}_{\ell+} + R_p^M \hat{\mathbf{P}}_{\ell-}) \right], \quad (1.21)$$

and

$$R_i^M \equiv \frac{R_i^{\ell b} e^{i\delta_0}}{1 + R_i^{v\ell} R_i^{\ell b} e^{i\delta}}, \quad i = s, p, \quad (1.22)$$

is defined as the multiple ( $M$ ) reflection coefficient. This coefficient depends on the thickness  $d$  of layer  $\ell$ , and most importantly on the position  $d_2$  of  $\mathcal{P}_\ell(2\omega)$  within this layer. The final results will depend on both  $d$  and  $d_2$ . However, we can also define an average  $\bar{R}_i^M$  as

$$\bar{R}_i^M \equiv \frac{1}{d} \int_0^d R_i^M(x) dx \propto \frac{1}{d} \int_0^d e^{i\alpha x} dx, \quad (1.23)$$

where

$$R_i^M(x) = \frac{R_i^{\ell b} e^{i\alpha x}}{1 + R_i^{v\ell} R_i^{\ell b} e^{i\delta}}, \quad (1.24)$$

and  $\alpha = 8\pi W_\ell / \lambda_0$ . We can evaluate the rightmost integral,

$$\begin{aligned} \frac{1}{d} \int_0^d e^{i\alpha x} dx &= \frac{1}{d} \frac{e^{i\alpha x}}{i\alpha} \Big|_0^d = \frac{1}{i\alpha d} (e^{i\alpha d} - 1) \\ &= \frac{1}{i\delta} (e^{i\delta} - 1) = \frac{1}{i\delta} e^{i\delta/2} \frac{(e^{i\delta/2} - e^{-i\delta/2})}{2i} = e^{i\delta/2} \text{sinc}(\delta/2). \end{aligned} \quad (1.25)$$

Therefore, we can establish the average value  $\bar{R}_i^M$  as

$$\bar{R}_i^M = \frac{R_i^{\ell b} e^{i\delta/2}}{1 + R_i^{v\ell} R_i^{\ell b} e^{i\delta}} \text{sinc}(\delta/2), \quad (1.26)$$

that only depends on  $d$  through the  $\delta$  term from Eq. (1.17).

To connect with the work in Ref. [4], where  $\mathcal{P}(2\omega)$  is located on top of the vacuum-surface interface and only the vacuum radiated beam and the first (and only) reflected beam need be considered, we take  $\ell = v$  and  $d_2 = 0$ , then  $T^{\ell v} = 1$ ,  $R^{v\ell} = 0$  and  $\delta_0 = 0$ , with which  $R_i^M = R_i^{vb}$ . Thus, Eq. (1.21) coincides with Eq. (3.8) of Ref. [4].

### 1.1.2 Multiple reflections for the linear field

For a more complete formulation, we must also consider the multiple reflections of the fundamental field  $\mathbf{E}_\ell(\omega)$  inside the thin  $\ell$  layer. In Fig. 1.2 I present the situation where  $\mathbf{E}_v(\omega)$  impinges from the vacuum side with an angle of incidence  $\theta_0$ . As the first transmitted beam is multiply reflected from the  $\ell b$  and the  $\ell v$  interfaces, it accumulates a phase difference of  $n\phi$ , with  $n = 1, 2, 3, \dots$ , given by

$$\begin{aligned} \varphi &= \frac{\omega}{c} (2L_1 n_\ell - L_2 n_v) \\ &= 4\pi \left( \frac{d}{\lambda_0} \right) w_\ell, \end{aligned} \quad (1.27)$$

where  $n_v = 1$ . Besides the equivalent of Eqs. (1.11) and (1.12) for  $\omega$ , we also need

$$\mathbf{t}^{v\ell} = \hat{\mathbf{s}} t_s^{v\ell} \hat{\mathbf{s}} + \hat{\mathbf{p}}_{\ell-} t_p^{v\ell} \hat{\mathbf{p}}_{v-}, \quad (1.28)$$

to write

$$\begin{aligned} \mathbf{E}(\omega) &= E_0 \left[ \mathbf{t}^{v\ell} + \mathbf{r}^{\ell b} \cdot \mathbf{t}^{v\ell} e^{i\varphi} + \mathbf{r}^{\ell b} \cdot \mathbf{r}^{\ell v} \cdot \mathbf{r}^{\ell b} \cdot \mathbf{t}^{v\ell} e^{i2\varphi} + \mathbf{r}^{\ell b} \cdot \mathbf{r}^{\ell v} \cdot \mathbf{r}^{\ell b} \cdot \mathbf{r}^{\ell v} \cdot \mathbf{r}^{\ell b} \cdot \mathbf{t}^{v\ell} e^{i3\varphi} + \dots \right] \cdot \hat{\mathbf{e}}^i \\ &= E_0 \left[ 1 + \left( 1 + \mathbf{r}^{\ell b} \cdot \mathbf{r}^{\ell v} e^{i\varphi} + (\mathbf{r}^{\ell b} \cdot \mathbf{r}^{\ell v})^2 e^{i2\varphi} + \dots \right) \cdot \mathbf{r}^{\ell b} e^{i\varphi} \right] \cdot \mathbf{t}^{v\ell} \cdot \hat{\mathbf{e}}^i \\ &= E_0 \left[ \hat{\mathbf{s}} t_s^{v\ell} (1 + r_s^M) \hat{\mathbf{s}} + t_p^{v\ell} (\hat{\mathbf{p}}_{\ell-} + \hat{\mathbf{p}}_{\ell+} r_p^M) \hat{\mathbf{p}}_{v-} \right] \cdot \hat{\mathbf{e}}^i, \end{aligned} \quad (1.29)$$

where  $E_0$  is the intensity of the fundamental field, and  $\hat{\mathbf{e}}^i$  is the unit vector of the incoming polarization, with  $i = s, p$ , and then,  $\hat{\mathbf{e}}^s = \hat{\mathbf{s}}$  and  $\hat{\mathbf{e}}^p = \hat{\mathbf{p}}_{v-}$ . Also,

$$r_i^M \equiv \frac{r_i^{\ell b} e^{i\varphi}}{1 + r_i^{v\ell} r_i^{\ell b} e^{i\varphi}}, \quad i = s, p. \quad (1.30)$$

$r_i^M$  is defined as the multiple (M) reflection coefficient for the fundamental field. We define  $\mathbf{E}_\ell^i(\omega) \equiv E_0 \mathbf{e}_\ell^{\omega, i}$  ( $i = s, p$ ), where

$$\mathbf{e}_\ell^{\omega, i} = \left[ \hat{\mathbf{s}} t_s^{v\ell} (1 + r_s^M) \hat{\mathbf{s}} + t_p^{v\ell} (\hat{\mathbf{p}}_{\ell-} + \hat{\mathbf{p}}_{\ell+} r_p^M) \hat{\mathbf{p}}_{v-} \right] \cdot \hat{\mathbf{e}}^i, \quad (1.31)$$

and using Eq. (1.5) we obtain that

$$\mathbf{e}_\ell^{\omega, p} = \frac{t_p^{v\ell}}{n_\ell} (r_p^{M+} \sin \theta_0 \hat{\mathbf{z}} + r_p^{M-} w_\ell \hat{\boldsymbol{\kappa}}), \quad (1.32)$$

for  $p$ -input polarization with  $\hat{\mathbf{e}}^i = \hat{\mathbf{p}}_{v-}$ , and

$$\mathbf{e}_\ell^{\omega, s} = t_s^{v\ell} r_s^{M+} \hat{\mathbf{s}}, \quad (1.33)$$

for  $s$ -input polarization with  $\hat{\mathbf{e}}^i = \hat{\mathbf{s}}$ , where

$$r_i^{M\pm} = 1 \pm r_i^M, \quad i = s, p. \quad (1.34)$$

### 1.1.3 Deriving the SSHG yield

The magnitude of the radiated field is given by  $E(2\omega) = \hat{\mathbf{e}}^F \cdot \mathbf{E}_\ell(2\omega)$ , where  $\hat{\mathbf{e}}^F$  is the unit vector of the final polarization with  $F = S, P$ , where  $\hat{\mathbf{e}}^S = \hat{\mathbf{s}}$  and  $\hat{\mathbf{e}}^P = \hat{\mathbf{P}}_{v+}$ . We expand the rightmost term in parenthesis of Eq. (1.21) as

$$\begin{aligned} \hat{\mathbf{P}}_{\ell+} + R_p^M \hat{\mathbf{P}}_{\ell-} &= \frac{\sin \theta_0 \hat{\mathbf{z}} - W_\ell \hat{\boldsymbol{\kappa}}}{N_\ell} + R_p^M \frac{\sin \theta_0 \hat{\mathbf{z}} + W_\ell \hat{\boldsymbol{\kappa}}}{N_\ell} \\ &= \frac{1}{N_\ell} (\sin \theta_0 R_p^{M+} \hat{\mathbf{z}} - W_\ell R_p^{M-} \hat{\boldsymbol{\kappa}}), \end{aligned} \quad (1.35)$$

where

$$R_i^{M\pm} \equiv 1 \pm R_i^M, \quad i = s, p. \quad (1.36)$$

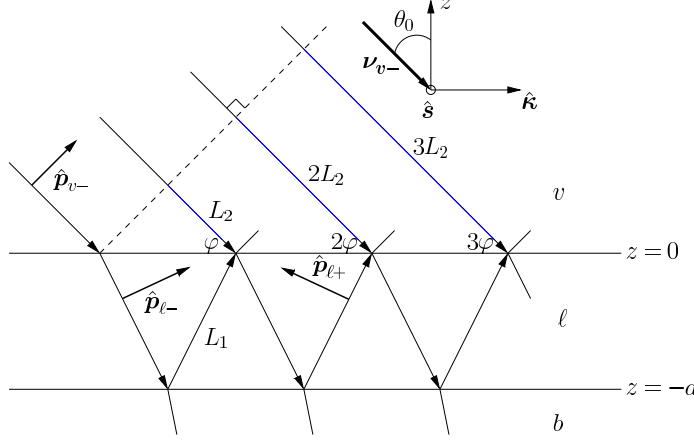


Figure 1.2: Sketch for the multiple reflected fundamental field  $\mathbf{E}(\omega)$ , which impinges from the vacuum side along the  $\hat{\kappa}z$ -plane.  $\theta_0$  and  $\nu_{v-}$  are the angle of incidence and wave vector, respectively. The arrows point along the direction of propagation. The  $p$ -polarization unit vectors  $\hat{\mathbf{p}}_{\beta\pm}$ , point along the downward ( $-$ ) or upward ( $+$ ) directions and are denoted with thick arrows, where  $\beta = v$  or  $\ell$ . The  $s$ -polarization unit vector  $\hat{\mathbf{s}}$  points out of the page.  $(1, 2, 3, \dots)\varphi$  denotes the phase difference for the multiple reflected beams with respect to the incident field, where the dotted line is perpendicular to this beam.

Using Eq. (1.14) we write Eq. (1.20) as

$$E(2\omega) = \frac{2\gamma i\omega}{cW_\ell} \hat{\mathbf{e}}^F \cdot \mathbf{H}_\ell \cdot \mathcal{P}_\ell(2\omega) = \frac{2\gamma i\omega}{cW_v} \mathbf{e}_\ell^{2\omega,F} \cdot \mathcal{P}_\ell(2\omega), \quad (1.37)$$

where

$$\mathbf{e}_\ell^{2\omega,F} = \hat{\mathbf{e}}^F \cdot \left[ \hat{\mathbf{s}} T_s^{v\ell} R_s^{M+} \hat{\mathbf{s}} + \hat{\mathbf{P}}_{v+} \frac{T_p^{v\ell}}{N_\ell} (\sin \theta_0 R_p^{M+} \hat{\mathbf{z}} - W_\ell R_p^{M-} \hat{\kappa}) \right]. \quad (1.38)$$

Replacing  $\mathbf{E}(\omega) \rightarrow E_0 \mathbf{e}_\ell^{\omega,i}$ , in Eq. (1.9), we obtain that

$$\mathcal{P}_\ell(2\omega) = \begin{cases} E_0^2 \chi : \mathbf{e}_\ell^{\omega,i} \mathbf{e}_\ell^{\omega,i} & (\text{CGS units}) \\ \epsilon_0 E_0^2 \chi : \mathbf{e}_\ell^{\omega,i} \mathbf{e}_\ell^{\omega,i} & (\text{MKS units}) \end{cases}, \quad (1.39)$$

where  $\mathbf{e}_\ell^{\omega,i}$  is given by Eq. (1.31), and thus Eq. (1.37) reduces to ( $W_v = \cos \theta_0$ )

$$E_\ell(2\omega) = \frac{2\eta i\omega}{c \cos \theta_0} \mathbf{e}_\ell^{2\omega,F} \cdot \chi : \mathbf{e}_\ell^{\omega,i} \mathbf{e}_\ell^{\omega,i}, \quad (1.40)$$

where  $\eta = 2\pi$  in CGS units and  $\eta = 1/2$  in MKS units. For ease of notation, we define

$$\Upsilon_{iF} \equiv \mathbf{e}_\ell^{2\omega,F} \cdot \chi : \mathbf{e}_\ell^{\omega,i} \mathbf{e}_\ell^{\omega,i}, \quad (1.41)$$

where  $i$  stands for the incoming polarization of the fundamental electric field given by  $\hat{\mathbf{e}}^i$  in Eq. (1.31), and  $F$  for the outgoing polarization of the SH electric field given by  $\hat{\mathbf{e}}^F$  in Eq. (1.38). I purposely omitted the full  $\chi(-2\omega; \omega, \omega)$  notation, and will do so from this point on.

From Eqs. (1.1) and (1.2) we obtain that in CGS units ( $\eta = 2\pi$ ),

$$\begin{aligned} |E(2\omega)|^2 &= |E_0|^4 \frac{16\pi^2\omega^2}{c^2 W_v^2} |\Upsilon_{iF}|^2 \\ \frac{c}{2\pi} |\sqrt{N_v} E(2\omega)|^2 &= \frac{32\pi^3\omega^2}{c^3 \cos^2 \theta_0} \left| \frac{\sqrt{N_v}}{n_\ell^2} \Upsilon_{iF} \right|^2 \left( \frac{c}{2\pi} |\sqrt{n_\ell} E_0|^2 \right)^2 \\ I(2\omega) &= \frac{32\pi^3\omega^2}{c^3 \cos^2 \theta_0} \left| \frac{\sqrt{N_v}}{n_\ell^2} \Upsilon_{iF} \right|^2 I^2(\omega) \\ \mathcal{R}_{iF}(2\omega) &= \frac{32\pi^3\omega^2}{c^3 \cos^2 \theta_0} \left| \frac{1}{n_\ell} \Upsilon_{iF} \right|^2, \end{aligned} \quad (1.42)$$

and in MKS units ( $\eta = 1/2$ ),

$$\begin{aligned} |E(2\omega)|^2 &= |E_0|^4 \frac{\omega^2}{c^2 W_v^2} \\ 2\epsilon_0 c |\sqrt{N_v} E(2\omega)|^2 &= \frac{2\epsilon_0 \omega^2}{c \cos^2 \theta_0} \left| \frac{\sqrt{N_v}}{n_\ell^2} \Upsilon_{iF} \right|^2 \frac{1}{4\epsilon_0^2 c^2} (2\epsilon_0 c |\sqrt{n_\ell} E_0|^2)^2 \\ I(2\omega) &= \frac{\omega^2}{2\epsilon_0 c^3 \cos^2 \theta_0} \left| \frac{\sqrt{N_v}}{n_\ell^2} \Upsilon_{iF} \right|^2 I^2(\omega) \\ \mathcal{R}_{iF}(2\omega) &= \frac{\omega^2}{2\epsilon_0 c^3 \cos^2 \theta_0} \left| \frac{1}{n_\ell} \Upsilon_{iF} \right|^2. \end{aligned} \quad (1.43)$$

Finally, we condense these results and establish the SSHG yield as

$$\mathcal{R}_{iF}(2\omega) \begin{cases} \frac{32\pi^3\omega^2}{c^3 \cos^2 \theta_0} \left| \frac{1}{n_\ell} \Upsilon_{iF} \right|^2 & (\text{CGS units}) \\ \frac{\omega^2}{2\epsilon_0 c^3 \cos^2 \theta_0} \left| \frac{1}{n_\ell} \Upsilon_{iF} \right|^2 & (\text{MKS units}) \end{cases}, \quad (1.44)$$

where  $N_v = 1$  and  $W_v = \cos \theta_0$ . In the MKS unit system  $\chi$  is given in  $\text{m}^2/\text{V}$ , since it is a surface second order nonlinear susceptibility, and  $\mathcal{R}_{iF}$  is given in  $\text{m}^2/\text{W}$ .

I include a full treatise on this exact procedure without considering the effects of multiple reflections in Appendix B.

## 1.2 $\mathcal{R}_{iF}$ for different polarization cases

We now have everything we need to derive explicit expressions for  $\mathcal{R}_{iF}$ , Eq. (1.44), for the most commonly used polarizations of incoming and outgoing fields ( $iF=pP$ ,  $pS$ ,  $sP$ , and  $sS$ ). For this, we must expand  $\Upsilon_{iF}$  from Eq. (1.41) for each case. By substituting Eqs. (1.7) and (1.8) into Eq. (1.38), we obtain

$$\mathbf{e}_\ell^{2\omega,P} = \frac{T_p^{v\ell}}{N_\ell} (\sin \theta_0 R_p^{M+} \hat{\mathbf{z}} - W_\ell R_p^{M-} \cos \phi \hat{\mathbf{x}} - W_\ell R_p^{M-} \sin \phi \hat{\mathbf{y}}), \quad (1.45)$$

for  $P$  ( $\hat{\mathbf{e}}^F = \hat{\mathbf{P}}_{v+}$ ) outgoing polarization, and

$$\mathbf{e}_\ell^{2\omega,S} = T_s^{v\ell} R_s^{M+} (-\sin \phi \hat{\mathbf{x}} + \cos \phi \hat{\mathbf{y}}). \quad (1.46)$$

Case	$\hat{\mathbf{e}}^F$	$\hat{\mathbf{e}}^i$	$\mathbf{e}_\ell^{2\omega,F}$	$\mathbf{e}_\ell^{\omega,i}\mathbf{e}_\ell^{\omega,i}$
$\mathcal{R}_{pP}$	$\hat{\mathbf{P}}_{v+}$	$\hat{\mathbf{p}}_{v-}$	Eq. (1.45)	Eq. (1.47)
$\mathcal{R}_{pS}$	$\hat{\mathbf{S}}$	$\hat{\mathbf{p}}_{v-}$	Eq. (1.46)	Eq. (1.47)
$\mathcal{R}_{sP}$	$\hat{\mathbf{P}}_{v+}$	$\hat{\mathbf{s}}$	Eq. (1.45)	Eq. (1.48)
$\mathcal{R}_{sS}$	$\hat{\mathbf{S}}$	$\hat{\mathbf{s}}$	Eq. (1.46)	Eq. (1.48)

Table 1.1: Polarization unit vectors for  $\hat{\mathbf{e}}^F$  and  $\hat{\mathbf{e}}^i$ , and equations describing  $\mathbf{e}_\ell^{2\omega,F}$  and  $\mathbf{e}_\ell^{\omega,i}\mathbf{e}_\ell^{\omega,i}$  for each polarization case.

(111)- $C_{3v}$	(110)- $C_{2v}$	(001)- $C_{4v}$
$\chi^{zzz}$ $\chi^{zxx} = \chi^{zyy}$ $\chi^{xxz} = \chi^{yyz}$ $\chi^{xxx} = -\chi^{xyy} = -\chi^{yyx}$	$\chi^{zzz}$ $\chi^{zxx} \neq \chi^{zyy}$ $\chi^{xxz} \neq \chi^{yyz}$	$\chi^{zzz}$ $\chi^{zxx} = \chi^{zyy}$ $\chi^{xxz} = \chi^{yyz}$

Table 1.2: Components of  $\chi$  for the (111), (110) and (001) crystallographic faces, belonging to the  $C_{3v}$ ,  $C_{2v}$ , and  $C_{4v}$ , symmetry groups, respectively. For the (111) surface we choose the  $x$  and  $y$  axes along the  $[1\bar{1}\bar{2}]$  and  $[1\bar{1}0]$  directions, respectively. For the (110) and (001) we consider the  $y$  axis perpendicular to the plane of symmetry.[10] We remark that in general  $\chi^{(111)} \neq \chi^{(110)} \neq \chi^{(001)}$ .

for  $S$  ( $\hat{\mathbf{e}}^F = \hat{\mathbf{s}}$ ) outgoing polarization.

Following a similar procedure, we use Eqs. (1.7) and (1.8) with Eq. (1.32), and obtain

$$\begin{aligned} \mathbf{e}_\ell^{\omega,p}\mathbf{e}_\ell^{\omega,p} = & \left(\frac{t_p^{v\ell}}{n_\ell}\right)^2 \left( (r_p^{M-})^2 w_\ell^2 \cos^2 \phi \hat{\mathbf{x}}\hat{\mathbf{x}} + 2(r_p^{M-})^2 w_\ell^2 \sin \phi \cos \phi \hat{\mathbf{x}}\hat{\mathbf{y}} \right. \\ & + 2r_p^{M+}r_p^{M-}w_\ell \sin \theta_0 \cos \phi \hat{\mathbf{x}}\hat{\mathbf{z}} + (r_p^{M-})^2 w_\ell^2 \sin^2 \phi \hat{\mathbf{y}}\hat{\mathbf{y}} \\ & \left. + 2r_p^{M+}r_p^{M-}w_\ell \sin \theta_0 \sin \phi \hat{\mathbf{y}}\hat{\mathbf{z}} + (r_p^{M+})^2 \sin^2 \theta_0 \hat{\mathbf{z}}\hat{\mathbf{z}} \right), \end{aligned} \quad (1.47)$$

for  $p$  incoming polarization ( $\hat{\mathbf{e}}^i = \hat{\mathbf{p}}_{v-}$ ), and with Eq. (1.33),

$$\mathbf{e}_\ell^{\omega,s}\mathbf{e}_\ell^{\omega,s} = \left(t_s^{v\ell}r_s^{M+}\right)^2 (\sin^2 \phi \hat{\mathbf{x}}\hat{\mathbf{x}} + \cos^2 \phi \hat{\mathbf{y}}\hat{\mathbf{y}} - 2 \sin \phi \cos \phi \hat{\mathbf{x}}\hat{\mathbf{y}}). \quad (1.48)$$

for  $s$  incoming polarization ( $\hat{\mathbf{e}}^i = \hat{\mathbf{s}}$ ).

I have summarized the combination of equations needed to derive the expressions for all four polarization cases of  $\mathcal{R}_{iF}$  in Table 1.1. In the following subsections we will derive the explicit expressions for  $\Upsilon_{iF}$  for the most general case where the surface has no symmetry other than that of noncentrosymmetry. We will then develop these expressions for particular cases of the most commonly investigated surfaces, the (111), (001), and (110) crystallographic faces. For ease of writing we split  $\Upsilon_{iF}$  as

$$\Upsilon_{iF} = \Gamma_{iF} r_{iF}. \quad (1.49)$$

Lastly, in Table 1.2 I list the nonzero components of  $\chi$  for each surface symmetry [10, 11].

I have provided the full, step-by-step derivation for all of these expressions in Appendix A, with and without the effects of multiple reflections. The avid reader should refer to that chapter if interested in deriving any of the expressions listed below.

### 1.2.1 $\mathcal{R}_{pP}$ ( $p$ -in, $P$ -out)

Per Table 1.1,  $\mathcal{R}_{pP}$  requires Eqs. (1.45) and (1.47). After some algebra, we obtain that

$$\Gamma_{pP} = \frac{T_p^{v\ell}}{N_\ell} \left( \frac{t_p^{v\ell}}{n_\ell} \right)^2, \quad (1.50)$$

and

$$\begin{aligned} r_{pP} = & -R_p^{M-} (r_p^{M-})^2 w_\ell^2 W_\ell \cos^3 \phi \chi^{xxx} - 2R_p^{M-} (r_p^{M-})^2 w_\ell^2 W_\ell \sin \phi \cos^2 \phi \chi^{xxy} \\ & - 2R_p^{M-} r_p^{M+} r_p^{M-} w_\ell W_\ell \sin \theta_0 \cos^2 \phi \chi^{xxz} - R_p^{M-} (r_p^{M-})^2 w_\ell^2 W_\ell \sin^2 \phi \cos \phi \chi^{xyy} \\ & - 2R_p^{M-} r_p^{M+} r_p^{M-} w_\ell W_\ell \sin \theta_0 \sin \phi \cos \phi \chi^{xyz} - R_p^{M-} (r_p^{M+})^2 W_\ell \sin^2 \theta_0 \cos \phi \chi^{xzz} \\ & - R_p^{M-} (r_p^{M-})^2 w_\ell^2 W_\ell \sin \phi \cos^2 \phi \chi^{yxx} - 2R_p^{M-} (r_p^{M-})^2 w_\ell^2 W_\ell \sin^2 \phi \cos \phi \chi^{yxy} \\ & - 2R_p^{M-} r_p^{M+} r_p^{M-} w_\ell W_\ell \sin \theta_0 \sin \phi \cos \phi \chi^{yxz} - R_p^{M-} (r_p^{M-})^2 w_\ell^2 W_\ell \sin^3 \phi \chi^{yyy} \\ & - 2R_p^{M-} r_p^{M+} r_p^{M-} w_\ell W_\ell \sin \theta_0 \sin^2 \phi \chi^{yyz} - R_p^{M-} (r_p^{M+})^2 W_\ell \sin^2 \theta_0 \sin \phi \chi^{yzz} \\ & + R_p^{M+} (r_p^{M-})^2 w_\ell^2 \sin \theta_0 \cos^2 \phi \chi^{zxx} + 2R_p^{M+} r_p^{M+} r_p^{M-} w_\ell \sin^2 \theta_0 \cos \phi \chi^{zxz} \\ & + 2R_p^{M+} (r_p^{M-})^2 w_\ell^2 \sin \theta_0 \sin \phi \cos \phi \chi^{zxy} + R_p^{M+} (r_p^{M-})^2 w_\ell^2 \sin \theta_0 \sin^2 \phi \chi^{zyy} \\ & + 2R_p^{M+} r_p^{M+} r_p^{M-} w_\ell \sin^2 \theta_0 \sin \phi \chi^{zzy} + R_p^{M+} (r_p^{M+})^2 \sin^3 \theta_0 \chi^{zzz}, \end{aligned} \quad (1.51)$$

where all 18 independent components of  $\chi$  for a surface with no symmetries, contribute to  $\mathcal{R}_{pP}$ . Recall that  $\chi^{ijk} = \chi^{ikj}$ . We will derive the expressions for each of the three surfaces being considered here, referring to Table 1.2. For the (111) surface we obtain

$$\begin{aligned} r_{pP}^{(111)} = & R_p^{M+} \sin \theta_0 \left[ (r_p^{M+})^2 \sin^2 \theta_0 \chi^{zzz} + (r_p^{M-})^2 w_\ell^2 \chi^{zxx} \right] \\ & - R_p^{M-} w_\ell W_\ell \left[ 2r_p^{M+} r_p^{M-} \sin \theta_0 \chi^{xxz} + (r_p^{M-})^2 w_\ell \chi^{xxx} \cos 3\phi \right], \end{aligned} \quad (1.52)$$

where the three-fold azimuthal symmetry of the SHG signal that is typical of the  $C_{3v}$  symmetry group, is seen in the  $3\phi$  argument of the cosine function. For the (110) surface, we have that

$$\begin{aligned} r_{pP}^{(110)} = & R_p^{M+} \sin \theta_0 \left[ (r_p^{M+})^2 \sin^2 \theta_0 \chi^{zzz} + (r_p^{M-})^2 w_\ell^2 \left( \frac{\chi^{zyy} + \chi^{zxx}}{2} + \frac{\chi^{zyy} - \chi^{zxx}}{2} \cos 2\phi \right) \right] \\ & - 2R_p^{M-} r_p^{M+} r_p^{M-} w_\ell W_\ell \sin \theta_0 \left( \frac{\chi^{yyz} + \chi^{xxz}}{2} + \frac{\chi^{yyz} - \chi^{xxz}}{2} \cos 2\phi \right). \end{aligned} \quad (1.53)$$

The two-fold azimuthal symmetry of the SHG signal that is typical of the  $C_{2v}$  symmetry group, is seen in the  $2\phi$  argument of the cosine function. For the (001) surface we simply make  $\chi^{zxx} = \chi^{zyy}$

and  $\chi^{xxz} = \chi^{yyz}$  as seen in Table 1.2, and the previous expression reduces to

$$\begin{aligned} r_{pP}^{(001)} &= R_p^{M+} \sin \theta_0 \left[ (r_p^{M+})^2 \sin^2 \theta_0 \chi^{zzz} + (r_p^{M-})^2 w_\ell^2 \chi^{zxx} \right] \\ &\quad - 2R_p^{M-} r_p^{M+} r_p^{M-} w_\ell W_\ell \sin \theta_0 \chi^{xxz}. \end{aligned} \quad (1.54)$$

This time, the azimuthal  $4\phi$  symmetry for the  $C_{4v}$  group of the (001) surface is absent in this expression since this contribution is only related to the bulk nonlinear quadrupolar SH term [10], that we neglect in this work.

### 1.2.2 $\mathcal{R}_{sP}$ (*s-in, P-out*)

Per Table 1.1,  $\mathcal{R}_{sP}$  requires Eqs. (1.45) and (1.48). After some algebra, we obtain that

$$\Gamma_{sP} = \frac{T_p^{v\ell}}{N_\ell} \left( t_s^{v\ell} r_s^{M+} \right)^2, \quad (1.55)$$

and

$$\begin{aligned} r_{sP} &= R_p^{M-} W_\ell (-\sin^2 \phi \cos \phi \chi^{xxx} + 2 \sin \phi \cos^2 \phi \chi^{xxy} - \cos^3 \phi \chi^{xyy}) \\ &\quad R_p^{M-} W_\ell (-\sin^3 \phi \chi^{yxx} + 2 \sin^2 \phi \cos \phi \chi^{yxy} - \sin \phi \cos^2 \phi \chi^{yyy}) \\ &\quad R_p^{M+} \sin \theta_0 (\sin^2 \phi \chi^{zxx} - 2 \sin \phi \cos \phi \chi^{zxy} + \cos^2 \phi \chi^{zyy}). \end{aligned} \quad (1.56)$$

In this case, 9 out of the 18 components of  $\chi$  for a surface with no symmetries, contribute to  $\mathcal{R}_{sP}$ . This is because there is no  $E_z(\omega)$  component, as the incoming polarization is *s*. From Table 1.2 we get,

$$r_{sP}^{(111)} = R_p^{M+} \sin \theta_0 \chi^{zxx} + R_p^{M-} W_\ell \chi^{xxx} \cos 3\phi, \quad (1.57)$$

for the (111) surface,

$$r_{sP}^{(110)} = R_p^{M+} \sin \theta_0 \left( \frac{\chi^{zxx} + \chi^{zyy}}{2} + \frac{\chi^{zyy} - \chi^{zxx}}{2} \cos 2\phi \right), \quad (1.58)$$

for the (110) surface, and

$$r_{sP}^{(001)} = R_p^{M+} \sin \theta_0 \chi^{zxx}, \quad (1.59)$$

for the (001) surface.

### 1.2.3 $\mathcal{R}_{pS}$ (*p-in, S-out*)

Per Table 1.1,  $\mathcal{R}_{pS}$  requires Eqs. (1.46) and (1.47). After some algebra, we obtain that

$$\Gamma_{pS} = T_s^{v\ell} R_s^{M+} \left( \frac{t_p^{v\ell}}{n_\ell} \right)^2, \quad (1.60)$$

and

$$\begin{aligned}
r_{pS} = & - (r_p^{M-})^2 w_\ell^2 \sin \phi \cos^2 \phi \chi^{xxx} - 2 (r_p^{M-})^2 w_\ell^2 \sin^2 \phi \cos \phi \chi^{xxy} \\
& - 2r_p^{M+} r_p^{M-} w_\ell \sin \theta_0 \sin \phi \cos \phi \chi^{xxz} - (r_p^{M-})^2 w_\ell^2 \sin^3 \phi \chi^{xyy} \\
& - 2r_p^{M+} r_p^{M-} w_\ell \sin \theta_0 \sin^2 \phi \chi^{xzy} - (r_p^{M+})^2 \sin^2 \theta_0 \sin \phi \chi^{xzz} \\
& + (r_p^{M-})^2 w_\ell^2 \cos^3 \phi \chi^{yxx} + 2 (r_p^{M-})^2 w_\ell^2 \sin \phi \cos^2 \phi \chi^{yxy} \\
& + 2r_p^{M+} r_p^{M-} w_\ell \sin \theta_0 \cos^2 \phi \chi^{yxz} + (r_p^{M-})^2 w_\ell^2 \sin^2 \phi \cos \phi \chi^{yyy} \\
& + 2r_p^{M+} r_p^{M-} w_\ell \sin \theta_0 \sin \phi \cos \phi \chi^{yzy} + (r_p^{M+})^2 \sin^2 \theta_0 \cos \phi \chi^{yzz}.
\end{aligned} \tag{1.61}$$

In this case, 12 out of the 18 components of  $\chi$  for a surface with no symmetries, contribute to  $\mathcal{R}_{pS}$ . This is because there is no  $\mathcal{P}_z(2\omega)$  component, as the outgoing polarization is  $S$ . From Table 1.2 we obtain,

$$r_{pS}^{(111)} = - (r_p^{M-})^2 w_\ell^2 \chi^{xxx} \sin 3\phi, \tag{1.62}$$

for the (111) surface,

$$r_{sP}^{(110)} = r_p^{M+} r_p^{M-} w_\ell \sin \theta_0 (\chi^{yyz} - \chi^{xxz}) \sin 2\phi, \tag{1.63}$$

for the (110) surface, finally,

$$r_{pS}^{(001)} = 0, \tag{1.64}$$

for the (001) surface, where the zero value is only surface related as we neglect the bulk nonlinear quadrupolar contribution [10].

#### 1.2.4 $\mathcal{R}_{ss}$ ( $s$ -in, $S$ -out)

Per Table 1.1,  $\mathcal{R}_{ss}$  requires Eqs. (1.46) and (1.48). After some algebra, we obtain that

$$\Gamma_{ss} = T_s^{v\ell} R_s^{M+} \left( t_s^{v\ell} r_s^{M+} \right)^2, \tag{1.65}$$

and

$$\begin{aligned}
r_{ss} = & - \sin^3 \phi \chi^{xxx} + 2 \sin^2 \phi \cos \phi \chi^{xxy} - \sin \phi \cos^2 \phi \chi^{xyy} \\
& + \sin^2 \phi \cos \phi \chi^{yxx} + \cos^3 \phi \chi^{yyy} - 2 \sin \phi \cos^2 \phi \chi^{yxy}.
\end{aligned} \tag{1.66}$$

In this case, only 6 out of the 18 components of  $\chi$  for a surface with no symmetries, contribute to  $\mathcal{R}_{ss}$ . This is because there is neither an  $E_z(\omega)$  component as the incoming polarization is  $s$ , nor a  $\mathcal{P}_z(2\omega)$  component as the outgoing polarization is  $S$ . From Table 1.2, we get

$$r_{ss}^{(111)} = \chi^{xxx} \sin 3\phi, \tag{1.67}$$

for the (111) surface,

$$r_{ss}^{(110)} = 0, \tag{1.68}$$

and

$$r_{ss}^{(001)} = 0, \tag{1.69}$$

for the (110) and (001) surfaces, respectively, both being zero as the bulk nonlinear quadrupolar contribution is not considered here [10].

Label	$\mathcal{P}(2\omega)$	$\mathbf{E}(\omega)$
3-layer	$\ell$	$\ell$
2-layer-fresnel	$v$	$b$
2-layer-bulk	$b$	$b$
3-layer-hybrid	$\ell$	$b$
2-layer-vacuum	$v$	$v$

Table 1.3: Summary of the SSHG yield models used throughout this work. “Label” is the name used in subsequent figures, while the remaining columns show in which medium we will consider the specified quantity.  $\ell$  is the thin layer below the surface of the material,  $v$  is the vacuum region, and  $b$  is the bulk region of the material.

### 1.3 Some scenarios of interest

In this section we present five different scenarios for placing the nonlinear polarization  $\mathcal{P}(2\omega)$  and the fundamental electric field  $\mathbf{E}(\omega)$ , which are alternatives to the three-layer model presented above. In what follows, we confine ourselves only to the (111) surface and the  $p$ -in  $P$ -out combination polarizations. This is the case where the proposed scenarios differ the most as the SSHG yield depends on all the finite  $\chi^{ijk}$  components for this surface. However, the other  $pS$ ,  $sP$ , and  $sS$  polarization cases, or the (110) or (001) surfaces could be worked out along the same lines described below. For all the scenarios we omit the multiple SH reflections by taking  $R_p^{M\pm} \rightarrow 1 \pm R_p^{\ell b}$  (Eq. (1.36)) and the linear multiple reflections by taking  $r_p^{M\pm} \rightarrow 1 \pm r_p^{\ell b}$  (Eq. (1.34)). Using the expressions in Eq. (1.14), we obtain the following useful relationships

$$\begin{aligned} r_p^{M+} &\rightarrow \frac{n_b}{n_\ell} t_p^{\ell b} \\ r_p^{M-} &\rightarrow \frac{n_\ell}{n_b} \frac{w_b}{w_\ell} t_p^{\ell b}, \end{aligned} \tag{1.70}$$

which will come in handy for expressing  $\Gamma_{pP}$  and  $r_{pP}^{(111)}$  in the forms presented below. Recall that these expressions are valid for the  $2\omega$  terms by simply capitalizing the relevant quantities as explained in Sec. 1.1. We summarize these scenarios in Table 1.3 for quick reference. The complete derivations for these different cases are included in Appendix C.

#### 1.3.1 The 3-layer model without multiple reflections

Using Eq. (1.70) in Eq. (1.52) with Eq. (1.50), we obtain

$$\Gamma_{pP} = \frac{T_p^{\ell v} T_p^{\ell b}}{N_\ell^2 N_b} \left( \frac{t_p^{v\ell} t_p^{\ell b}}{n_\ell^2 n_b} \right)^2, \tag{1.71}$$

and

$$\begin{aligned} r_{pP}^{(111)} &= N_b^2 \sin \theta_0 \left( n_b^4 \sin^2 \theta_0 \chi^{zzz} + n_\ell^4 w_b^2 \chi^{zxx} \right) \\ &- N_\ell^2 n_\ell^2 w_b W_b \left( 2n_b^2 \sin \theta_0 \chi^{xxz} + n_\ell^2 w_b \chi^{xxx} \cos(3\phi) \right). \end{aligned} \tag{1.72}$$

Now that we have neglected multiple SH reflections, we can use these two expressions for  $\Gamma_{pP}$  and  $r_{pP}$  to obtain the next four scenarios by using the choices described in each subsection below. Note that by neglecting the multiple reflections, the thickness  $d$  of layer  $\ell$  disappears from the formulation, and the location of the nonlinear polarization sheet  $\mathbf{P}(\mathbf{r}, t)$  (Eq. (1.3)) at  $d_2$  (see Fig. 1.1) is immaterial.

### 1.3.2 The two layer, or Fresnel (2-layer-fresnel) model

Historically, this is the model most used in the literature. In Chap. 2, we will see how the 3-layer model, presented in the previous sections, offers a significant improvement over this model.

In the 2-layer-fresnel model, we consider that  $\mathcal{P}(2\omega)$  is evaluated in the vacuum region, while the fundamental fields are evaluated in the bulk region [10, 4]. To do this, we evaluate the  $2\omega$  radiations factors in the vacuum by taking  $\ell = v$ , thus  $\epsilon_\ell(2\omega) = 1$ ,  $T_p^{\ell v} = 1$ , and  $T_p^{\ell b} = T_p^{vb}$ . We also evaluate the fundamental field inside medium  $b$  by taking  $\ell = b$ , thus  $\epsilon_\ell(\omega) = \epsilon_b(\omega)$ ,  $t_p^{v\ell} = t_p^{vb}$ , and  $t_p^{\ell b} = 1$ . With these choices, Eqs. (1.71) and (1.72) reduce to

$$\Gamma_{pP} = \frac{T_p^{vb}(t_p^{vb})^2}{n_b^2 N_b}, \quad (1.73)$$

and

$$r_{pP}^{(111)} = N_b^2 \sin \theta_0 \left( \sin^2 \theta_0 \chi^{zzz} + w_b^2 \chi^{zxx} \right) - w_b W_b \left( 2 \sin \theta_0 \chi^{xxz} + w_b \chi^{xxx} \cos(3\phi) \right). \quad (1.74)$$

These expressions are in perfect agreement with Refs. [10] and [4].

### 1.3.3 The 2-layer-bulk model: evaluating $\mathcal{P}(2\omega)$ and $\mathbf{E}(\omega)$ in the bulk

We follow the same procedure as above considering that both the  $2\omega$  and  $1\omega$  terms will be evaluated in the bulk, by taking  $\ell = b$ . Thus,  $\epsilon_\ell(2\omega) = \epsilon_b(2\omega)$ ,  $T_p^{v\ell} = T_p^{vb}$ ,  $T_p^{\ell b} = 1$ , and  $\epsilon_\ell(\omega) = \epsilon_b(\omega)$ ,  $t_p^{v\ell} = t_p^{vb}$ , and  $t_p^{\ell b} = 1$ . With these choices Eqs. (1.71) and (1.72) reduce to

$$\Gamma_{pP} = \frac{T_p^{vb}(t_p^{vb})^2}{n_b^2 N_b}, \quad (1.75)$$

and

$$r_{pP}^{(111)} = \sin^3 \theta_0 \chi^{zzz} + w_b^2 \sin \theta_0 \chi^{zxx} - 2w_b W_b \sin \theta_0 \chi^{xxz} - w_b^2 W_b \chi^{xxx} \cos 3\phi. \quad (1.76)$$

### 1.3.4 The 2-layer-vacuum model: evaluating $\mathcal{P}(2\omega)$ and $\mathbf{E}(\omega)$ in the vacuum

We consider both  $\mathcal{P}(2\omega)$  and the fundamental fields to be evaluated in the vacuum. We take  $\ell = v$ , thus  $\epsilon_\ell(2\omega) = 1$ ,  $T_p^{\ell v} = 1$ ,  $T_p^{\ell b} = T_p^{vb}$ , and  $\epsilon_\ell(\omega) = 1$ ,  $t_p^{v\ell} = 1$ , and  $t_p^{\ell b} = t_p^{vb}$ . With these choices Eqs. (1.71) and (1.72) reduce to

$$\Gamma_{pP} = \frac{T_p^{vb}(t_p^{vb})^2}{n_b^2 N_b}, \quad (1.77)$$

and

$$r_{pP}^{(111)} = n_b^4 N_b^2 \sin^3 \theta_0 \chi^{zzz} + N_b^2 w_b^2 \sin \theta_0 \chi^{zxx} - 2n_b^2 w_b W_b \sin \theta_0 \chi^{xxz} - w_b^2 W_b \chi^{xxx} \cos 3\phi. \quad (1.78)$$

### 1.3.5 The 3-layer-hybrid model: evaluating $\mathcal{P}(2\omega)$ in $\ell$ and $\mathbf{E}(\omega)$ in the bulk

Again, we follow the same procedure as above considering that  $2\omega$  terms are evaluated in the thin layer  $\ell$ , and the  $1\omega$  terms will be evaluated in the bulk by taking  $\ell = b$ , thus  $\epsilon_\ell(\omega) = \epsilon_b(\omega)$ ,  $t_p^{v\ell} = t_p^{vb}$ , and  $t_p^{\ell b} = 1$ . With these choices Eqs. (1.71) and (1.72) reduce to

$$\Gamma_{pP}^{\ell b} = \frac{T_p^{v\ell} T_p^{\ell b} (t_p^{vb})^2}{N_\ell^2 n_b^2 N_b}, \quad (1.79)$$

and

$$r_{pP}^{(111)} = N_b^2 \sin^3 \theta_0 \chi^{zzz} + N_b^2 k_b^2 \sin \theta_0 \chi^{zxx} - 2N_\ell^2 w_b W_b \sin \theta_0 \chi^{xxz} - N_\ell^2 w_b^2 W_b \chi^{xxx} \cos 3\phi. \quad (1.80)$$

## 1.4 About coding the SSHG yield

Github repository (<https://github.com/roguephysicist/SHGYield>)

```

1 ONEE = np.linspace(0.01, 10, 1000) # 1ω energy array
2
3 # The prefactor,  $\omega^2/2\epsilon_0c^3 \cos^2 \theta_0$ 
4 PREFACCTOR = (ONEE**2)/(2*EPS0*HBAR**2 * LSPEED**3 * math.cos(THETA0)**2)
5
6 nl = np.sqrt(epsl1w) # The index of refraction,  $n_\ell = \sqrt{\epsilon_\ell(\omega)}$ 
7 Nl = np.sqrt(epsl2w) # The index of refraction,  $N_\ell = \sqrt{\epsilon_\ell(2\omega)}$ 
8
9 # The wave vectors,  $w_\ell = \sqrt{\epsilon_\ell(\omega) - \sin^2 \theta_0}$ , etc.
10 wb1w = np.sqrt(epsb1w - (math.sin(THETA0)**2))
11 wb2w = np.sqrt(epsb2w - (math.sin(THETA0)**2))
12 wl1w = np.sqrt(epsl1w - (math.sin(THETA0)**2))
13 wl2w = np.sqrt(epsl2w - (math.sin(THETA0)**2))
14
15 # The Fresnel factors,  $r_s^{lb} = (w_\ell - w_b)/(w_\ell + w_b)$ , etc.
16 tvls = (2*math.cos(THETA0))/(math.cos(THETA0) + wl1w)
17 Tvlp = (2*math.cos(THETA0)*Nl)/(math.cos(THETA0)*epsl2w + wl2w)
18 rvlps = (math.cos(THETA0) - wl1w)/(math.cos(THETA0) + wl1w)
19 rlbs = (wl1w - wb1w)/(wl1w + wb1w)
20 Rvlp = (math.cos(THETA0)*epsl2w - wl2w)/(math.cos(THETA0)*epsl2w + wl2w)
21 Rlbp = (wl2w*epsb2w - wb2w*epsl2w)/(wl2w*epsb2w + wb2w*epsl2w)
22
23 #  $\delta = 8\pi(d/\lambda_0)W_\ell$ ,  $\varphi = 4\pi(d/\lambda_0)w_\ell$ 
24 delta = 8*math.pi*((ONEE*THICKNESS*1e-9)/(PLANCK*LSPEED))*wl2w
25 varphi = 4*math.pi*((ONEE*THICKNESS*1e-9)/(PLANCK*LSPEED))*wl1w
26
27 #  $r_s^M = (r_s^{lb} e^{i\varphi})/(1 + r_s^{v\ell} r_s^{lb} e^{i\varphi})$ , etc.
28 rmS = ((rlbs*np.exp(1j*varphi))/(1 + rvlps*rlbs*np.exp(1j * varphi)))
29 RMpav = (Rlbp*np.exp(1j*delta/2)*(2/delta)*np.sin(delta/2))* \
30           (1 + Rvlp*Rlbp*np.exp(1j*delta))**-1
31 rMplus = 1 + rmS
32 RMplusP = 1 + RMpav
33 RMminusP = 1 - RMpav
34
35 #  $\Gamma_{sP} = (T_p^{v\ell}/N_\ell) (t_s^{v\ell} r_s^{M+})^2$ 
36 GammasP = (Tvlp/Nl)*(tvls*rMplus)**2
37
38 #  $r_{sP} = -R_p^{M-} W_\ell \sin^2 \phi \cos \phi \chi^{xxx} + R_p^{M-} W_\ell 2 \sin \phi \cos^2 \phi \chi^{xyy} - \dots$ 
39 rsP = - (RMminusP*wl2w*math.sin(PHI)**2*math.cos(PHI) * XXX) \
40       + (RMminusP*wl2w*2*math.sin(PHI)*math.cos(PHI)**2 * XXY) \
41       - (RMminusP*wl2w*math.cos(PHI)**3 * XYY) \
42       - (RMminusP*wl2w*math.sin(PHI)**3 * YXX) \
43       + (RMminusP*wl2w*2*math.sin(PHI)**2*math.cos(PHI) * YYX) \
44       - (RMminusP*wl2w*math.sin(PHI)*math.cos(PHI)**2 * YYY) \
45       + (RMplusP*math.sin(THETA0)*math.sin(PHI)**2 * ZXX) \
46       - (RMplusP*math.sin(THETA0)*2*math.sin(PHI)*math.cos(PHI) * ZXY) \
47       + (RMplusP*math.sin(THETA0)*math.cos(PHI)**2 * ZYY)
48
49 #  $\mathcal{R}_{sP} = (\omega^2/2\epsilon_0c^3 \cos^2 \theta_0) |n_\ell^{-1} \Gamma_{sP} r_{sP}|^2$ 
50 RsP = PREFACCTOR * np.absolute((1/nl) * GammasP * rsP)**2

```

Figure 1.3: A simplified example of using Python code to calculate  $\mathcal{R}_{sP}$ .

# Chapter 2

# Results

## Outline

---

2.1	Results for the Si(001)(2×1) surface . . . . .	19
2.1.1	Calculating $\chi^{xxx}$ . . . . .	20
2.1.1.1	Full-slab results . . . . .	21
2.1.1.2	Half-slab vs full-slab . . . . .	22
2.1.1.3	Half-slab results . . . . .	24
2.1.2	Overview of the calculated $\mathcal{R}$ spectra . . . . .	25
2.2	Results for the Si(111)(1×1):H surface . . . . .	26
2.2.1	Calculating $\chi^{xxx}$ . . . . .	28
2.2.2	Comparing the theoretical $\mathcal{R}$ to experiment . . . . .	30
2.2.2.1	Overview of the calculated $\mathcal{R}$ spectra . . . . .	30
2.2.2.2	$\mathcal{R}_{pP}$ ( $p$ -in, $P$ -out) . . . . .	31
2.2.2.3	Calculated $\mathcal{R}_{pP}$ compared to experiment . . . . .	34
2.2.2.4	Calculated $\mathcal{R}_{sP}$ compared to experiment . . . . .	37
2.2.2.5	Calculated $\mathcal{R}_{pS}$ compared to experiment . . . . .	38

---

In this chapter, we will review the results for the calculation of the nonlinear susceptibility,  $\chi$ , and the SSHG yield,  $\mathcal{R}_{iF}$ , for the the Si(001)(2×1) and the Si(111)(1×1):H surfaces. These results are the direct product of all the theory derived in Chapters ?? and 1. These example surfaces provide the perfect testbed for the theory developed in this work, and the resulting spectra yield insight into the various key aspects of the theory.

The first part focuses on using the Si(001)(2×1) surface to review and compare the enhancements that we have added to the framework for calculating  $\chi$ . This surface is presented in a special configuration that allows us to test each improvement made on the theory; namely, the use of the cut function for extracting the surface susceptibility, the effect of the scissors operator, and the addition of  $\mathcal{V}^{\text{nl}}$ . I will also present a very brief overview of the calculated SSHG yield, but with no comparison to experimental data as there is very little available for this surface.

The second part features the Si(111)(1×1):H, which is experimentally well-characterized, and thus provides an excellent platform with which to test our robust formulation for the SSHG yield. We will first compare the calculated  $\chi^{xxx}$  component with experimental data from Ref. [12]. This will provide a nice confirmation of everything we learned from the Si(001)(2×1) surface. We will then review the calculated spectra for different polarization cases of the incoming fields, and compare them to experimental data from Refs. [13, 14, 15], over a wide energy range covering both the E<sub>1</sub> and E<sub>2</sub> critical point transitions for bulk Si. We will find that this new formalism, that is developed from the 3-layer model and includes the effect of multiple reflections in the material, compares quite favorably with the experimental data. The quality of these calculations affords us some insight into how the SSHG spectrum can be affected by several physical factors.

## 2.1 Results for the Si(001)(2×1) surface

In this section, let us review the characteristics of the Si(001)(2×1) surface we will be using for the subsequent calculations. This surface provides an excellent test case to check the consistency of our approach for calculating  $\chi$  with the new elements described in Chap. ???. For this, I have selected a clean Si(001) surface with a 2×1 surface reconstruction. The slab for such a surface could be made centrosymmetric by creating the front and back surfaces with the same 2×1 reconstruction. However, this particular slab has the lower surface terminated with hydrogen, producing a terminated, “ideal” bulk Si surface. The H atoms saturate the dangling bonds of the bulk-like Si atoms at the surface, as seen in Fig. 2.1. Consider the  $z$  coordinate pointing out of the surface with the  $x$  coordinate along the crystallographic [011] direction, parallel to the dimers.

The self-consistent ground state and the Kohn-Sham states were calculated in the DFT-LDA framework using the plane-wave ABINIT code [16, 17], using Troullier-Martins pseudopotentials [18] that are fully separable nonlocal pseudopotentials in the Kleinman-Bylander form [19]. The contribution of  $\mathbf{v}^{\text{nl}}$  and  $\mathcal{V}^{\text{nl}}$  to Eq. (??) was carried out using the DP code [20].

The surface was studied with the experimental lattice constant of 5.43 Å. Structural optimizations were also performed with the ABINIT code. The geometry optimization was carried out in slabs of 12 atomic layers, where the central four layers were fixed at the bulk positions. The structures were relaxed until the Cartesian force components were less than 5 meV/Å. The geometry optimization for the clean surface gives a dimer buckling of 0.721 Å, and a dimer length of 2.301 Å. For the dihydride surface, the obtained Si-H bond distance was 1.48 Å. These results are in good agreement with previous theoretical studies [21, 6]. The vacuum size is equivalent to one quarter the size of the slab, avoiding the effects produced by possible wave-function tunneling from the contiguous surfaces of the full crystal formed by the repeated super-cell scheme [6].

Spin-orbit, local field, and electron-hole attraction [22] effects on the SHG process are all neglected. Although these are important factors in the optical response of a semiconductor, their efficient calculation is still theoretically and numerically challenging and under debate. This merits further study but is beyond the scope of this thesis. For a given slab size, I found the converged spectra to obtain the relevant parameters. The most important of these are: an energy cutoff of 10 Ha for the 16, 24, and 32 layered slabs and 13 Ha for the 40 layer slab, an equal number of conduction and valence bands, and a set of 244  $\mathbf{k}$  points in the irreducible Brillouin zone, which are equivalent to 1058  $\mathbf{k}$  points when disregarding symmetry relations. The  $\mathbf{k}$  points are used for the linear analytic tetrahedron method for evaluating the 3D Brillouin Zone (BZ) integrals, where special care was taken to examine the double resonances of Eq. (??) [23]. Note that the Brillouin

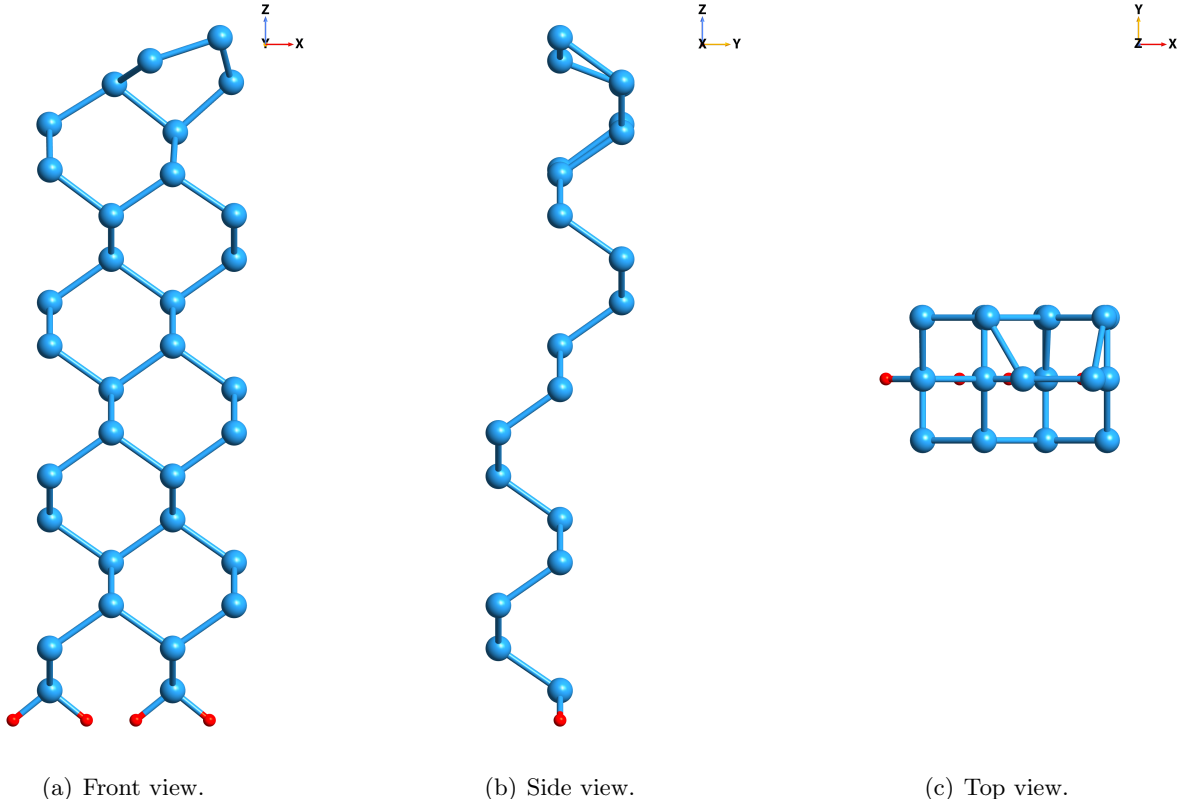


Figure 2.1: Several views of the slab used to represent the Si(001)(2×1) surface. This particular slab has 16 Si atomic layers (large blue balls) with two H atomic layers (small red balls).

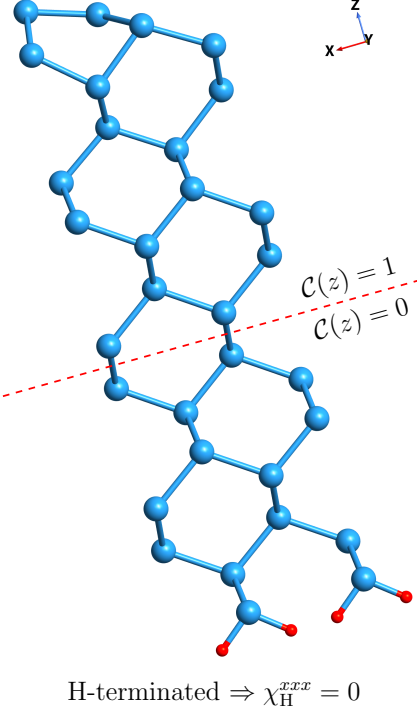
zone for the slab geometry collapses to a 2D-zone, with only one  $\mathbf{k}$ -point along the  $z$ -axis.

$T_{nm}^{ab} = (i/\hbar)[r^b, v^{nl,a}]_{nm}$  must be evaluated in order to obtain Eqs. (??) and (??) that are required for Eq. (??). Computing second-order derivatives is necessary, making the numerical procedure very time consuming. This adds significantly to the already lengthy time needed for the calculation of the  $\mathbf{v}^{nl}$  contribution that is proportional only to the first-order derivatives. Memory requirements are also greatly increased for both  $\mathbf{v}^{nl}$  and  $[r, \mathbf{v}^{nl}]$ . However, the contribution from  $[r, \mathbf{v}^{nl}]$  is very small [24] and it is therefore neglected in this work.

### 2.1.1 Calculating $\chi^{xxx}$

The idea behind the special slab configuration, pictured in Fig. 2.2, is that the crystalline symmetry of the H terminated surface imposes that  $\chi_H^{xxx} = 0$ . The  $2 \times 1$  surface has no such restrictions, so naturally  $\chi_{2 \times 1}^{xxx} \neq 0$ . This is due to the fact that along the  $y$  direction there is a mirror plane for the H-saturated surface (causing centrosymmetry), whereas for the  $2 \times 1$  surface this mirror is lost as the dimers are asymmetric along  $x$ . Thus, calculating  $\chi^{xxx}$  for the full-slab, or the upper half-slab containing the  $2 \times 1$  surface [25] should yield the same result, since the contribution from the H saturated surface is zero regardless. The following relationship must be satisfied for this particular

$2\times 1$  reconstruction  $\Rightarrow \chi_{2\times 1}^{xxx} \neq 0$



H-terminated  $\Rightarrow \chi_H^{xxx} = 0$

Figure 2.2: The slab for the Si(001)( $2\times 1$ ) surface. The front (upper) surface is in a  $2\times 1$ , clean reconstruction, and the rear (lower) surfaces is H-terminated, with “ideal” bulk-like atomic positions. The dangling bonds are H-saturated.

slab,

$$\chi_{\text{half-slab}}^{xxx} = \chi_{\text{full-slab}}^{xxx},$$

where  $\chi_{\text{half-slab}}^{xxx}$  is calculated using  $\mathcal{C}(z) = 1$  for the upper half containing the  $2\times 1$  surface reconstruction (see Fig. 2.2), and  $\chi_{\text{full-slab}}^{xxx}$  is calculated using  $\mathcal{C}(z) = 1$  for the entire slab. Again, the dihydride surface on the lower half of the slab must have  $\chi_{\text{half-slab}}^{xxx} = 0$ .

Note that all spectra for  $\chi^{xxx}$  presented in this section were calculated with a Gaussian broadening of 0.15 eV.

### 2.1.1.1 Full-slab results

Fig. 2.3 shows  $|\chi_{\text{full-slab}}^{xxx}|$  for the slab with 16, 24, 32, and 40 Si atomic layers, without the contribution of  $\mathbf{v}^{\text{nl}}$ , and with no scissors correction. Since the clean Si(001) surface is in a  $2\times 1$  reconstruction there are two atoms per atomic layer. Thus, the total number of atoms per slab is twice the number of atomic layers of the slab. The slabs were extended in the  $z$  directions in steps of 8 layers of bulk-like atomic positions. Note that the response differs substantially for 16 and 24 layers but is quite similar for 32 and 40 layers. As explained above, the calculation of the  $\mathbf{v}^{\text{nl}}$  contribution is computationally expensive, so it is crucial to minimize the number of atoms in the calculation. I consider a slab with 32 Si atomic layers as a good compromise between the

convergence of  $\chi_{\text{full-slab}}^{xxx}$  as a function of the number of layers in the slab, and the computational expense.

### 2.1.1.2 Half-slab vs full-slab

Now that we have established an adequate number of layers to attain convergence, we can proceed to study the spectra produced from the slab with 32 atomic layers. Fig. 2.4 presents a comparison between  $\chi_{\text{half-slab}}^{xxx}$  and  $\chi_{\text{full-slab}}^{xxx}$  for four different scenarios: with and without the effects of  $\mathbf{v}^{\text{nl}}$ , and with two values for the scissors correction,  $\hbar\Delta$ . I have chosen a scissors value of  $\hbar\Delta = 0.5$  eV, that is the GW gap reported in Refs. [26, 27]. This is justified by the fact that the surface states from the clean  $2\times 1$  surface are rigidly shifted and maintain their dispersion relation with respect to the LDA value, according to the GW calculations of Ref. [26].

We can appreciate that the difference between the half-slab and full-slab responses is quite small for all four scenarios. Indeed, when the value  $|\chi^{xxx}|$  is large, the difference between the two is quite small; when  $|\chi^{xxx}|$  is small, the difference increases slightly but the spectra is so close to zero that it is negligible. Of course, the difference between the two would decrease as the number of atomic layers increases. Note how 32 layers in the slab is more than enough to confirm that the extraction of the surface second-harmonic susceptibility from the  $2\times 1$  surface is readily possible using the formalism contained in Eq. (??). Calculating the response from the lower half of the slab substantiates that  $|\chi_{\text{half-slab}}^{xxx}| \approx 0$  for the dihydride surface (not shown).

This confirms the validity of the theory developed in ?? and is an important result of this work. Through the proposed layer formalism, we can calculate the surface  $\chi^{\text{abc}}$  component including the contribution from the nonlocal part of the pseudopotentials, and part of the many-body effects through the scissors correction. Therefore, this scheme is robust and versatile and should work for any crystalline surface.

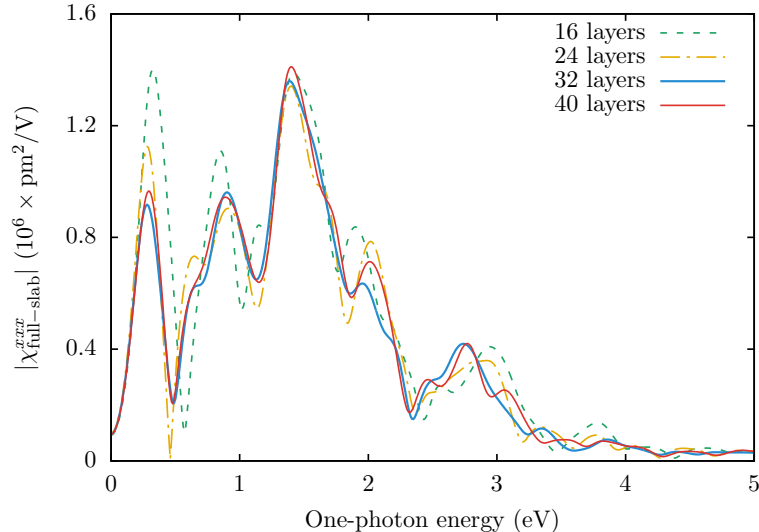


Figure 2.3:  $|\chi_{\text{full-slab}}^{xxx}|$  vs  $\hbar\omega$  for the slab with 16, 24, 32, and 40 atomic Si layers. Adequate convergence is achieved after 32 layers. The spectra presented here do not include the contribution from  $\mathbf{v}^{\text{nl}}$ , with a scissors value of  $\hbar\Delta = 0$  eV.

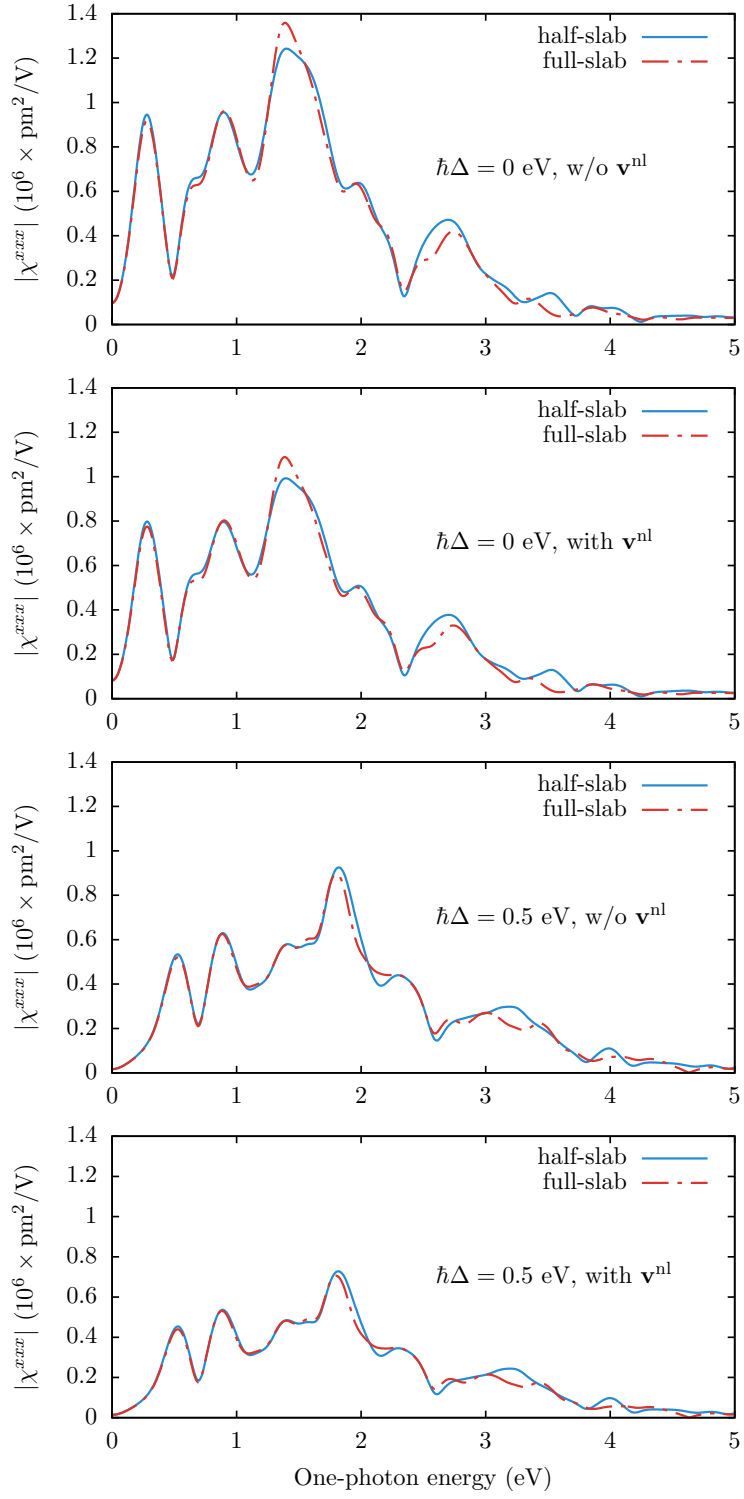


Figure 2.4:  $\chi_{\text{half-slab}}^{xxx}$  and  $\chi_{\text{full-slab}}^{xxx}$  vs  $\hbar\omega$  for four different combinations: with and without the effects of  $\mathbf{v}^{\text{nl}}$ , and with two values for the scissors correction,  $\hbar\Delta$ .

### 2.1.1.3 Half-slab results

I proceed to explain some of the features seen in  $|\chi_{\text{half-slab}}^{xxx}|$  that is obtained when setting  $\mathcal{C}(z) = 1$  for the upper half containing the  $2 \times 1$  surface reconstruction, as seen in Fig. 2.2. From Fig. 2.4, we note a series of resonances that derive from the  $1\omega$  and  $2\omega$  terms in Eq. (??). Notice that the  $2\omega$  resonances start below  $E_g/2$ , where  $E_g$  is the band gap (0.53 eV for LDA, and 1.03 eV if the scissor is used with  $\hbar\Delta = 0.5$  eV). These resonances come from the electronic states of the  $2 \times 1$  surface, that lie inside the bulk band gap of Si and are the well known electronic surface states [26].

Fig. 2.5 shows that the inclusion of  $\mathbf{v}^{\text{nl}}$  reduces the value of  $|\chi_{\text{half-slab}}^{xxx}|$  by 15-20%. This demonstrates the importance of this contribution for a fully correct SSHG calculation. This is in agreement with the analysis for bulk semiconductors [28]. However, the inclusion of  $\mathbf{v}^{\text{nl}}$  does not change the spectral shape of  $|\chi_{\text{half-slab}}^{xxx}|$ . We can confirm that this is not unique for this specific scissors shift, as we can appreciate from the upper two panels of Fig. 2.4, with  $\hbar\Delta = 0$  eV.

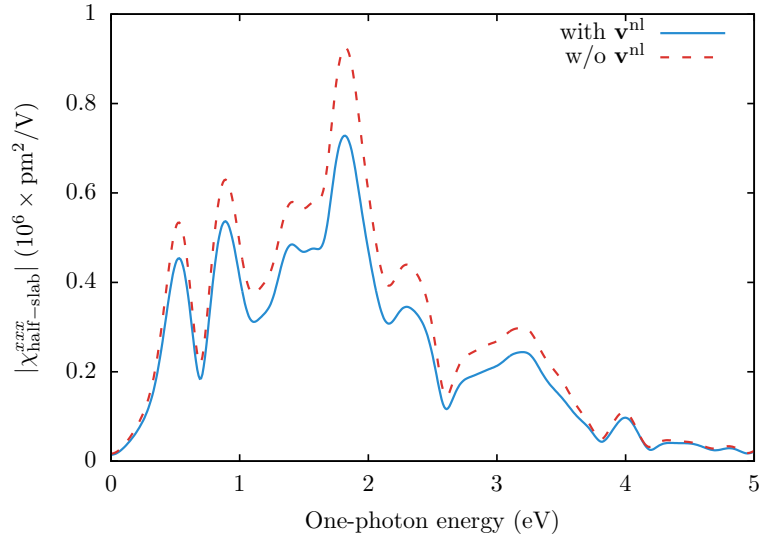


Figure 2.5:  $\chi_{\text{half-slab}}^{xxx}$  vs  $\hbar\omega$ , with and without the contribution from  $\mathbf{v}^{\text{nl}}$ . This spectrum has a scissors value of  $\hbar\Delta = 0.5$  eV.

To demonstrate the effect of the scissors correction, I considered two different finite values for  $\hbar\Delta$ . The first, with a value of  $\hbar\Delta = 0.5$  eV that is used in the previous results, is the “average” GW gap taken from Ref. [26] that is in agreement with Ref. [27]. The second, with a value of  $\hbar\Delta = 0.63$  eV is the “average” gap taken from Ref. [29], where more  $\mathbf{k}$  points in the Brillouin zone were used to calculate the GW value. Fig. 2.6 shows that the scissors correction shifts the spectra from its LDA value to higher energies, as expected. However, contrary to the case of linear optics [30], the shift introduced by the scissors correction is not rigid, which is consistent with the work of Ref. [23]. This is because the second-harmonic optical response mixes  $1\omega$  and  $2\omega$  transitions (see Eq. (??)), and accounts for the non-rigid shift. The reduction of the spectral strength is in agreement with previous calculations for bulk systems [23, 31, 32].

When comparing  $|\chi_{\text{half-slab}}^{xxx}|$  for the two finite values of  $\hbar\Delta$ , it is clear that the first two peaks are almost rigidly shifted with a small difference in height while the rest of the peaks are modified substantially. This behavior comes from the fact that the first two peaks are almost exclusively

related to the  $2\omega$  resonances of Eq. (??). The other peaks are a combination of  $1\omega$  and  $2\omega$  resonances and yield a more varied spectrum. Note that for large-gap materials the  $1\omega$  and  $2\omega$  resonances would be split, producing a small interference effect. The  $2\omega$  resonances would still strongly depend on the surface states. Thus, small changes in the scissors shift can affect the SSH susceptibility spectrum quite dramatically. In Ref. [33], the authors already noted that the nonlinear optical response of bulk materials is more influenced by the electronic structure of the material than the linear case. For the case of semiconductor surfaces, the problem is even more intricate due to the presence of electronic surface states.

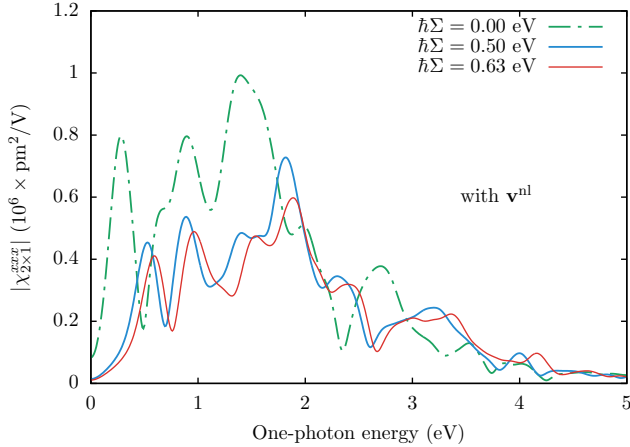


Figure 2.6:  $\chi_{\text{half-slab}}^{xxx}$  vs  $\hbar\omega$  for a slab with 32 atomic Si layers plus one H layer, for three different values of the scissors correction,  $\hbar\Delta$ .

The high sensitivity of SSHG to the energy position of surface states, as seen in Fig. 2.6, makes SSHG a good benchmark tool for spectroscopically testing the validity of the inclusion of many-body effects, and in particular the quasi-particle correction to the electronic states. Although local fields are neglected, in principle they should be quite small parallel to the interface as the electric field is continuous.  $\chi^{xxx}$  should have a relatively small influence from these local fields. Excitonic effects should also be explored, but their efficient calculation is theoretically and numerically challenging [22] and far beyond the scope of this work. Unfortunately the experimental measurement of the  $\chi^{xxx}$  component is difficult as the SH radiated intensity would be proportional not only to this component but also to the other components of  $\chi$ . However, I will present this exact comparison later on in Sec. 2.2.1 for the Si(111)(1×1):H surface.

### 2.1.2 Overview of the calculated $\mathcal{R}$ spectra

In Figs. 2.7 and 2.8, I present the results for the calculation of the SSHG yield for our test surface. The  $2\times 1$  surface reconstruction yields a Class 1, primitive triclinic system with all 18 components independent from each other [11]. We cannot take advantage of any symmetry relations for this surface. However, this is no problem for the robust formulation we derived in Chapter 1 that can accommodate all 18 components disregarding any surface symmetries. Calculating all 18 components is obviously more time consuming, but they can be efficiently parallelized so very little time is actually lost.

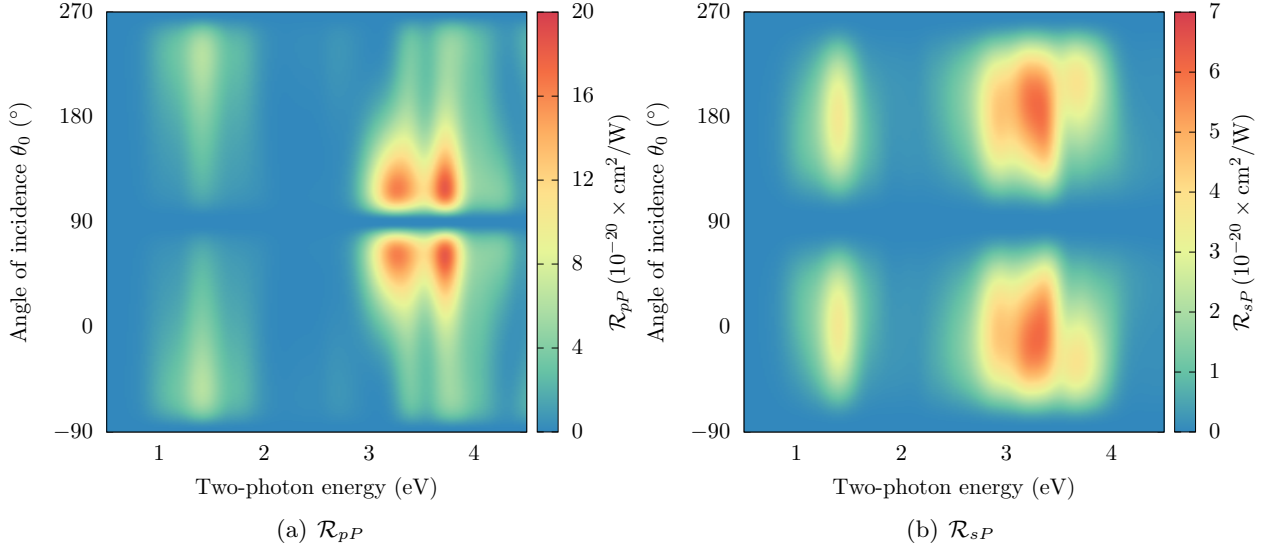


Figure 2.7:  $\mathcal{R}$  for outgoing  $P$  polarization, versus the angle of incidence ( $\theta_0$ ) for the Si(001)(2×1) surface. The scissor shift used was  $\hbar\Delta = 0.5$  eV. Both figures consider an azimuthal angle of  $\phi = 45^\circ$ . All curves are broadened with  $\sigma = 0.10$  eV.

Fig. 2.7 presents the results for the SSHG yield with outgoing  $P$  polarization. I set a fixed azimuthal angle of  $\phi = 45^\circ$  and then varied the incoming angle  $\theta_0$  from  $-90^\circ$  to  $270^\circ$ . We can clearly see that the surface states associated with the  $2\times 1$  reconstruction produce significant intensity between 1-2 eV in the two-photon energy range. This is consistent with the findings presented in the previous section and in Ref. [34]. The intensity of the peak related to the surface states is significantly lower than the peaks produced in the 2.5-4 eV two-photon energy range. Overall peak intensity is quite high for this surface, which is consistent as it is highly non-centrosymmetric. The spectrum for  $\mathcal{R}_{pP}$  is very consistent with other calculations of this type [35], and even with some limited experimental data [36].

Fig. 2.8 presents the results for the SSHG yield with outgoing  $S$  polarization. They are quite similar to what we observed in Fig. 2.7, with a peak related to the surface states between 1-2 eV, and a larger set of peaks between 2.4-4 eV in the two-photon energy range. These spectra have a clear maxima around  $\theta_0 = 0^\circ$  and  $\theta_0 = 180^\circ$ .

These plots are presented for mainly illustrative purposes, as there is little experimental data to compare with the theoretical spectrum. However, these kinds of plots will be quite useful to the experimentalist interested in this kind of spectroscopy. Excellent intensity for all polarization cases can be obtained for small beam angles, such as  $\theta_0 = 30^\circ$ .

## 2.2 Results for the Si(111)(1×1):H surface

We will now focus our attention on the Si(111)(1×1):H surface. This surface is a  $C_{3v}$ , primitive hexagonal system with only 4 nonzero components independent from each other, as shown in Table 1.2 [11, 10, 4]. It is composed of stacked layers with one Si atom each, with one H atom

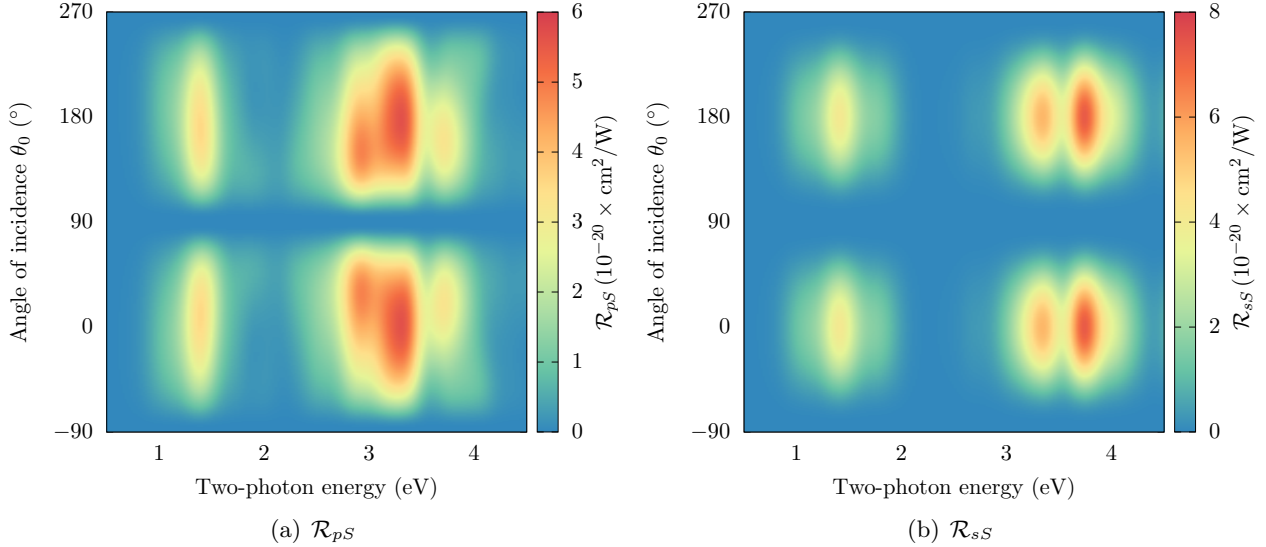


Figure 2.8:  $\mathcal{R}$  for outgoing  $S$  polarized fields, versus the angle of incidence ( $\theta_0$ ) for the Si(001)( $2 \times 1$ ) surface. The scissor shift used was  $\hbar\Delta = 0.5$  eV. Both figures consider an azimuthal angle of  $\phi = 45^\circ$ . All curves are broadened with  $\sigma = 0.10$  eV.

terminating each surface. The added H saturates the surface Si dangling bonds and eliminates any surface-related electronic states in the band gap. Here, the top and bottom surfaces are mirror images (see Fig. 2.9); this provides the centrosymmetry that necessitates the use of the cut function to extract the nonzero surface response. In Sec. 2.2.1 we will compare the spectrum produced by using relaxed and unrelaxed coordinates, so it is worth reviewing this concept here. The specifics of this process are as follows.

The relaxation process was done by my colleague, Nicolas Tancogne-Dejean [35]. The structure was initially constructed with the experimental lattice constant of 5.43 Å, and then performed structural optimizations with the ABINIT [16, 17] code. It was then relaxed until the Cartesian force components were less than 5 meV/Å, yielding a final Si-H bond distance of 1.50 Å. The energy cutoff used was 20 Ha, and Troullier-Martin LDA pseudopotentials were used [18]. The resulting atomic positions are in good agreement with previous theoretical studies [37, 38, 39, 40, 14], as well as the experimental value for the Si-H distance [41].

I also evaluated the number of layers required for convergence (like Sec. 2.1.1.1) and settled on a slab with 48 atomic Si planes. The geometric optimizations mentioned above are therefore carried out on slabs of 48 atomic layers without fixing any atoms to the bulk positions. Fig. 2.9 depicts a sample slab with 16 layers of Si. The surface susceptibilities must be extracted from only half of the slab. This encompasses 24 layers of Si and the single layer of H that terminates the top surface. The vacuum size is equivalent to one quarter the size of the slab, avoiding the effects produced by possible wave-function tunneling from the contiguous surfaces of the full crystal formed by the repeated super-cell scheme [6].

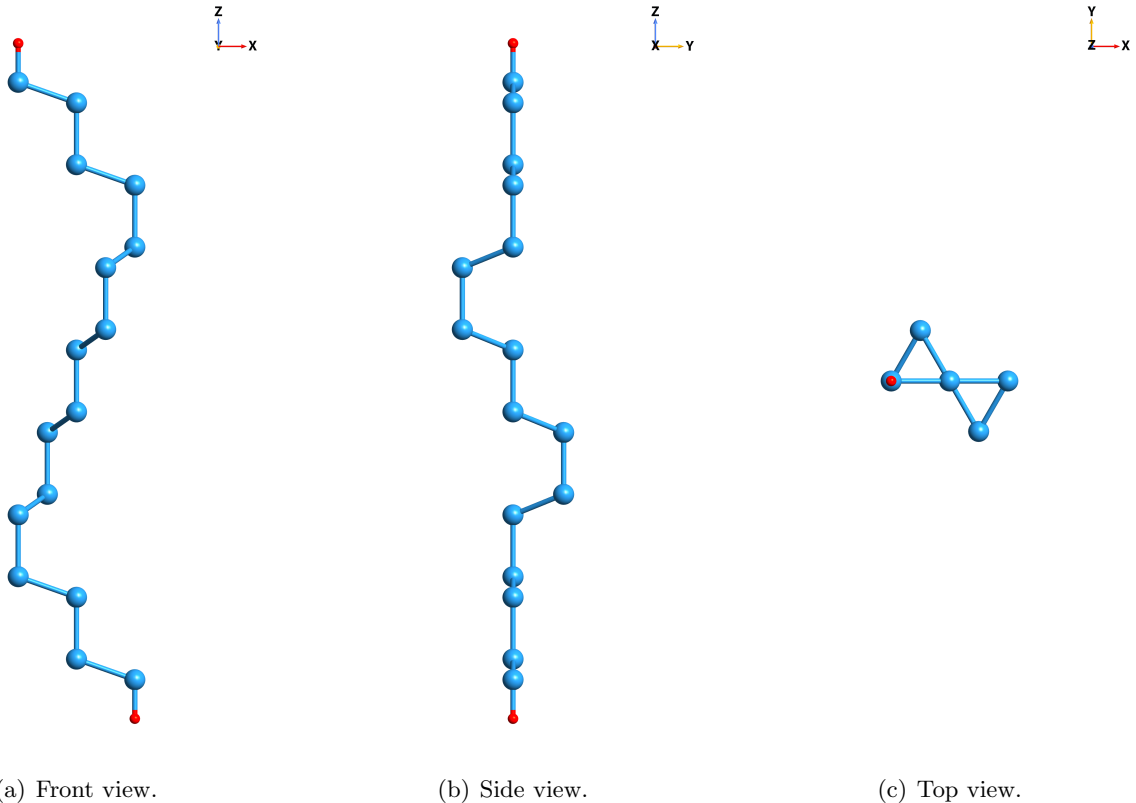


Figure 2.9: Several views of the slab used to represent the Si(111)(1×1):H surface. This particular slab has 16 Si atomic layers (large blue balls) with two H atomic layers (small red balls).

The electronic wave-functions,  $\psi_{n\mathbf{k}}(\mathbf{r})$ , were also calculated with the ABINIT code using a planewave basis set with an energy cutoff of 15 Hartrees.  $\chi^{abc}$  was properly converged with 576  $\mathbf{k}$  points in the irreducible Brillouin zone, which are equivalent to 1250  $\mathbf{k}$  points when disregarding symmetry relations. The contribution of  $\mathcal{V}^{nl}$  in Eq. (??) was carried out using the DP[20] code with a basis set of 3000 planewaves. Convergence for the number of bands was achieved at 200, which includes 97 occupied bands and 103 unoccupied bands.

All spectra were produced using a scissors value of 0.7 eV in the  $\chi^{abc}$  and  $\epsilon_\ell(\omega)$  calculations. This value was obtained from Ref. [42], in which the authors carry out a  $G_0W_0$  calculation on this surface for increasing numbers of layers. They calculated the LDA and  $G_0W_0$  band gaps, and found that the difference between the two tends towards  $\sim 0.7$  eV as more layers are added, culminating in a value of 0.68 eV for bulk Si. This calculation is completely *ab-initio*, so I consider 0.7 eV to be a very reasonable value for the scissors correction.

### 2.2.1 Calculating $\chi^{xxx}$

The pioneering work presented in Ref. [14] showed the effect of artificially moving the atomic position on the resulting SSHG spectra. In this section, I will address the more practical and relevant case of atomic relaxation. More precisely, I compare the fully relaxed structure described

above with an unrelaxed structure where all the Si atoms are at the ideal bulk positions. Note that in both cases, the Si-H bond distance is the same 1.5 Å. The unrelaxed coordinates use the same parameters mentioned above. Fortunately, there exists experimental data that can be compared to the calculated  $\chi^{xxx}$  for this surface, taken from Ref. [12]. This data provides an excellent point of comparison as it was presented in absolute units and was measured at a very low temperature of 80 K.

Fig. 2.10 depicts the spectra from the relaxed and unrelaxed coordinates compared to experiment. The theoretical curves were calculated with a scissors shift of  $\hbar\Delta = 0.7$  eV, as mentioned in the previous section. The relaxed coordinates have a peak position that is very slightly blueshifted with respect to the experimental peak near 1.7 eV. In contrast, the unrelaxed coordinates have a peak that is redshifted close to 0.05 eV from experiment. There is also a feature between 1.5 eV and 1.6 eV that appears in the relaxed spectrum that coincides partially with the experimental data. Both theoretical curves have half the intensity of the experimental peak. It is important to note that this data was taken at low temperature (80 K); this further favors the comparison, as the theory neglects the effects of temperature. As is shown in Ref. [12], the peaks in the spectrum redshift as the temperature increases. Intensity for both the relaxed and unrelaxed curves are roughly half the intensity of the experimental spectrum. I have converted the units of the experimental data from CGS to MKS units for easier comparison.

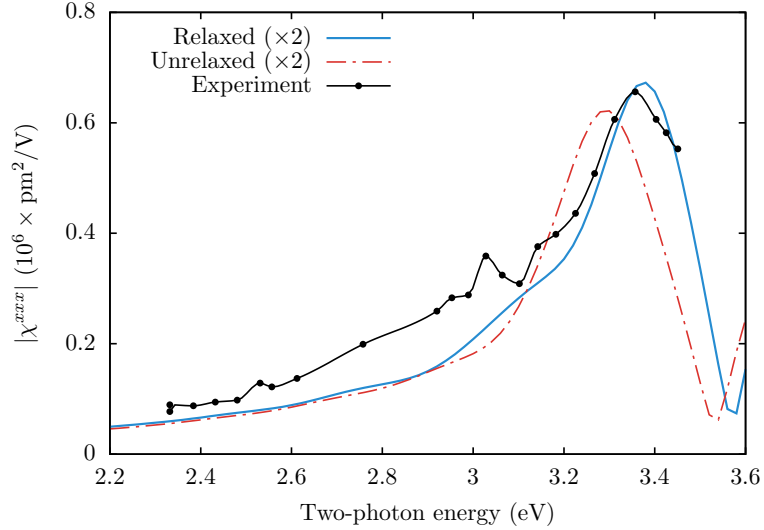


Figure 2.10: Comparison of  $\chi^{xxx}$  calculated using relaxed and unrelaxed atomic positions, with the experimental data presented in Ref. [12]. The theoretical curves were calculated with a scissors shift of  $\hbar\Delta = 0.7$  eV, and are broadened with  $\sigma = 0.075$  eV. Experimental data was taken at 80 K.

We can conclude that the most accurate theoretical results are produced by using relaxed atomic positions for the calculation of  $\chi$ . Although this process can be very time consuming for large numbers of atoms, this should be considered a crucial step. This also further demonstrates that SSHG is very sensitive to the surface atomic positions. In particular, these results show that a correct value of the Si-H bond length is not enough to obtain the most accurate SSHG spectra, and that a full relaxation of the structure is required. Additionally, it seems that the theory may

coincide better with experiments that are conducted under very low temperature conditions.

### 2.2.2 Comparing the theoretical $\mathcal{R}$ to experiment

All calculations presented from this point on were done using the relaxed atomic positions described in the previous section. I will now present the theoretical SSHG yield for the Si(111)(1×1):H surface compared to experiments from Refs. [15, 14, 13]. These comparisons are good benchmarks to test the complete formalism for calculating the SSHG yield.

The method of calculation is as follows. I first calculated  $\varepsilon_b(\omega)$ ,  $\varepsilon_\ell(\omega)$ , and then  $\chi^{abc}$  from Eq. (??). I used these for the Fresnel factors and in Eqs. (1.52), (1.62), and (1.57), and finally, those into Eq. (1.44) to obtain the theoretical SSHG yield for different polarizations that can then be compared with the experimental data. Remember that a scissors shift of  $\hbar\Delta = 0.7$  eV is used for all the  $\chi^{abc}$  components. These were also broadened with a Gaussian broadening of  $\sigma = 0.05$  eV, while the calculated  $\mathcal{R}$  spectra feature a broadening of  $\sigma = 0.10$  eV. These values were selected so that the theoretical calculation best represents the lineshape of the experimental spectrum.

#### 2.2.2.1 Overview of the calculated $\mathcal{R}$ spectra

We will carefully review and compare the calculated  $\mathcal{R}$  for each different polarization case in the following sections. However, I first want to present a general overview of the theoretical SSHG yield, as I did in Sec. 2.1.2. In Figs. 2.11 and 2.12, I present these results over a two-photon energy range of 2.5–5 eV. This range corresponds to the experimental measurements featured in Refs. [14] and [13]. Note that the SSHG yield drops to zero very rapidly before for energy values under 3 eV. This is because of the lack of surface states due to the surface H-saturation.

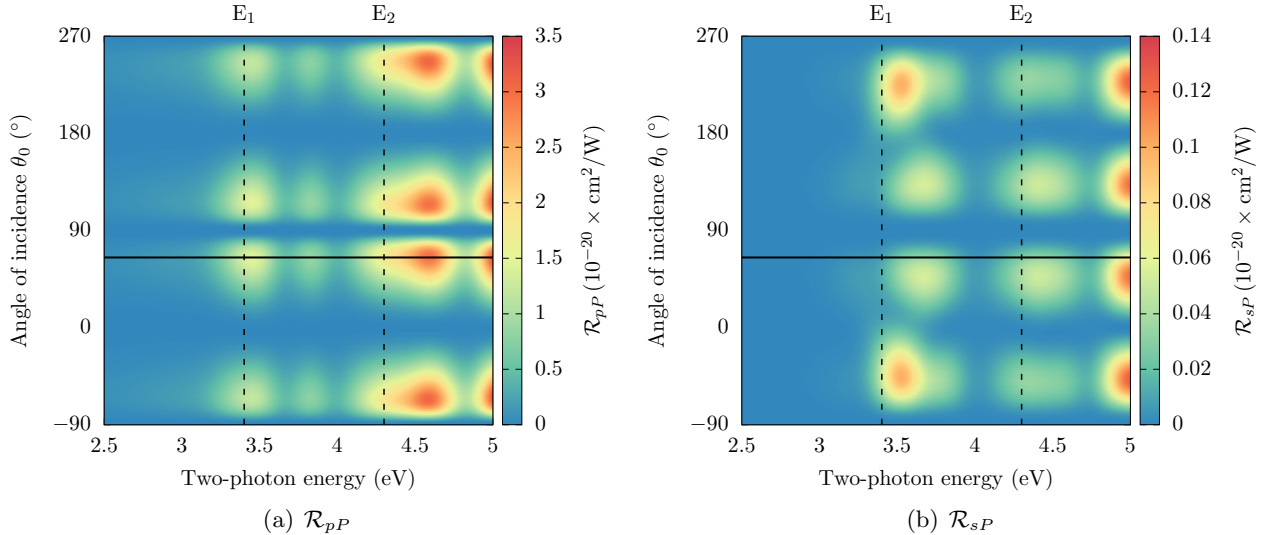


Figure 2.11:  $\mathcal{R}$  for outgoing  $P$  polarization, versus the angle of incidence ( $\theta_0$ ) for the Si(111)(1×1):H surface. A scissors shift of  $\hbar\Delta = 0.7$  eV is applied. The solid line represents  $\theta_0 = 65^\circ$ , and the dotted lines represent the  $E_1$  and  $E_2$  Si critical points. Both figures consider an azimuthal angle of  $\phi = 30^\circ$ . All curves are broadened with  $\sigma = 0.10$  eV.

I have included some helpful markers in these figures. First, the solid black line represents an angle incidence of  $\theta_0 = 65^\circ$ . This is one of two angles that we will consider for the remainder of this chapter; in particular, this is the angle used in the experiment from Ref. Refs. [14]. It is clear that they chose this particular angle to maximize the  $\mathcal{R}_{pP}$  output. Second, the dashed black lines represent the  $E_1 \sim 3.4$  eV and  $E_2 \sim 4.3$  eV critical points of bulk Si [43]. For the outgoing  $P$  polarization in Fig. 2.11, we can see that the calculated SSHG yield does have peaks around those energy values. We will review this in much further detail below.

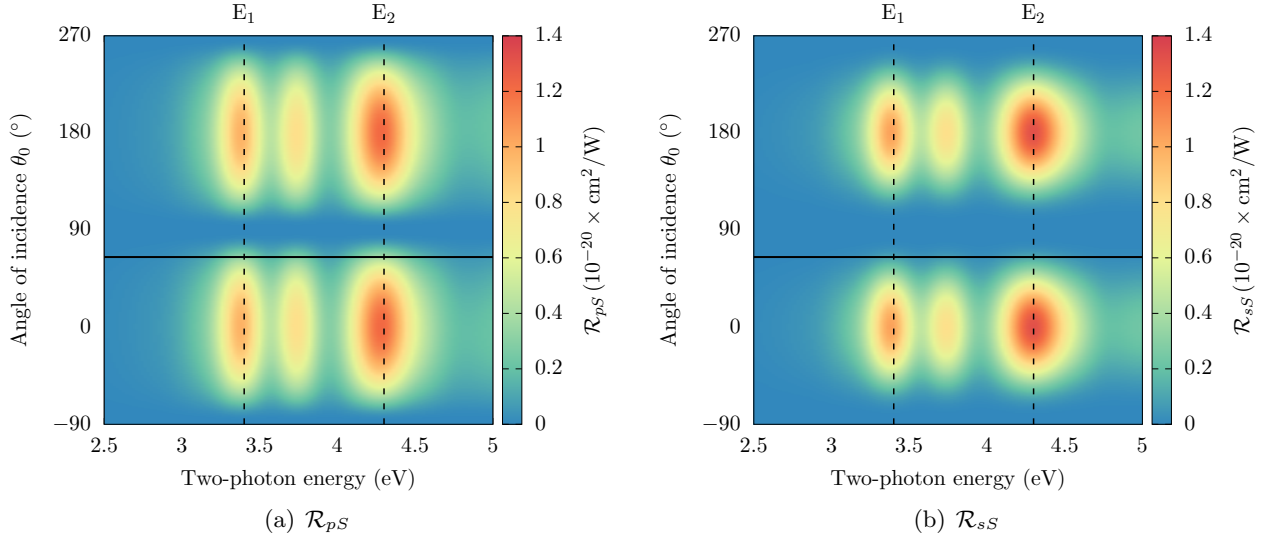


Figure 2.12:  $\mathcal{R}$  for outgoing  $S$  polarized fields, versus the angle of incidence ( $\theta_0$ ) for the Si(111)(1×1):H surface. A scissors shift of  $\hbar\Delta = 0.7$  eV is applied. The solid line represents  $\theta_0 = 65^\circ$ , and the dotted lines represent the  $E_1$  and  $E_2$  Si critical points. Both figures consider an azimuthal angle of  $\phi = 30^\circ$ . All curves are broadened with  $\sigma = 0.10$  eV.

We see similar characteristics, for Fig. 2.12 with the outgoing  $S$  polarization cases. Indeed, the theoretical peak values seem to match quite well with the critical points. Again, we will review these findings in much more detail below. Note that I will omit  $\mathcal{R}_{sS}$  from this point forward, as I do not have any experimental data to compare it with.

### 2.2.2.2 $\mathcal{R}_{pP}$ ( $p$ -in, $P$ -out)

HERE HERE HERE HERE HERE

I think we should first review how the inclusion of multiple reflections affects the produced spectra.

We consider a Si(111)(1×1):H surface as a test case for the three layer model and to study the effects that multiple reflections have on the SSHG radiation. This surface is well characterized experimentally,[15, 14, 13] and there has been success in reproducing these experimental results using the three layer model without multiple reflections.[44] The details of the *ab initio* calculation of  $\chi^{ijk}$  are not needed for the following discussion, and are left for the reader in Ref. [44]. However, we mention that we apply a scissors shift of 0.7 eV to the theoretical spectra. In a first approximation,

this includes the effects of the electronic many-body interactions within the independent particle approach for the *ab initio* calculation. This 0.7 eV value allows the SH resonant peaks to acquire their corresponding energy positions, and is calculated with what is known as a  $G_0W_0$  calculation [44]. We are interested in finding the thickness of the layer  $\ell$  where  $\chi^{ijk} \neq 0$ . For this surface, we found well-converged results for a thickness of  $\sim 5$  nm, that is equivalent to 24 atomic sheets of Si along the (111) direction. As this represents only the upper half of the slab, we find it reasonable to choose the thickness of the layer  $\ell$  to be between  $d \sim 5 - 10$  nm. This corresponds to a half-slab comprised of 24 to 48 atomic layers to get well-converged values of  $\chi^{ijk}$ .

We begin our comparisons in Fig. 2.13, in which we compare the theoretical results for the SHG radiation with the experimental results from Ref. [14]. The theoretical curves that include multiple reflections are featured with the average value  $\bar{R}_i^M$ , Eq. (1.26), with two values for the total thickness,  $d$ , and Eqs. (1.50) and (1.52). We contrast these with the standard three layer model excluding the effects of multiple reflections from Sec. 1.3.1. We see that the  $E_2$  peak is blueshifted by around 0.3 eV, and the yield does not go to zero after 4.75 eV.  $\mathcal{R}_{pP}$  is by far the most involved calculation out of the four different polarization cases, since it includes all four nonzero components. In particular,  $\chi^{zzz}$  and  $\chi^{xxz}$  include out-of-plane incoming fields. These are affected by local field effects that can change both intensity and peak position.[35] Including these effects is computationally very expensive and is beyond the scope of this paper. We speculate that  $\mathcal{R}_{pP}$  requires the proper inclusion of these effects in order to accurately describe the experimental peaks.

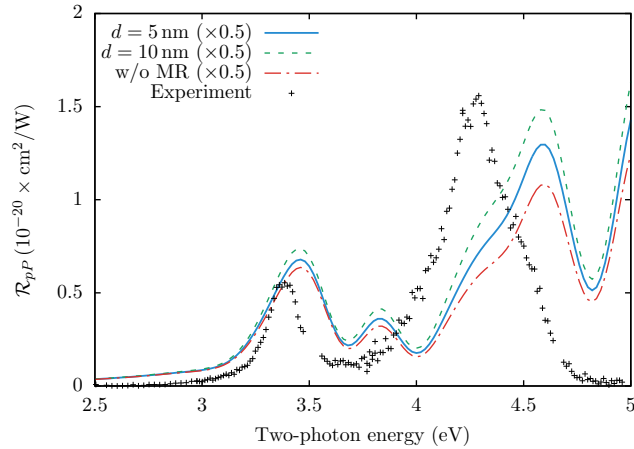


Figure 2.13: Comparison between the three layer model with the effects of multiple reflections for two different values of the total layer thickness  $d$ , with the standard three layer model without the effects of multiple reflections, and the experimental data from Ref. [14]. We take  $\theta = 65^\circ$ ,  $\phi = 30^\circ$ , and a scissors value of  $\hbar\Delta = 0.7$  eV. The  $\chi^{ijk}$  components are broadened with  $\sigma = 0.05$  eV, and then  $\mathcal{R}_{pP}$  is broadened with  $\sigma = 0.10$  eV.

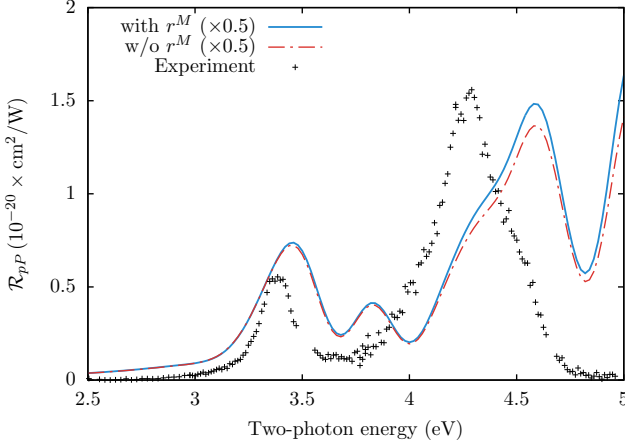


Figure 2.14: Comparison between theoretical models (see Table 1.3) and experiment for  $\mathcal{R}_{pP}$ , for  $\theta = 65^\circ$ , and a scissors value of  $\hbar\Delta = 0.7\text{eV}$ . The  $\chi^{ijk}$  components are broadened with  $\sigma = 0.05\text{eV}$ , and then  $\mathcal{R}_{pP}$  is broadened with  $\sigma = 0.10\text{eV}$ . Experimental data taken from Ref. [15], measured at room temperature.

In Fig. 2.15, we compare the theoretical results for the SSHG yield with the experimental results from Ref. [14]. We mention that the experimental results were produced with an angle of incidence of  $\theta = 65^\circ$ , and an azimuthal angle of  $\phi = 30^\circ$ , which eliminates the contribution from  $\chi^{xxx}$  from Eq. (1.52). First, we note that the experimental spectrum shows two very well defined resonances which come from electronic transitions from the valence to the conduction bands around the well known  $E_1 \sim 3.4\text{ eV}$  and  $E_2 \sim 4.3\text{ eV}$  critical points of Si [43]. As can be seen, the theoretical results reproduce the features of the spectrum, although we see that the  $E_2$  peak is blueshifted by around 0.3 eV. Here we focus on the SSHG yield itself rather than on the physics that lead to such a blueshifted theoretical spectrum. The interested reader can refer to Ref. [44] for those details.

All curves in this figure that include multiple reflections consider  $d = 10\text{ nm}$ . We compare the theoretical SSHG yield for  $d_2 = 0\text{ nm}$  and  $d_2 = 10\text{ nm}$ , with the SSHG yield that neglects multiple reflections. When  $d_2 = 0\text{ nm}$ , we have placed the polarization sheet at the bottom of the layer region. This minimizes the effect of the multiple reflections, and thus the curve is very similar to the three layer model that neglects multiple reflections entirely. When  $d_2 = 10\text{ nm}$ , the polarization sheet is placed at the top of the layer region. This maximizes the effect of the multiple reflections and therefore leads to the largest yield. We also notice that the average value obtained by using  $\bar{R}_i^M$  (Eq. (1.23)) is intermediate between  $d_2 = 0$  and  $d_2 = 10\text{ nm}$ , as expected. This is very similar to selecting  $d_2 = d/2$ , which can be interpreted as placing the nonlinear polarization sheet  $\mathbf{P}(\mathbf{r}, t)$  at the middle of layer  $\ell$ . It is important to remark that these enhancements are larger for  $E_2$  than for  $E_1$ . This can be understood from the fact that the corresponding  $\lambda_0$  for  $E_1$  is larger than that of  $E_2$ . From Eqs. (1.16), (1.17), and (1.27), we see that the phase shifts are larger for  $E_2$  than for  $E_1$ , producing a larger enhancement of the SSHG yield at  $E_2$  from the multiple reflections. As the phase shifts grow with  $d$ , so does the enhancement caused by the multiple reflections. We have verified that the effects of the multiple reflections from the linear field are significantly smaller than those of the SH field. This is clear since the phase shift of Eq. (1.27) is not only a factor of 2

smaller than that of Eqs. (1.16) and (1.17), but also  $w_\ell < W_\ell$ .

From this figure, it becomes evident that the inclusion of multiple reflections is crucial to obtain a better agreement between the theoretical SSHG yield and the experimental spectrum. This is particularly true for larger energies, such as  $E_2$ , as  $\lambda_0$  becomes smaller and the multiple reflection effects become more noticeable. The selected value for  $d \ll \lambda_0$ , that comes naturally from the *ab initio* calculation of  $\chi^{ijk}$  is thus very reasonable in order to model a thin surface layer below the vacuum region where the nonlinear SH conversion takes place.

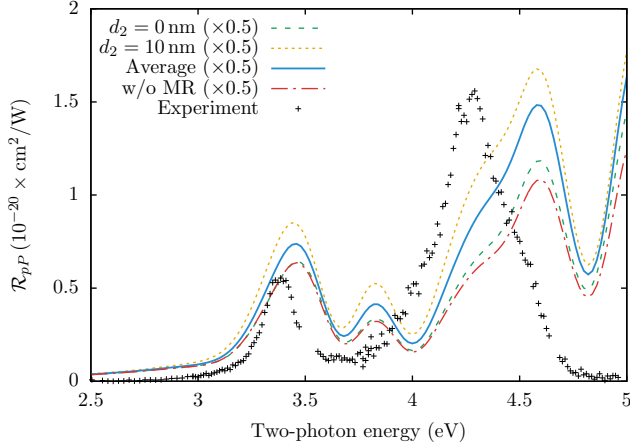


Figure 2.15: Comparison between the three layer model with the effects of multiple reflections for two different values of  $d_2$ , using the average value  $\bar{R}_i^M$  Eq. of Eq. (1.26), the three layer model without the effects of multiple reflections, and the experimental data from Ref. [14]. All curves that include multiple reflections consider a layer  $\ell$  thickness of  $d = 10$  nm.

### 2.2.2.3 Calculated $\mathcal{R}_{pP}$ compared to experiment

I present  $\mathcal{R}_{pP}$  compared to experimental data from Ref. [14] in Fig. 2.16. Note that peak position for the 3-layer model is similar to experiment with the overall intensity being only two times larger. The  $E_2$  peak is blueshifted by around 0.3 eV, and the yield does not go to zero after 4.75 eV. The 2-layer-fresnel model produces a spectrum with peak positions that are close to the experiment, but are 20 times more intense. The calculated  $E_2$  peak is similar, but the  $E_1$  peak lacks the sharpness present in the experiment. The 2-layer-bulk model is almost identical in lineshape to the 3-layer model, but with eight times less intensity.

From Eq. (1.52), it is clear that  $\mathcal{R}_{pP}$  has several  $2\omega$  terms that will change between models; this will have a deep effect on the lineshape. Additionally,  $\Gamma_{pP}^\ell$  also has  $\varepsilon_\ell(2\omega)$  in the denominator, and so we have a significant difference in both lineshape and intensity between the 2-layer-fresnel and the other two models. Again, as in the previous sections for  $\mathcal{R}_{pS}$  and  $\mathcal{R}_{sP}$ , the 3-layer model is the closest in intensity to the experiment. Additionally, Ref. [45] shows that low temperature measurements of  $\mathcal{R}_{pP}$  will blueshift the spectrum away from room temperature measurements such as those shown in Figs. 2.16 and 2.18, and towards the theoretical results.

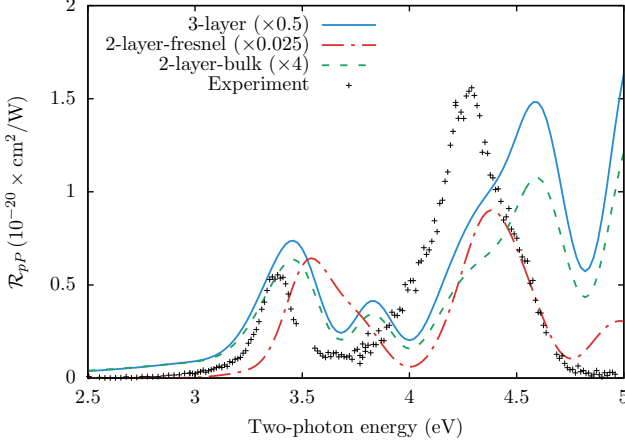


Figure 2.16: Comparison between theoretical models (see Table 1.3) and experiment for  $\mathcal{R}_{pP}$ , for  $\theta = 65^\circ$ , and a scissors value of  $\hbar\Delta = 0.7 \text{ eV}$ . All theoretical curves are broadened with  $\sigma = 0.10 \text{ eV}$ . Experimental data taken from Ref. [14], measured at room temperature.

I'll take this moment to present some auxiliary results from Sec. 1.3 in Fig. 2.17. Refer to Table 1.3 and Sec. 1.3, and note that there are two additional models that we have ignored thus far. The 3-layer-hybrid (Sec. 1.3.5) evaluates  $\mathcal{P}(2\omega)$  in the thin layer  $\ell$  defined by  $\epsilon_{ell}$ , while the fundamental fields are evaluated in the bulk region defined by  $\epsilon_b$ .

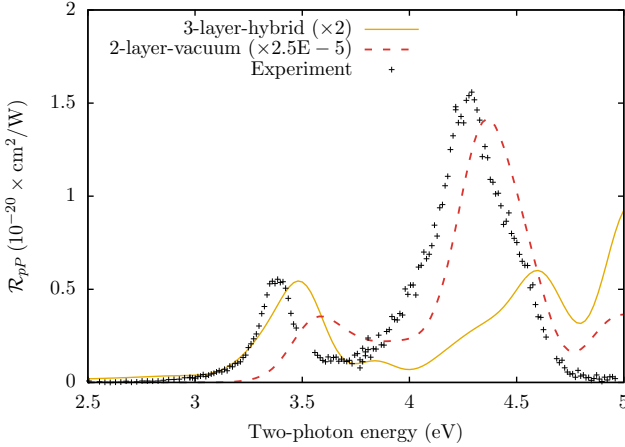


Figure 2.17: Other models.

It is immediately apparent that the 3-layer-hybrid model shares the same lineshape as 3-layer and 2-layer-bulk models, see Fig. 2.16. This is entirely consistent as  $\epsilon_b$  and  $\epsilon_\ell$  differ only in intensity; this model is intermediate in intensity between the other two. The 3-layer model is still closer to experiment, but this is an interesting alternative. On the other hand, the 2-layer-vacuum model has the most extreme intensity difference with the experiment, over 5 orders of magnitude higher. The lineshape reproduces the E<sub>2</sub> peak quite well, but lacks a sharp E<sub>1</sub> peak with poor peak position. Clearly, the screening provided by  $\epsilon_b$  and  $\epsilon_\ell$  are necessary for accurate results.

Reviewing Eq. (1.52), we see that  $\mathcal{R}_{pP}$  is by far the most involved calculation, since it includes all four nonzero components. In particular,  $\chi^{zzz}$  and  $\chi^{xxz}$  include out-of-plane incoming fields. These are affected by local field effects[35] that reveal the inhomogeneities in the material, which are by far more prevalent perpendicular to the surface than in the surface plane. This can be evidenced for Si, as Reflectance Anisotropy Spectroscopy (RAS) measurements are well described by *ab initio* calculations neglecting local field effects.[46, 47] It is therefore expected that the out-of-plane components will be more sensitive to the inclusion of local fields. These will not change the transition energies, only their relative weights of the resonant peaks,[35] but including these effects is challenging to compute,[7] and beyond the scope of this paper. We speculate that  $\mathcal{R}_{pP}$  requires the proper inclusion of these effects in order to accurately describe the experimental peaks.

In Fig. 2.18, I compare the theoretical spectra to results from Ref. [15]. The 3-layer model is, as before, close to the experiment in both peak position and intensity. Intensity is almost the same the experimental value. This provides a more compelling argument against the 2-layer-fresnel model than Fig. 2.16. The 2-layer-fresnel model is 20 times more intense and blueshifted by around 0.1 eV. As mentioned above, this surface is of very high quality with measurements taken shortly after surface preparation. The 2-layer-bulk model is intermediate between the other two models in both intensity and lineshape. Under these conditions, the 3-layer model very accurately reproduces the  $E_1$  peak over the 2-layer-fresnel and 2-layer-bulk models.

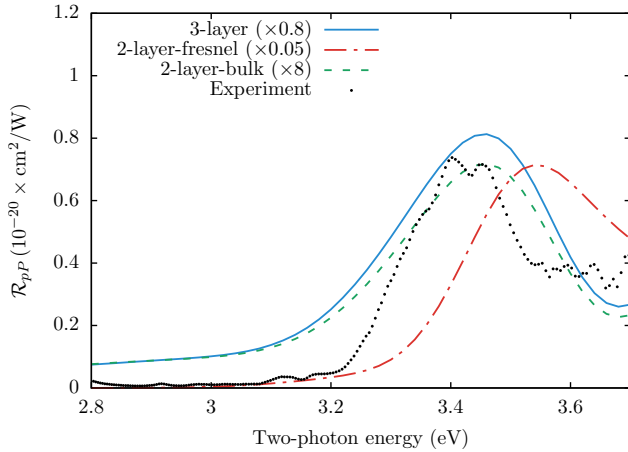


Figure 2.18: Comparison between theoretical models (see Table 1.3) and experiment for  $\mathcal{R}_{pP}$ , for  $\theta = 45^\circ$ , and a scissors value of  $\hbar\Delta = 0.7$  eV. All theoretical curves are broadened with  $\sigma = 0.075$  eV. Experimental data taken from Ref. [15], measured at room temperature.

Lastly,  $GW$  transition energies are needed for linear optics and SHG. Doing a Bethe-Salpeter calculation for SSHG will undoubtedly improve the position and the amplitude of the peaks, but is far beyond current capabilities [48]. I kept the scissors shift constant throughout these calculations as I want to keep this calculation at the *ab initio* level. Remember that the choice of  $\hbar\Delta = 0.7$  eV for the scissors shift comes from a  $GW$  calculation [42]. As explained in Fig. 2.22, the lack of surface states causes an almost rigid shift of the spectra by applying the scissors correction. I have checked that it is not possible to have a single scissors value that can reproduce the energy positions of both the  $E_1$  and the  $E_2$  peaks. Of course, the experimental temperature at which the

spectra is measured should be taken into account in a more complete formulation. However, these calculations are always restricted to  $T = 0$  K.

#### 2.2.2.4 Calculated $\mathcal{R}_{sP}$ compared to experiment

Next, I analyze and compare the calculated  $\mathcal{R}_{sP}$  spectra with experimental data from Ref. [14]. The calculation adheres to the experimental setup by taking an angle of incidence  $\theta = 65^\circ$  and an azimuthal angle  $\phi = 30^\circ$ . As seen in Fig. 2.19, the overall intensity of  $\mathcal{R}_{sP}$  is one order of magnitude lower than  $\mathcal{R}_{pS}$ . The experimental data is far noisier than in the other cases but the E<sub>1</sub> and E<sub>2</sub> peaks are still discernible. As with the previous comparisons, the 3-layer model is the closest match in both intensity and lineshape to the experimental spectrum. It produces a curve that is very close to the experimental intensity with good proportional heights for the calculated E<sub>1</sub> and E<sub>2</sub> peaks. In contrast, the 2-layer-fresnel model is 100 times more intense than experiment and produces an enlarged E<sub>2</sub> peak. The 2-layer-bulk model is ten times smaller with a very similar lineshape to the 3-layer model.

The differences between the 2-layer-fresnel and 2-layer-bulk models are not derived from Eq. (1.57), as the  $\varepsilon_b(2\omega)$  does not change and the second term vanishes for this azimuthal angle of  $\phi = 30$ . However,  $\Gamma_{sP}^\ell$  does cause a significant change in the intensity as there is an  $\varepsilon_\ell(2\omega)$  term in the denominator. This will become  $\varepsilon_v(2\omega) = 1$  for the 2-layer-fresnel model, and  $\varepsilon_b(2\omega)$  in the bulk model. This accounts for the significant difference between the intensity of the two models, while the lineshape remains mostly consistent.

At higher energies, the theoretical curve is blueshifted as compared to the experiment. The best explanation for this is the inclusion of the scissor operator, which does not adequately correct the transitions occurring at these higher energies. A full GW calculation would be well suited for this task, but is well beyond the scope of this work.

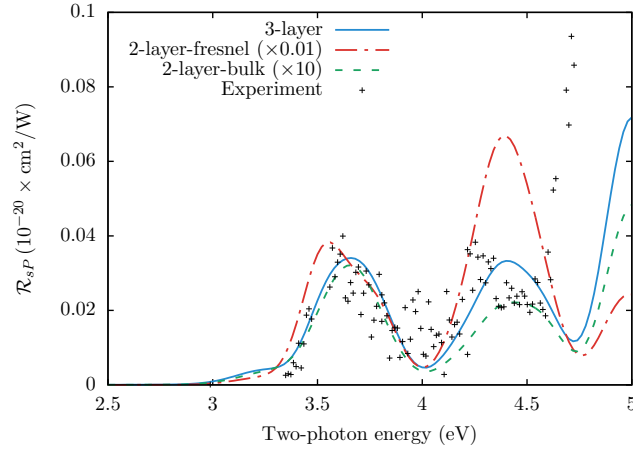


Figure 2.19: Comparison between theoretical models (see Table 1.3) and experiment for  $\mathcal{R}_{sP}$ , for  $\theta = 65^\circ$ , and a scissors value of  $\hbar\Delta = 0.7$  eV. All theoretical curves are broadened with  $\sigma = 0.075$  eV. Experimental data taken from Ref. [14], measured at room temperature.

### 2.2.2.5 Calculated $\mathcal{R}_{pS}$ compared to experiment

I first compare the calculated  $\mathcal{R}_{pS}$  spectra with room temperature experimental data from Ref. [14]. Adhering to the experimental setup, I set an angle of incidence  $\theta = 65^\circ$  and an azimuthal angle of  $\phi = 30^\circ$  with respect to the  $x$ -axis. This azimuthal angle maximizes  $r_{pS}$ , as shown in Eq. (1.62). Fig. 2.20, shows that all three models reproduce the lineshape of the experimental spectrum which includes the peaks corresponding to both the E<sub>1</sub> (3.4 eV) and E<sub>2</sub> (4.3 eV) critical points of bulk silicon, and a smaller feature at around 3.8 eV. The calculated E<sub>1</sub> and E<sub>2</sub> peaks are redshifted by 0.1 eV and 0.06 eV, respectively, compared with the experimental peaks.

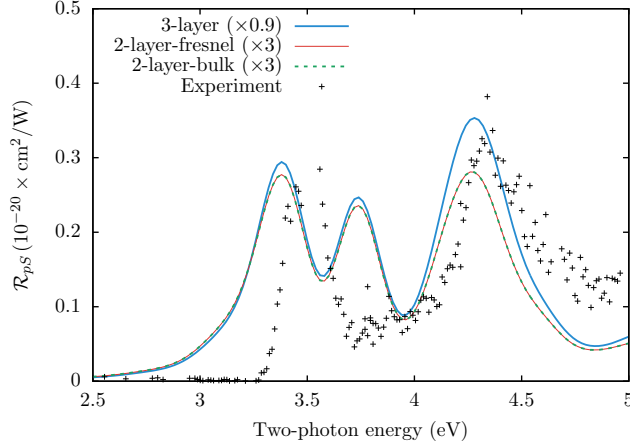


Figure 2.20: Comparison between theoretical models (see Table 1.3) and experiment for  $\mathcal{R}_{pS}$ , for  $\theta = 65^\circ$ , and a scissors value of  $\hbar\Delta = 0.7$  eV. All theoretical curves are broadened with  $\sigma = 0.075$  eV. Experimental data taken from Ref. [14], measured at room temperature.

The main issue to address here is the discrepancy between the intensity of the E<sub>1</sub> peak. In the theoretical curves, the peaks differ only slightly in overall intensity. Conversely, the experimental E<sub>1</sub> peak is significantly smaller than the E<sub>2</sub> peak. This may be due to the effects of oxidation on the surface. Ref. [13] features similar data to those of Ref. [14] but focuses on the effects of surface oxidation. From Ref. [13] it is clear that as time passes during the experiment, the surface becomes more oxidized and the E<sub>1</sub> peak diminishes substantially, as shown by the experimental data taken 5 hours after initial H-termination. This may be enough time to slightly reduce the E<sub>1</sub> peak intensity, as can be observed here.

In Fig. 2.21, I compare the theoretical  $\mathcal{R}_{pS}$  with experimental data from Ref. [15]; this data, however, only encompasses the E<sub>1</sub> peaks, and was obtained at room temperature. This calculation uses an angle of incidence  $\theta = 45^\circ$  and an azimuthal angle  $\phi = 30^\circ$  to match the experimental conditions. As in the previous comparison, the E<sub>1</sub> peak is slightly redshifted compared to experiment. The intensity of the theoretical yield is smaller than the experimental yield for all three models. The measurements presented in Ref. [15] were taken very shortly after the surface had been prepared, and the surface itself was prepared with a high degree of quality and measured at room temperature. Peak position compared to theory is slightly improved under these conditions. As before, the 3-layer model is closer in intensity to the experimental spectrum.

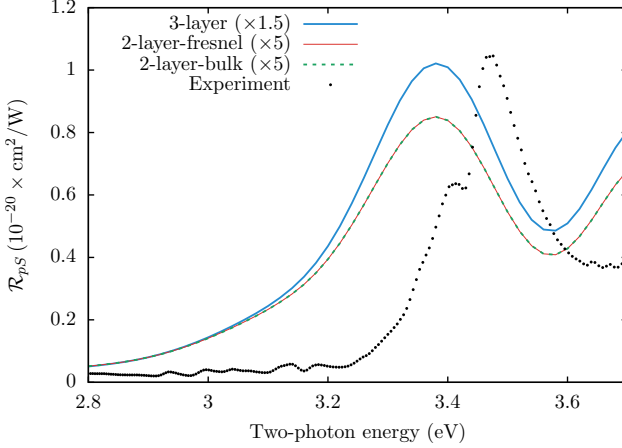


Figure 2.21: Comparison between theoretical models (see Table 1.3) and experiment for  $\mathcal{R}_{pS}$ , for  $\theta = 45^\circ$ . We use a scissors value of  $\hbar\Delta = 0.7$  eV. All theoretical curves are broadened with  $\sigma = 0.075$  eV. Experimental data taken from Ref. [15], measured at room temperature.

From Fig. 2.10, I presented that our calculation for  $\chi^{xxx}$  coincides with the measurement taken at a low temperature of 80 K. It is well known that temperature causes shifting in the peak position of SSHG spectra [45]. As  $\mathcal{R}_{pS}$  only depends on this component (see Eq. (1.62)), the position of the theoretical peak should be correct in Figs. 2.20 and 2.21. Thus, the difference in peak position should stem from the higher temperature at which the experiments were measured.

Both the 2-layer-fresnel and 2-layer-bulk models are identical and roughly four times smaller than the experiment. It is clear from Eq. (1.62) that  $\mathcal{R}_{pS}$  only has  $1\omega$  terms ( $\varepsilon_\ell(\omega)$  and  $k_b$ ). For both of these models, the fundamental fields are evaluated in the bulk, which means that the only change to Eq. (1.62) is that  $\varepsilon_\ell(\omega) \rightarrow \varepsilon_b(\omega)$ . Additionally,  $\Gamma_{pS}^\ell$  also remains identical between the two models and has no  $2\omega$  terms in the denominator. Therefore,  $r_{pS}$  is identical between these two models. Ultimately, the intensity of the 3-layer model is the closest to the experiment.

Per Eq. (1.62), the intensity of  $\mathcal{R}_{pS}$  depends only on  $\chi^{xxx}$ , which is not affected by local field effects [35]. These effects are neglected in this calculation, but  $\mathcal{R}_{pS}$  maintains an accurate lineshape and provides a good quantitative description of the experimental SSHG yield. Note that both the calculated and experimental spectra show two-photon resonances at the energies corresponding to the critical point transitions of bulk Si. Note also that the SSHG yield drops rapidly to zero below  $E_1$ , which is consistent with the absence of surface states due to the H saturation on the surface. This observation holds true for all three polarization cases studied for this surface.

Lastly, in Fig. 2.22 I provide an overview of the different levels of approximation proposed in this article. All curves here were calculated using the 3-layer model. The long dashed line depicts the effect of excluding the contribution from the nonlocal part of the pseduopotentials. This is consistent with the results reported in Ref. [34], where the exclusion of this term increases the intensity of the components of  $\chi$  by approximately 15% to 20%. Note that the  $E_1$  peak is larger than the  $E_2$  peak, contrasting with the experiment, where the  $E_1$  peak is smaller than  $E_2$ . Lastly, the thin solid line depicts the full calculation with a scissors value of  $\hbar\Delta = 0$ . The spectrum is almost rigidly redshifted as this H-saturated surface has no electronic surface states [34]. Thus, this demonstrates the importance of including the scissors correction to accurately reproduce the

experimental spectrum. In summary, the inclusion of the contribution from the nonlocal part of the pseudopotentials and the scissors operator on top of the 3-layer model produces spectra with a lineshape and intensity that compare favorably with the experimental data.

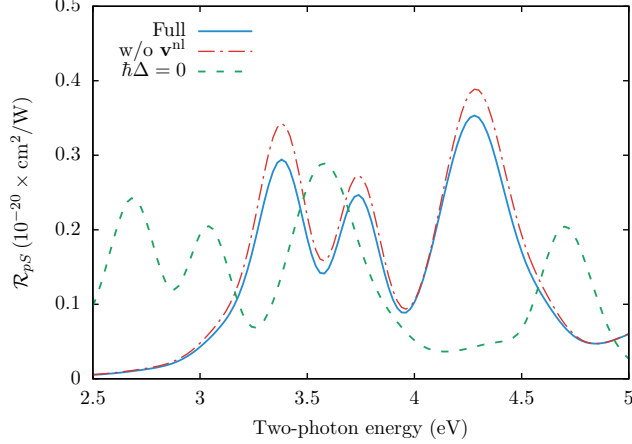


Figure 2.22: Calculated results for  $\mathcal{R}_{pS}$  for the different levels of approximation proposed in this article. All curves were calculated using the 3-layer model. We take  $\theta = 65^\circ$  for this plot. See text for full details. All curves are broadened with  $\sigma = 0.075$  eV.

# Chapter 3

## Final Remarks

### Outline

---

3.1 Conclusions . . . . .	41
3.2 Future Work . . . . .	42

---

### 3.1 Conclusions

I was able to learn and successfully apply the XP2SHG/SFG technique to a series of nanoparticles that were unfortunately not of sufficient optical quality to yield meaningful results. This was accomplished by using established methods (with the help of very capable people) to study samples that were not properly characterized. The obvious solution to this would have been to use other nanoparticles, but it was very much beyond my possibilities to obtain other samples within the time constraints imposed by my visit to the Femtosecond Spectroscopy group.

My suggestions for a revisionary work are the following.

**Better quality samples.** The scattering problem can be completely eliminated with samples that are in good physical condition.

**Well characterized samples.** The purpose of this work was to characterize the nanoparticles via nonlinear spectroscopy. However, these measurements work much better if applied in conjunction with previous studies of the samples, such as TEM scans, linear measurements, etc.

**Apply the XP2SFG technique to metallic nanoparticles.** There are few references available on sum frequency studies involving metallic nanoparticles, especially in the two beam configuration. I think that using proper samples with a NOPA in the XP2SFG configuration would provide excellent characterization of the samples and interesting results.

## 3.2 Future Work

I think that every work of experimental science has its fair share of setbacks, complications, and difficulties. Sometimes the work itself can be very difficult or even dangerous. Other times, the work is so cutting edge that problems have to be solved as they come without the help of literature. Regardless of the scope of the work, *all* experimentation is very touch-and-go business – you arm yourself with the best tools available for the job and hope for the best. This work had its share of complications and setbacks, chief amongst these was the constant breakdown of lasers in both countries. Then, the poor quality of the samples which only came to light after they were in place and ready to be measured. Lastly, the lack of information about the samples did not allow for the systematic study needed to get the most out of this project.

Fortunately, Stephen Jay Gould once said that, “Honorable errors do not count as failures in science, but as seeds for progress in the quintessential activity of correction.” With that in mind I summarize what was learned from this.

First, the XP2SHG/SFG technique is fairly unique and specialized even amongst groups that are dedicated to surface optics and nonlinear optical techniques. Learning how this technique works and how it is used will be invaluable for future work in this field. Actually having seen it in use, and then using it for myself in the company of the people who pioneered it was a rewarding and educational experience.

Second, while the results were inconclusive, the types of measurements done on these types of samples are new and unexplored. There is much work to be done with these kinds of materials and I hope that this work can serve as a starting point for other interested scientists. I have no doubt in my mind that better samples would have yielded excellent new results.

Lastly, this entire work helped broaden my knowledge of nonlinear optics in general, as well as the many experimental techniques used everyday by scientists everywhere. Even so, I only possess a very small portion of the “big picture” needed to understand every aspect of this work. There is still a lot to be learned about surface optics and nonlinear techniques and I hope that this work, at the very least, will pique the readers’ interest on these topics.

## Appendix A

# Derived expressions for the SHG yield

## Outline

---

A.1	Some useful expressions . . . . .	43
A.1.1	$2\omega$ terms . . . . .	44
A.1.2	$1\omega$ terms . . . . .	45
A.1.3	Nonzero components of $\chi(-2\omega; \omega, \omega)$ . . . . .	46
A.2	$\mathcal{R}_{pP}$ . . . . .	47
A.2.1	For the (111) surface . . . . .	48
A.2.2	For the (110) surface . . . . .	51
A.2.3	For the (001) surface . . . . .	52
A.3	$\mathcal{R}_{pS}$ . . . . .	53
A.3.1	For the (111) surface . . . . .	54
A.3.2	For the (110) surface . . . . .	54
A.3.3	For the (001) surface . . . . .	55
A.4	$\mathcal{R}_{sP}$ . . . . .	55
A.4.1	For the (111) surface . . . . .	56
A.4.2	For the (110) surface . . . . .	57
A.4.3	For the (001) surface . . . . .	57
A.5	$\mathcal{R}_{ss}$ . . . . .	58
A.5.1	For the (111) surface . . . . .	58
A.5.2	For the (110) surface . . . . .	59
A.5.3	For the (001) surface . . . . .	59

---

### A.1 Some useful expressions

We are interested in finding

$$\Upsilon = \mathbf{e}_\ell^{2\omega} \cdot \boldsymbol{\chi} : \mathbf{e}_\ell^\omega \mathbf{e}_\ell^\omega$$

for each different polarization case. We choose the plane of incidence along the  $\kappa z$  plane, and define

$$\hat{\boldsymbol{\kappa}} = \cos \phi \hat{\mathbf{x}} + \sin \phi \hat{\mathbf{y}}, \quad (\text{A.1})$$

and

$$\hat{\mathbf{s}} = -\sin \phi \hat{\mathbf{x}} + \cos \phi \hat{\mathbf{y}}, \quad (\text{A.2})$$

where  $\phi$  the angle with respect to the  $x$  axis.

### A.1.1 $2\omega$ terms

Including multiple reflecions, the  $\mathbf{e}_\ell^{2\omega}$  term is

$$\mathbf{e}_\ell^{2\omega} = \hat{\mathbf{e}}^{\text{out}} \cdot \left[ \hat{\mathbf{s}} T_s^{v\ell} R_s^{M+} \hat{\mathbf{s}} + \hat{\mathbf{P}}_{v+} \frac{T_p^{v\ell}}{N_\ell} (\sin \theta_0 R_p^{M+} \hat{\mathbf{z}} - W_\ell R_p^{M-} \hat{\boldsymbol{\kappa}}) \right], \quad (\text{A.3})$$

and neglecting the multiple reflections reduces this expression to

$$\mathbf{e}_\ell^{2\omega} = \hat{\mathbf{e}}^{\text{out}} \cdot \left[ \hat{\mathbf{s}} T_s^{v\ell} T_s^{\ell b} \hat{\mathbf{s}} + \hat{\mathbf{P}}_{v+} \frac{T_p^{v\ell} T_p^{\ell b}}{N_\ell^2 N_b} (N_b^2 \sin \theta_0 \hat{\mathbf{z}} - N_\ell^2 W_b \hat{\boldsymbol{\kappa}}) \right]. \quad (\text{A.4})$$

We first expand these equations for clarity. Substituting Eqs. (A.1) and (A.2) into Eq. (A.3),

$$\begin{aligned} \mathbf{e}_\ell^{2\omega} = & \hat{\mathbf{e}}^{\text{out}} \cdot \left[ \hat{\mathbf{s}} T_s^{v\ell} R_s^{M+} (-\sin \phi \hat{\mathbf{x}} + \cos \phi \hat{\mathbf{y}}) \right. \\ & \left. + \hat{\mathbf{P}}_{v+} \frac{T_p^{v\ell}}{N_\ell} (\sin \theta_0 R_p^{M+} \hat{\mathbf{z}} - W_\ell R_p^{M-} \cos \phi \hat{\mathbf{x}} - W_\ell R_p^{M-} \sin \phi \hat{\mathbf{y}}) \right]. \end{aligned}$$

We now have  $\mathbf{e}_\ell^{2\omega}$  in terms of  $\hat{\mathbf{P}}_{v+}$ ,

$$\mathbf{e}_\ell^{2\omega} = \frac{T_p^{v\ell}}{N_\ell} (\sin \theta_0 R_p^{M+} \hat{\mathbf{z}} - W_\ell R_p^{M-} \cos \phi \hat{\mathbf{x}} - W_\ell R_p^{M-} \sin \phi \hat{\mathbf{y}}), \quad (\text{A.5})$$

and in terms of  $\hat{\mathbf{s}}$ ,

$$\mathbf{e}_\ell^{2\omega} = T_s^{v\ell} R_s^{M+} (-\sin \phi \hat{\mathbf{x}} + \cos \phi \hat{\mathbf{y}}). \quad (\text{A.6})$$

If we wish to neglect the effects from the multiple reflections, we do the exact same for Eq. (A.4), and get the following term for  $\hat{\mathbf{P}}_{v+}$ ,

$$\mathbf{e}_\ell^{2\omega} = \frac{T_p^{v\ell} T_p^{\ell b}}{N_\ell^2 N_b} (N_b^2 \sin \theta_0 \hat{\mathbf{z}} - N_\ell^2 W_b \cos \phi \hat{\mathbf{x}} - N_\ell^2 W_b \sin \phi \hat{\mathbf{y}}), \quad (\text{A.7})$$

and  $\hat{\mathbf{s}}$ ,

$$\mathbf{e}_\ell^{2\omega} = T_s^{v\ell} T_s^{\ell b} [-\sin \phi \hat{\mathbf{x}} + \cos \phi \hat{\mathbf{y}}]. \quad (\text{A.8})$$

### A.1.2 $1\omega$ terms

We have that the  $\mathbf{e}_\ell^\omega$  term is

$$\mathbf{e}_\ell^\omega = \left[ \hat{\mathbf{s}} t_s^{v\ell} r_s^{M+} \hat{\mathbf{s}} + \frac{t_p^{v\ell}}{n_\ell} (r_p^{M+} \sin \theta_0 \hat{\mathbf{z}} + r_p^{M-} w_\ell \hat{\boldsymbol{\kappa}}) \hat{\mathbf{p}}_{v-} \right] \cdot \hat{\mathbf{e}}^{\text{in}}.$$

We are interested in finding  $\mathbf{e}_\ell^\omega \mathbf{e}_\ell^\omega$  for both polarizations. For  $\hat{\mathbf{e}}^{\text{in}} = \hat{\mathbf{p}}_{v-}$  we have

$$\mathbf{e}_\ell^\omega = \frac{t_p^{v\ell}}{n_\ell} (r_p^{M+} \sin \theta_0 \hat{\mathbf{z}} + r_p^{M-} w_\ell \cos \phi \hat{\mathbf{x}} + r_p^{M-} w_\ell \sin \phi \hat{\mathbf{y}}),$$

so

$$\begin{aligned} \mathbf{e}_\ell^\omega \mathbf{e}_\ell^\omega &= \left( \frac{t_p^{v\ell}}{n_\ell} \right)^2 \left( (r_p^{M-})^2 w_\ell^2 \cos^2 \phi \hat{\mathbf{x}} \hat{\mathbf{x}} + 2(r_p^{M-})^2 w_\ell^2 \sin \phi \cos \phi \hat{\mathbf{x}} \hat{\mathbf{y}} \right. \\ &\quad + 2r_p^{M+} r_p^{M-} w_\ell \sin \theta_0 \cos \phi \hat{\mathbf{x}} \hat{\mathbf{z}} + (r_p^{M-})^2 w_\ell^2 \sin^2 \phi \hat{\mathbf{y}} \hat{\mathbf{y}} \\ &\quad \left. + 2r_p^{M+} r_p^{M-} w_\ell \sin \theta_0 \sin \phi \hat{\mathbf{z}} \hat{\mathbf{y}} + (r_p^{M+})^2 \sin^2 \theta_0 \hat{\mathbf{z}} \hat{\mathbf{z}} \right), \end{aligned} \quad (\text{A.9})$$

and for  $\hat{\mathbf{e}}^{\text{in}} = \hat{\mathbf{s}}$ ,

$$\mathbf{e}_\ell^\omega \mathbf{e}_\ell^\omega = \left( t_s^{v\ell} r_s^{M+} \right)^2 (\sin^2 \phi \hat{\mathbf{x}} \hat{\mathbf{x}} + \cos^2 \phi \hat{\mathbf{y}} \hat{\mathbf{y}} - 2 \sin \phi \cos \phi \hat{\mathbf{x}} \hat{\mathbf{y}}). \quad (\text{A.10})$$

Neglecting the effects of the multiple reflections for the  $\mathbf{e}_\ell^\omega$  term yields

$$\mathbf{e}_\ell^\omega = \left[ \hat{\mathbf{s}} t_s^{v\ell} t_s^{\ell b} \hat{\mathbf{s}} + \frac{t_p^{v\ell} t_p^{\ell b}}{n_\ell^2 n_b} (n_b^2 \sin \theta_0 \hat{\mathbf{z}} + n_\ell^2 w_b \hat{\boldsymbol{\kappa}}) \hat{\mathbf{p}}_{v-} \right] \cdot \hat{\mathbf{e}}^{\text{in}}.$$

For all cases, we require a  $\mathbf{e}_\ell^\omega \mathbf{e}_\ell^\omega$  product. For brevity, we will directly list these terms for both polarizations. For  $\hat{\mathbf{e}}^{\text{in}} = \hat{\mathbf{p}}_{v-}$ ,

$$\begin{aligned} \mathbf{e}_\ell^\omega \mathbf{e}_\ell^\omega &= \left( \frac{t_p^{v\ell} t_p^{\ell b}}{n_\ell^2 n_b} \right)^2 (n_\ell^4 w_b^2 \cos^2 \phi \hat{\mathbf{x}} \hat{\mathbf{x}} + 2n_\ell^4 w_b^2 \sin \phi \cos \phi \hat{\mathbf{x}} \hat{\mathbf{y}} \\ &\quad + 2n_\ell^2 n_b^2 w_b \sin \theta_0 \cos \phi \hat{\mathbf{x}} \hat{\mathbf{z}} + n_\ell^4 w_b^2 \sin^2 \phi \hat{\mathbf{y}} \hat{\mathbf{y}} \\ &\quad + 2n_\ell^2 n_b^2 w_b \sin \theta_0 \sin \phi \hat{\mathbf{y}} \hat{\mathbf{z}} + n_b^4 \sin^2 \theta_0 \hat{\mathbf{z}} \hat{\mathbf{z}}), \end{aligned} \quad (\text{A.11})$$

and for  $\hat{\mathbf{e}}^{\text{in}} = \hat{\mathbf{s}}$ ,

$$\mathbf{e}_\ell^\omega \mathbf{e}_\ell^\omega = \left( t_s^{v\ell} t_s^{\ell b} \right)^2 (\sin^2 \phi \hat{\mathbf{x}} \hat{\mathbf{x}} + \cos^2 \phi \hat{\mathbf{y}} \hat{\mathbf{y}} - 2 \sin \phi \cos \phi \hat{\mathbf{x}} \hat{\mathbf{y}}). \quad (\text{A.12})$$

We summarize these expressions in Table A.1. In order to derive the equations for a given polarization case, we refer to the equations listed there. Then it is simply a matter of multiplying the terms correctly and obtaining the appropriate components of  $\chi(-2\omega; \omega, \omega)$ .

### A.1.3 Nonzero components of $\chi(-2\omega; \omega, \omega)$

For a (111) surface with  $C_{3v}$  symmetry, we have the following nonzero components:

$$\begin{aligned}\chi_{xxx} &= -\chi_{xyy} = -\chi_{yyx}, \\ \chi_{xxz} &= \chi_{yyz}, \\ \chi_{zxx} &= \chi_{zyy}, \\ \chi_{zzz}.\end{aligned}\tag{A.13}$$

For a (110) surface with  $C_{2v}$  symmetry, we have the following nonzero components:

$$\chi_{xxz}, \chi_{yyz}, \chi_{zxx}, \chi_{zyy}, \chi_{zzz}.\tag{A.14}$$

Lastly, for a (001) surface with  $C_{4v}$  symmetry, we have the following nonzero components:

$$\begin{aligned}\chi_{xxz} &= \chi_{yyz}, \\ \chi_{zxx} &= \chi_{zyy}, \\ \chi_{zzz}.\end{aligned}\tag{A.15}$$

Case	$\hat{\mathbf{e}}^{\text{out}}$	$\hat{\mathbf{e}}^{\text{in}}$	$\mathbf{e}_\ell^{2\omega}$	$\mathbf{e}_\ell^\omega \mathbf{e}_\ell^\omega$
$\mathcal{R}_{pP}$	$\hat{\mathbf{P}}_{v+}$	$\hat{\mathbf{p}}_{v-}$	Eq. (A.5) or (A.7)	Eq. (A.9) or Eq. (A.11)
$\mathcal{R}_{pS}$	$\hat{\mathbf{s}}$	$\hat{\mathbf{p}}_{v-}$	Eq. (A.6) or (A.8)	Eq. (A.9) or Eq. (A.11)
$\mathcal{R}_{sP}$	$\hat{\mathbf{P}}_{v+}$	$\hat{\mathbf{s}}$	Eq. (A.5) or (A.7)	Eq. (A.10) or Eq. (A.12)
$\mathcal{R}_{sS}$	$\hat{\mathbf{s}}$	$\hat{\mathbf{s}}$	Eq. (A.6) or (A.8)	Eq. (A.10) or Eq. (A.12)

Table A.1: Polarization unit vectors for  $\hat{\mathbf{e}}^{\text{out}}$  and  $\hat{\mathbf{e}}^{\text{in}}$ , and equations describing  $\mathbf{e}_\ell^{2\omega}$  and  $\mathbf{e}_\ell^\omega \mathbf{e}_\ell^\omega$  for each polarization case. When there are two equations to choose from, the former includes the effects of multiple reflections, and the latter neglects them.

## A.2 $\mathcal{R}_{pP}$

Per Table A.1,  $\mathcal{R}_{pP}$  requires Eqs. (A.5) and (A.9). After some algebra, we obtain that

$$\Upsilon_{pP}^{\text{MR}} = \Gamma_{pP}^{\text{MR}} \left[ -R_p^{M-} (r_p^{M-})^2 w_\ell^2 W_\ell \cos^3 \phi \chi_{xxx} \right. \\ - 2R_p^{M-} (r_p^{M-})^2 w_\ell^2 W_\ell \sin \phi \cos^2 \phi \chi_{xxy} \\ - 2R_p^{M-} r_p^{M+} r_p^{M-} w_\ell W_\ell \sin \theta_0 \cos^2 \phi \chi_{xxz} \\ - R_p^{M-} (r_p^{M-})^2 w_\ell^2 W_\ell \sin^2 \phi \cos \phi \chi_{xyy} \\ - 2R_p^{M-} r_p^{M+} r_p^{M-} w_\ell W_\ell \sin \theta_0 \sin \phi \cos \phi \chi_{xyz} \\ - R_p^{M-} (r_p^{M+})^2 W_\ell \sin^2 \theta_0 \cos \phi \chi_{xzz} \\ - R_p^{M-} (r_p^{M-})^2 w_\ell^2 W_\ell \sin \phi \cos^2 \phi \chi_{yxx} \\ - 2R_p^{M-} (r_p^{M-})^2 w_\ell^2 W_\ell \sin^2 \phi \cos \phi \chi_{yxy} \\ - 2R_p^{M-} r_p^{M+} r_p^{M-} w_\ell W_\ell \sin \theta_0 \sin \phi \cos \phi \chi_{yxz} \\ - R_p^{M-} (r_p^{M-})^2 w_\ell^2 W_\ell \sin^3 \phi \chi_{yyy} \\ - 2R_p^{M-} r_p^{M+} r_p^{M-} w_\ell W_\ell \sin \theta_0 \sin^2 \phi \chi_{yyz} \\ - R_p^{M-} (r_p^{M+})^2 W_\ell \sin^2 \theta_0 \sin \phi \chi_{yzz} \\ + R_p^{M+} (r_p^{M-})^2 w_\ell^2 \sin \theta_0 \cos^2 \phi \chi_{zxx} \\ + 2R_p^{M+} r_p^{M+} r_p^{M-} w_\ell \sin^2 \theta_0 \cos \phi \chi_{zxz} \\ + 2R_p^{M+} (r_p^{M-})^2 w_\ell^2 \sin \theta_0 \sin \phi \cos \phi \chi_{zxy} \\ + R_p^{M+} (r_p^{M-})^2 w_\ell^2 \sin \theta_0 \sin^2 \phi \chi_{zyy} \\ + 2R_p^{M+} r_p^{M+} r_p^{M-} w_\ell \sin^2 \theta_0 \sin \phi \chi_{zzy} \\ \left. + R_p^{M+} (r_p^{M+})^2 \sin^3 \theta_0 \chi_{zzz} \right], \quad (\text{A.16})$$

We take this opportunity to introduce a quantity that will be repeated throughout this section,

$$\Gamma_{pP}^{\text{MR}} = \frac{T_p^{v\ell}}{N_\ell} \left( \frac{t_p^{v\ell}}{n_\ell} \right)^2. \quad (\text{A.17})$$

If we neglect the multiple reflections, as described in the manuscript, we have that

$$\begin{aligned}
\Upsilon_{pP} = \Gamma_{pP} & \left[ -N_\ell^2 W_b \left( +n_\ell^4 w_b^2 \cos^3 \phi \chi_{xxx} + 2n_\ell^4 w_b^2 \sin \phi \cos^2 \phi \chi_{xxy} \right. \right. \\
& + 2n_b^2 n_\ell^2 w_b \sin \theta_0 \cos^2 \phi \chi_{xxz} + n_\ell^4 w_b^2 \sin^2 \phi \cos \phi \chi_{xyy} \\
& \left. \left. + 2n_b^2 n_\ell^2 w_b \sin \theta_0 \sin \phi \cos \phi \chi_{xyz} + n_b^4 \sin^2 \theta_0 \cos \phi \chi_{xzz} \right) \right. \\
& - N_\ell^2 W_b \left( +n_\ell^4 w_b^2 \sin \phi \cos^2 \phi \chi_{yxx} + 2n_\ell^4 w_b^2 \sin^2 \phi \cos \phi \chi_{yxy} \right. \\
& + 2n_b^2 n_\ell^2 w_b \sin \theta_0 \sin \phi \cos \phi \chi_{yxz} + n_\ell^4 w_b^2 \sin^3 \phi \chi_{yyy} \\
& \left. \left. + 2n_b^2 n_\ell^2 w_b \sin \theta_0 \sin^2 \phi \chi_{yyz} + n_b^4 \sin^2 \theta_0 \sin \phi \chi_{yzz} \right) \right. \\
& + N_b^2 \sin \theta_0 \left( +n_\ell^4 w_b^2 \cos^2 \phi \chi_{zxx} + 2n_\ell^4 w_b^2 \sin \phi \cos \phi \chi_{zxy} \right. \\
& + n_\ell^4 w_b^2 \sin^2 \phi \chi_{zyy} + 2n_\ell^2 n_b^2 w_b \sin \theta_0 \cos \phi \chi_{zzx} \\
& \left. \left. + 2n_\ell^2 n_b^2 w_b \sin \theta_0 \sin \phi \chi_{zzy} + n_b^4 \sin^2 \theta_0 \chi_{zzz} \right) \right], \tag{A.18}
\end{aligned}$$

and again we introduce a quantity that will be repeated throughout this section,

$$\Gamma_{pP} = \frac{T_p^{v\ell} T_p^{\ell b}}{N_\ell^2 N_b} \left( \frac{t_p^{v\ell} t_p^{\ell b}}{n_\ell^2 n_b} \right)^2. \tag{A.19}$$

### A.2.1 For the (111) surface

We take Eqs. (A.16) and (A.13), eliminate the components that do not contribute, and apply the symmetry relations as follows,

$$\begin{aligned}
\Upsilon_{pP}^{\text{MR},(111)} = \Gamma_{pP}^{\text{MR}} & \left[ -R_p^{M-} (r_p^{M-})^2 w_\ell^2 W_\ell \cos^3 \phi \chi_{xxx} \right. \\
& + R_p^{M-} (r_p^{M-})^2 w_\ell^2 W_\ell \sin^2 \phi \cos \phi \chi_{xxx} \\
& + 2R_p^{M-} (r_p^{M-})^2 w_\ell^2 W_\ell \sin^2 \phi \cos \phi \chi_{xxx} \\
& - 2R_p^{M-} r_p^{M+} r_p^{M-} w_\ell W_\ell \sin \theta_0 \cos^2 \phi \chi_{xxz} \\
& - 2R_p^{M-} r_p^{M+} r_p^{M-} w_\ell W_\ell \sin \theta_0 \sin^2 \phi \chi_{xxz} \\
& + R_p^{M+} (r_p^{M-})^2 w_\ell^2 \sin \theta_0 \cos^2 \phi \chi_{zxx} \\
& + R_p^{M+} (r_p^{M-})^2 w_\ell^2 \sin \theta_0 \sin^2 \phi \chi_{zxx} \\
& \left. + R_p^{M+} (r_p^{M+})^2 \sin^3 \theta_0 \chi_{zzz} \right].
\end{aligned}$$

We reduce terms,

$$\begin{aligned}
\Upsilon_{pP}^{\text{MR},(111)} &= \Gamma_{pP}^{\text{MR}} \left[ R_p^{M-} (r_p^{M-})^2 w_\ell^2 W_\ell (3 \sin^2 \phi \cos \phi - \cos^3 \phi) \chi_{xxx} \right. \\
&\quad - 2R_p^{M-} r_p^{M+} r_p^{M-} w_\ell W_\ell \sin \theta_0 (\sin^2 \phi + \cos^2 \phi) \chi_{xxz} \\
&\quad + R_p^{M+} (r_p^{M+})^2 w_\ell^2 \sin \theta_0 (\sin^2 \phi + \cos^2 \phi) \chi_{zxx} \\
&\quad \left. + R_p^{M+} (r_p^{M+})^2 \sin^3 \theta_0 \chi_{zzz} \right] \\
&= \Gamma_{pP}^{\text{MR}} \left[ R_p^{M+} \sin \theta_0 \left( (r_p^{M+})^2 \sin^2 \theta_0 \chi_{zzz} + (r_p^{M-})^2 w_\ell^2 \chi_{zxx} \right) \right. \\
&\quad \left. - R_p^{M-} w_\ell W_\ell \left( 2r_p^{M+} r_p^{M-} \sin \theta_0 \chi_{xxz} + (r_p^{M-})^2 w_\ell \chi_{xxx} \cos 3\phi \right) \right] \\
&= \Gamma_{pP}^{\text{MR}} r_{pP}^{\text{MR},(111)},
\end{aligned}$$

where

$$\begin{aligned}
r_{pP}^{\text{MR},(111)} &= R_p^{M+} \sin \theta_0 \left( (r_p^{M+})^2 \sin^2 \theta_0 \chi_{zzz} + (r_p^{M-})^2 w_\ell^2 \chi_{zxx} \right) \\
&\quad - R_p^{M-} w_\ell W_\ell \left( 2r_p^{M+} r_p^{M-} \sin \theta_0 \chi_{xxz} + (r_p^{M-})^2 w_\ell \chi_{xxx} \cos 3\phi \right). \tag{A.20}
\end{aligned}$$

If we wish to neglect the effects of the multiple reflections, we follow the exact same procedure but starting with Eq. (A.18),

$$\begin{aligned}
\Upsilon_{pP}^{(111)} &= \Gamma_{pP} \left[ + n_b^4 N_b^2 \sin^3 \theta_0 \chi_{zzz} \right. \\
&\quad + n_\ell^4 N_b^2 w_b^2 \sin \theta_0 \cos^2 \phi \chi_{zxx} \\
&\quad + n_\ell^4 N_b^2 w_b^2 \sin \theta_0 \sin^2 \phi \chi_{zxx} \\
&\quad - 2n_b^2 n_\ell^2 N_\ell^2 w_b W_b \sin \theta_0 \cos^2 \phi \chi_{xxz} \\
&\quad - 2n_b^2 n_\ell^2 N_\ell^2 w_b W_b \sin \theta_0 \sin^2 \phi \chi_{xxz} \\
&\quad - n_\ell^4 N_\ell^2 w_b^2 W_b \cos^3 \phi \chi_{xxx} \\
&\quad + n_\ell^4 N_\ell^2 w_b^2 W_b \sin^2 \phi \cos \phi \chi_{xxx} \\
&\quad \left. + 2n_\ell^4 N_\ell^2 w_b^2 W_b \sin^2 \phi \cos \phi \chi_{xxx} \right],
\end{aligned}$$

and reduce,

$$\begin{aligned}
\Upsilon_{pP}^{(111)} &= \Gamma_{pP} \left[ + n_b^4 N_b^2 \sin^3 \theta_0 \chi_{zzz} \right. \\
&\quad + n_\ell^4 N_b^2 w_b^2 \sin \theta_0 (\sin^2 \phi + \cos^2 \phi) \chi_{zxx} \\
&\quad - 2n_b^2 n_\ell^2 N_\ell^2 w_b W_b \sin \theta_0 (\sin^2 \phi + \cos^2 \phi) \phi \chi_{xxz} \\
&\quad \left. + n_\ell^4 N_\ell^2 w_b^2 W_b (3 \sin^2 \phi \cos \phi - \cos^3 \phi) \chi_{xxx} \right] \\
&= \Gamma_{pP} \left[ N_b^2 \sin \theta_0 (n_b^4 \sin^2 \theta_0 \chi_{zzz} + n_\ell^4 w_b^2 \chi_{zxx}) \right. \\
&\quad \left. - n_\ell^2 N_\ell^2 w_b W_b (2n_b^2 \sin \theta_0 \chi_{xxz} + n_\ell^2 w_b \chi_{xxx} \cos 3\phi) \right] \\
&= \Gamma_{pP} r_{pP}^{(111)},
\end{aligned}$$

where

$$\begin{aligned}
r_{pP}^{(111)} &= N_b^2 \sin \theta_0 (n_b^4 \sin^2 \theta_0 \chi_{zzz} + n_\ell^4 w_b^2 \chi_{zxx}) \\
&\quad - n_\ell^2 N_\ell^2 w_b W_b (2n_b^2 \sin \theta_0 \chi_{xxz} + n_\ell^2 w_b \chi_{xxx} \cos 3\phi).
\end{aligned} \tag{A.21}$$

### A.2.2 For the (110) surface

We take Eqs. (A.16) and (A.14), eliminate the components that do not contribute, and apply the symmetry relations as follows,

$$\begin{aligned}
\Upsilon_{pP}^{\text{MR},(110)} &= \Gamma_{pP}^{\text{MR}} \left[ R_p^{M+} (r_p^{M+})^2 \sin^3 \theta_0 \chi_{zzz} \right. \\
&\quad + R_p^{M+} (r_p^{M-})^2 w_\ell^2 \sin \theta_0 \sin^2 \phi \chi_{zyy} \\
&\quad + R_p^{M+} (r_p^{M-})^2 w_\ell^2 \sin \theta_0 \cos^2 \phi \chi_{zxx} \\
&\quad - 2R_p^{M-} r_p^{M+} r_p^{M-} w_\ell W_\ell \sin \theta_0 \sin^2 \phi \chi_{yyz} \\
&\quad \left. - 2R_p^{M-} r_p^{M+} r_p^{M-} w_\ell W_\ell \sin \theta_0 \cos^2 \phi \chi_{xxz} \right] \\
&= \Gamma_{pP}^{\text{MR}} \left[ R_p^{M+} \sin \theta_0 \left( (r_p^{M+})^2 \sin^2 \theta_0 \chi_{zzz} \right. \right. \\
&\quad + (r_p^{M-})^2 w_\ell^2 \left( \frac{1}{2}(1 - \cos 2\phi) \chi_{zyy} + \frac{1}{2}(\cos 2\phi + 1) \chi_{zxx} \right) \\
&\quad \left. \left. - 2R_p^{M-} r_p^{M+} r_p^{M-} w_\ell W_\ell \sin \theta_0 \left( \frac{1}{2}(1 - \cos 2\phi) \chi_{yyz} \right. \right. \right. \\
&\quad \left. \left. \left. + \frac{1}{2}(\cos 2\phi + 1) \chi_{xxz} \right) \right] \\
&= \Gamma_{pP}^{\text{MR}} \left[ R_p^{M+} \sin \theta_0 \left( (r_p^{M+})^2 \sin^2 \theta_0 \chi_{zzz} \right. \right. \\
&\quad + (r_p^{M-})^2 w_\ell^2 \left( \frac{\chi_{zyy} + \chi_{zxx}}{2} + \frac{\chi_{zyy} - \chi_{zxx}}{2} \cos 2\phi \right) \\
&\quad \left. \left. - 2R_p^{M-} r_p^{M+} r_p^{M-} w_\ell W_\ell \sin \theta_0 \left( \frac{\chi_{yyz} + \chi_{xxz}}{2} + \frac{\chi_{yyz} - \chi_{xxz}}{2} \cos 2\phi \right) \right] \\
&= \Gamma_{pP}^{\text{MR}} r_{pP}^{\text{MR},(110)},
\end{aligned}$$

where

$$\begin{aligned}
r_{pP}^{\text{MR},(110)} &= R_p^{M+} \sin \theta_0 \left( (r_p^{M+})^2 \sin^2 \theta_0 \chi_{zzz} \right. \\
&\quad + (r_p^{M-})^2 w_\ell^2 \left( \frac{\chi_{zyy} + \chi_{zxx}}{2} + \frac{\chi_{zyy} - \chi_{zxx}}{2} \cos 2\phi \right) \\
&\quad \left. - 2R_p^{M-} r_p^{M+} r_p^{M-} w_\ell W_\ell \sin \theta_0 \left( \frac{\chi_{yyz} + \chi_{xxz}}{2} + \frac{\chi_{yyz} - \chi_{xxz}}{2} \cos 2\phi \right) \right). \tag{A.22}
\end{aligned}$$

If we wish to neglect the effects of the multiple reflections, we follow the exact same procedure

but starting with Eq. (A.18),

$$\begin{aligned}
\Upsilon_{pP}^{(110)} &= \Gamma_{pP} \left[ N_b^2 \sin \theta_0 \left( n_b^4 \sin^2 \theta_0 \chi_{zzz} + n_\ell^4 w_b^2 (\sin^2 \phi \chi_{zyy} + \cos^2 \phi \chi_{zxx}) \right) \right. \\
&\quad \left. - 2n_b^2 n_\ell^2 N_\ell^2 w_b W_b \sin \theta_0 (\sin^2 \phi \chi_{yyz} + \cos^2 \phi \chi_{xxz}) \right] \\
&= \Gamma_{pP} \left[ N_b^2 \sin \theta_0 \left( n_b^4 \sin^2 \theta_0 \chi_{zzz} \right. \right. \\
&\quad \left. + n_\ell^4 w_b^2 \left( \frac{\chi_{zyy} + \chi_{zxx}}{2} + \frac{\chi_{zyy} - \chi_{zxx}}{2} \cos 2\phi \right) \right) \\
&\quad \left. - 2n_b^2 n_\ell^2 N_\ell^2 w_b W_b \sin \theta_0 \left( \frac{\chi_{yyz} + \chi_{xxz}}{2} + \frac{\chi_{yyz} - \chi_{xxz}}{2} \cos 2\phi \right) \right] \\
&= \Gamma_{pP} r_{pP}^{(110)},
\end{aligned}$$

where

$$\begin{aligned}
r_{pP}^{(110)} &= N_b^2 \sin \theta_0 \left[ n_b^4 \sin^2 \theta_0 \chi_{zzz} + n_\ell^4 w_b^2 \left( \frac{\chi_{zyy} + \chi_{zxx}}{2} + \frac{\chi_{zyy} - \chi_{zxx}}{2} \cos 2\phi \right) \right] \\
&\quad - 2n_b^2 n_\ell^2 N_\ell^2 w_b W_b \sin \theta_0 \left( \frac{\chi_{yyz} + \chi_{xxz}}{2} + \frac{\chi_{yyz} - \chi_{xxz}}{2} \cos 2\phi \right).
\end{aligned} \tag{A.23}$$

### A.2.3 For the (001) surface

We take Eqs. (A.16) and (A.14), eliminate the components that do not contribute, and apply the symmetry relations as follows,

$$\begin{aligned}
\Upsilon_{pP}^{\text{MR},(001)} &= \Gamma_{pP}^{\text{MR}} \left[ R_p^{M+} (r_p^{M+})^2 \sin^3 \theta_0 \chi_{zzz} \right. \\
&\quad + R_p^{M+} (r_p^{M-})^2 w_\ell^2 \sin \theta_0 \sin^2 \phi \chi_{zxx} \\
&\quad + R_p^{M+} (r_p^{M-})^2 w_\ell^2 \sin \theta_0 \cos^2 \phi \chi_{zxx} \\
&\quad - 2R_p^{M-} r_p^{M+} r_p^{M-} w_\ell W_\ell \sin \theta_0 \sin^2 \phi \chi_{xxz} \\
&\quad \left. - 2R_p^{M-} r_p^{M+} r_p^{M-} w_\ell W_\ell \sin \theta_0 \cos^2 \phi \chi_{xxz} \right] \\
&= \Gamma_{pP}^{\text{MR}} \left[ R_p^{M+} \sin \theta_0 \left( (r_p^{M+})^2 \sin^2 \theta_0 \chi_{zzz} + (r_p^{M-})^2 w_\ell^2 \chi_{zxx} \right) \right. \\
&\quad \left. - 2R_p^{M-} r_p^{M+} r_p^{M-} w_\ell W_\ell \sin \theta_0 \chi_{xxz} \right] \\
&= \Gamma_{pP}^{\text{MR}} r_{pP}^{\text{MR},(001)},
\end{aligned}$$

where

$$\begin{aligned} r_{pP}^{\text{MR},(001)} = & R_p^{M+} \sin \theta_0 \left( (r_p^{M+})^2 \sin^2 \theta_0 \chi_{zzz} + (r_p^{M-})^2 w_\ell^2 \chi_{zxx} \right) \\ & - 2R_p^{M-} r_p^{M+} r_p^{M-} w_\ell W_\ell \sin \theta_0 \chi_{xxz}, \end{aligned} \quad (\text{A.24})$$

If we wish to neglect the effects of the multiple reflections, we follow the exact same procedure but starting with Eq. (A.18),

$$\begin{aligned} \Upsilon_{pP}^{(001)} = & \Gamma_{pP} [N_b^2 \sin \theta_0 (n_b^4 \sin^2 \theta_0 \chi_{zzz} + n_\ell^4 w_b^2 \chi_{zxx}) \\ & - 2n_b^2 n_\ell^2 N_\ell^2 w_b W_b \sin \theta_0 \chi_{xxz}] \\ = & \Gamma_{pP} r_{pp}^{(001)}, \end{aligned}$$

where

$$\begin{aligned} r_{pP}^{(001)} = & N_b^2 \sin \theta_0 (n_b^4 \sin^2 \theta_0 \chi_{zzz} + n_\ell^4 w_b^2 \chi_{zxx}) \\ & - 2n_b^2 n_\ell^2 N_\ell^2 w_b W_b \sin \theta_0 \chi_{xxz}. \end{aligned} \quad (\text{A.25})$$

### A.3 $\mathcal{R}_{pS}$

Per Table A.1,  $\mathcal{R}_{pS}$  requires Eqs. (A.6) and (A.9). After some algebra, we obtain that

$$\begin{aligned} \Upsilon_{pS}^{\text{MR}} = & \Gamma_{pS}^{\text{MR}} [ - (r_p^{M-})^2 w_\ell^2 \sin \phi \cos^2 \phi \chi_{xxx} - 2(r_p^{M-})^2 w_\ell^2 \sin^2 \phi \cos \phi \chi_{xxy} \\ & - 2r_p^{M+} r_p^{M-} w_\ell \sin \theta_0 \sin \phi \cos \phi \chi_{xxz} - (r_p^{M-})^2 w_\ell^2 \sin^3 \phi \chi_{xyy} \\ & - 2r_p^{M+} r_p^{M-} w_\ell \sin \theta_0 \sin^2 \phi \chi_{xzy} - (r_p^{M+})^2 \sin^2 \theta_0 \sin \phi \chi_{xzz} \\ & + (r_p^{M-})^2 w_\ell^2 \cos^3 \phi \chi_{yxx} + 2(r_p^{M-})^2 w_\ell^2 \sin \phi \cos^2 \phi \chi_{yxy} \\ & + 2r_p^{M+} r_p^{M-} w_\ell \sin \theta_0 \cos^2 \phi \chi_{yxz} + (r_p^{M-})^2 w_\ell^2 \sin^2 \phi \cos \phi \chi_{yyy} \\ & + 2r_p^{M+} r_p^{M-} w_\ell \sin \theta_0 \sin \phi \cos \phi \chi_{yzy} + (r_p^{M+})^2 \sin^2 \theta_0 \cos \phi \chi_{yzz} ]. \end{aligned} \quad (\text{A.26})$$

We take this opportunity to introduce a quantity that will be repeated throughout this section,

$$\Gamma_{pS}^{\text{MR}} = T_s^{v\ell} R_s^{M+} \left( \frac{t_p^{v\ell}}{n_\ell} \right)^2 \quad (\text{A.27})$$

If we neglect the multiple reflections, as described in the manuscript, we have that

$$\begin{aligned} \Upsilon_{pS} = & \Gamma_{pS} [ - n_\ell^4 w_b^2 \sin \phi \cos^2 \phi \chi_{xxx} - 2n_\ell^4 w_b^2 \sin^2 \phi \cos \phi \chi_{xxy} \\ & - 2n_\ell^2 n_b^2 w_b \sin \theta_0 \sin \phi \cos \phi \chi_{xxz} - n_\ell^4 w_b^2 \sin^3 \phi \chi_{xyy} \\ & - 2n_\ell^2 n_b^2 w_b \sin \theta_0 \sin^2 \phi \chi_{xzy} - n_b^4 \sin^2 \theta_0 \sin \phi \chi_{xzz} \\ & + n_\ell^4 w_b^2 \cos^3 \phi \chi_{yxx} + 2n_\ell^4 w_b^2 \sin \phi \cos^2 \phi \chi_{yxy} \\ & + 2n_\ell^2 n_b^2 w_b \sin \theta_0 \cos^2 \phi \chi_{yxz} + n_\ell^4 w_b^2 \sin^2 \phi \cos \phi \chi_{yyy} \\ & + 2n_\ell^2 n_b^2 w_b \sin \theta_0 \sin \phi \cos \phi \chi_{yzy} + n_b^4 \sin^2 \theta_0 \cos \phi \chi_{yzz} ], \end{aligned} \quad (\text{A.28})$$

and again we introduce a quantity that will be repeated throughout this section,

$$\Gamma_{pS} = T_s^{v\ell} T_s^{\ell b} \left( \frac{t_p^{v\ell} t_p^{\ell b}}{n_\ell^2 n_b} \right)^2. \quad (\text{A.29})$$

### A.3.1 For the (111) surface

We take Eqs. (A.26) and (A.13), eliminate the components that do not contribute, and apply the symmetry relations as follows,

$$\begin{aligned}\Upsilon_{pS}^{\text{MR},(111)} &= \Gamma_{pS}^{\text{MR}} [2r_p^{M+}r_p^{M-}w_\ell \sin \theta_0 \sin \phi \cos \phi \chi_{xxz} \\ &\quad - 2r_p^{M+}r_p^{M-}w_\ell \sin \theta_0 \sin \phi \cos \phi \chi_{xxz} \\ &\quad - (r_p^{M-})^2 w_\ell^2 \sin \phi \cos^2 \phi \chi_{xxx} \\ &\quad - 2(r_p^{M-})^2 w_\ell^2 \sin \phi \cos^2 \phi \chi_{xxx} \\ &\quad + (r_p^{M-})^2 w_\ell^2 \sin^3 \phi \chi_{xxx}].\end{aligned}$$

We reduce terms,

$$\begin{aligned}\Upsilon_{pS}^{\text{MR},(111)} &= \Gamma_{pS}^{\text{MR}} [(r_p^{M-})^2 w_\ell^2 (\sin^3 \phi - 3 \sin \phi \cos^2 \phi) \chi_{xxx}] \\ &= \Gamma_{pS}^{\text{MR}} [-(r_p^{M-})^2 w_\ell^2 \chi_{xxx} \sin 3\phi] \\ &= \Gamma_{pS}^{\text{MR}} r_{pS}^{\text{MR},(111)},\end{aligned}$$

where

$$r_{pS}^{\text{MR},(111)} = -(r_p^{M-})^2 w_\ell^2 \chi_{xxx} \sin 3\phi. \quad (\text{A.30})$$

If we wish to neglect the effects of the multiple reflections, we follow the exact same procedure but starting with Eq. (A.28),

$$\begin{aligned}\Upsilon_{pS} &= \Gamma_{pS} [n_\ell^4 w_b^2 (\sin^3 \phi - 3 \sin \phi \cos^2 \phi) \chi_{xxx}] \\ &= \Gamma_{pS} [-n_\ell^4 w_b^2 \chi_{xxx} \sin 3\phi] \\ &= \Gamma_{pS} r_{pS}^{(111)},\end{aligned} \quad (\text{A.31})$$

where

$$r_{pS}^{(111)} = -n_\ell^4 w_b^2 \chi_{xxx} \sin 3\phi, \quad (\text{A.32})$$

and we use  $\Gamma_{pS}$  instead of  $\Gamma_{pS}^{\text{MR}}$ .

### A.3.2 For the (110) surface

We take Eqs. (A.26) and (A.14), eliminate the components that do not contribute, and apply the symmetry relations as follows,

$$\begin{aligned}\Upsilon_{pS}^{\text{MR},(110)} &= \Gamma_{pS}^{\text{MR}} [2r_p^{M+}r_p^{M-}w_\ell \sin \theta_0 \sin \phi \cos \phi (\chi_{yyz} - \chi_{xxz})] \\ &= \Gamma_{pS}^{\text{MR}} [r_p^{M+}r_p^{M-}w_\ell \sin \theta_0 (\chi_{yyz} - \chi_{xxz}) \sin 2\phi] \\ &= \Gamma_{pS}^{\text{MR}} r_{pS}^{\text{MR},(110)}.\end{aligned}$$

where

$$r_{pS}^{\text{MR},(110)} = r_p^{M+} r_p^{M-} w_\ell \sin \theta_0 (\chi_{yyz} - \chi_{xxz}) \sin 2\phi. \quad (\text{A.33})$$

If we neglect the effects of the multiple reflections as mentioned above, we have

$$r_{pS}^{(110)} = n_\ell^2 n_b^2 w_b \sin \theta_0 (\chi_{yyz} - \chi_{xxz}) \sin 2\phi, \quad (\text{A.34})$$

and we use  $\Gamma_{pS}$  instead of  $\Gamma_{pS}^{\text{MR}}$ .

### A.3.3 For the (001) surface

We take Eqs. (A.26) and (A.14), eliminate the components that do not contribute, and apply the symmetry relations as follows,

$$\begin{aligned} \Upsilon_{pS}^{\text{MR},(001)} &= \Gamma_{pS}^{\text{MR}} [ -2r_p^{M+} r_p^{M-} w_\ell \sin \theta_0 \sin \phi \cos \phi \chi_{xxz} \\ &\quad + 2r_p^{M+} r_p^{M-} w_\ell \sin \theta_0 \sin \phi \cos \phi \chi_{xxz} ] = 0. \end{aligned}$$

Neglecting the effects of multiple reflections will obviously yield the same result, thus

$$\Upsilon_{pS}^{\text{MR},(001)} = \Upsilon_{pS}^{(001)} = 0. \quad (\text{A.35})$$

## A.4 $\mathcal{R}_{sP}$

Per Table A.1,  $\mathcal{R}_{sP}$  requires Eqs. (A.5) and (A.10). After some algebra, we obtain that

$$\begin{aligned} \Upsilon_{sP}^{\text{MR}} &= \Gamma_{sP}^{\text{MR}} \left[ R_p^{M-} W_\ell (-\sin^2 \phi \cos \phi \chi_{xxx} + 2 \sin \phi \cos^2 \phi \chi_{xxy} - \cos^3 \phi \chi_{xyy}) \right. \\ &\quad + R_p^{M-} W_\ell (-\sin^3 \phi \chi_{yxx} + 2 \sin^2 \phi \cos \phi \chi_{yyx} - \sin \phi \cos^2 \phi \chi_{yyy}) \\ &\quad \left. + R_p^{M+} \sin \theta_0 (\sin^2 \phi \chi_{zxx} - 2 \sin \phi \cos \phi \chi_{zxy} + \cos^2 \phi \chi_{zyy}) \right]. \end{aligned} \quad (\text{A.36})$$

We take this opportunity to introduce a quantity that will be repeated throughout this section,

$$\Gamma_{sP}^{\text{MR}} = \frac{T_p^{v\ell}}{N_\ell} \left( t_s^{v\ell} r_s^{M+} \right)^2 \quad (\text{A.37})$$

If we neglect the multiple reflections, as described in the manuscript, we have that

$$\begin{aligned} \Upsilon_{sP} &= \Gamma_{sP} \left[ N_\ell^2 W_b (-\sin^2 \phi \cos \phi \chi_{xxx} + 2 \sin \phi \cos^2 \phi \chi_{xxy} - \cos^3 \phi \chi_{xyy}) \right. \\ &\quad + N_\ell^2 W_b (-\sin^3 \phi \chi_{yxx} + 2 \sin^2 \phi \cos \phi \chi_{yyx} - \sin \phi \cos^2 \phi \chi_{yyy}) \\ &\quad \left. + N_b^2 \sin \theta_0 (+\sin^2 \phi \chi_{zxx} - 2 \sin \phi \cos \phi \chi_{zxy} + \cos^2 \phi \chi_{zyy}) \right], \end{aligned} \quad (\text{A.38})$$

and again we introduce a quantity that will be repeated throughout this section,

$$\Gamma_{sP} = \frac{T_p^{v\ell} T_p^{\ell b}}{N_\ell^2 N_b} \left( t_s^{v\ell} t_s^{\ell b} \right)^2. \quad (\text{A.39})$$

### A.4.1 For the (111) surface

We take Eqs. (A.36) and (A.13), eliminate the components that do not contribute, and apply the symmetry relations as follows,

$$\begin{aligned}\Upsilon_{sP}^{\text{MR},(111)} &= \Gamma_{sP}^{\text{MR}} \left[ + R_p^{M-} W_\ell \cos^3 \phi \chi_{xxx} \right. \\ &\quad - R_p^{M-} W_\ell \sin^2 \phi \cos \phi \chi_{xxx} \\ &\quad - 2R_p^{M-} W_\ell \sin^2 \phi \cos \phi \chi_{xxx} \\ &\quad + R_p^{M+} \sin \theta_0 \sin^2 \phi \chi_{zxx} \\ &\quad \left. + R_p^{M+} \sin \theta_0 \cos^2 \phi \chi_{zxx} \right].\end{aligned}$$

We reduce terms,

$$\begin{aligned}\Upsilon_{sP}^{\text{MR},(111)} &= \Gamma_{sP}^{\text{MR}} \left[ R_p^{M-} W_\ell (\cos^3 \phi - 3 \sin^2 \phi \cos \phi) \chi_{xxx} \right. \\ &\quad \left. + R_p^{M+} \sin \theta_0 (\sin^2 \phi + \cos^2 \phi) \chi_{zxx} \right] \\ &= \Gamma_{sP}^{\text{MR}} \left[ R_p^{M-} W_\ell \chi_{xxx} \cos 3\phi + R_p^{M+} \sin \theta_0 \chi_{zxx} \right] \\ &= \Gamma_{sP}^{\text{MR}} r_{sP}^{\text{MR},(111)},\end{aligned}$$

where

$$r_{sP}^{\text{MR},(111)} = R_p^{M+} \sin \theta_0 \chi_{zxx} + R_p^{M-} W_\ell \chi_{xxx} \cos 3\phi. \quad (\text{A.40})$$

If we wish to neglect the effects of the multiple reflections, we follow the exact same procedure but starting with Eq. (A.38),

$$\begin{aligned}\Upsilon_{sP}^{(111)} &= \Gamma_{sP} \left[ - N_\ell^2 W_b \sin^2 \phi \cos \phi \chi_{xxx} \right. \\ &\quad + N_\ell^2 W_b \cos^3 \phi \chi_{xxx} \\ &\quad - 2N_\ell^2 W_b \sin^2 \phi \cos \phi \chi_{yyx} \\ &\quad + N_b^2 \sin \theta_0 \sin^2 \phi \chi_{zxx} \\ &\quad \left. + N_b^2 \sin \theta_0 \cos^2 \phi \chi_{zxx} \right],\end{aligned}$$

and reduce,

$$\begin{aligned}\Upsilon_{sP}^{(111)} &= \Gamma_{sP} \left[ N_\ell^2 W_b (\cos^3 \phi - 3 \sin^2 \phi \cos \phi) \chi_{xxx} \right. \\ &\quad \left. + N_b^2 \sin \theta_0 (\sin^2 \phi + \cos^2 \phi) \chi_{zxx} \right] \\ &= \Gamma_{sP} \left[ N_\ell^2 W_b \chi_{xxx} \cos 3\phi + N_b^2 \sin \theta_0 \chi_{zxx} \right] \\ &= \Gamma_{sP} r_{sP}^{(111)},\end{aligned}$$

where

$$r_{sP}^{(111)} = N_b^2 \sin \theta_0 \chi_{zxx} + N_\ell^2 W_b \chi_{xxx} \cos 3\phi. \quad (\text{A.41})$$

### A.4.2 For the (110) surface

We take Eqs. (A.36) and (A.14), eliminate the components that do not contribute, and apply the symmetry relations as follows,

$$\begin{aligned}
\Upsilon_{sP}^{\text{MR},(110)} &= \Gamma_{sP}^{\text{MR}} [R_p^{M+} \sin \theta_0 (\sin^2 \phi \chi_{zxx} + \cos^2 \phi \chi_{zyy})] \\
&= \Gamma_{sP}^{\text{MR}} \left[ R_p^{M+} \sin \theta_0 \left( \frac{1}{2}(1 - \cos 2\phi) \chi_{zxx} + \frac{1}{2}(\cos 2\phi + 1) \chi_{zyy} \right) \right] \\
&= \Gamma_{sP}^{\text{MR}} \left[ R_p^{M+} \sin \theta_0 \left( \frac{\chi_{zyy} + \chi_{zxx}}{2} + \frac{\chi_{zyy} - \chi_{zxx}}{2} \cos 2\phi \right) \right] \\
&= \Gamma_{sP}^{\text{MR}} r_{sP}^{\text{MR},(110)},
\end{aligned}$$

where

$$r_{sP}^{\text{MR},(110)} = R_p^{M+} \sin \theta_0 \left( \frac{\chi_{zxx} + \chi_{zyy}}{2} + \frac{\chi_{zyy} - \chi_{zxx}}{2} \cos 2\phi \right). \quad (\text{A.42})$$

If we wish to neglect the effects of the multiple reflections, we follow the exact same procedure but starting with Eq. (A.38),

$$\begin{aligned}
\Upsilon_{sP}^{(110)} &= \Gamma_{sP} [N_b^2 \sin \theta_0 (\sin^2 \phi \chi_{zxx} + \cos^2 \phi \chi_{zyy})] \\
&= \Gamma_{sP} \left[ N_b^2 \sin \theta_0 \left( \frac{1}{2}(1 - \cos 2\phi) \chi_{zxx} + \frac{1}{2}(\cos 2\phi + 1) \chi_{zyy} \right) \right] \\
&= \Gamma_{sP} \left[ N_b^2 \sin \theta_0 \left( \frac{\chi_{zxx} + \chi_{zyy}}{2} + \frac{\chi_{zyy} - \chi_{zxx}}{2} \cos 2\phi \right) \right] \\
&= \Gamma_{sP} r_{sP}^{(110)},
\end{aligned}$$

where

$$r_{sP}^{(110)} = N_b^2 \sin \theta_0 \left( \frac{\chi_{zxx} + \chi_{zyy}}{2} + \frac{\chi_{zyy} - \chi_{zxx}}{2} \cos 2\phi \right). \quad (\text{A.43})$$

### A.4.3 For the (001) surface

We take Eqs. (A.36) and (A.14), eliminate the components that do not contribute, and apply the symmetry relations as follows,

$$\begin{aligned}
\Upsilon_{sP}^{\text{MR},(001)} &= \Gamma_{sP}^{\text{MR}} [R_p^{M+} \sin \theta_0 (\sin^2 \phi + \cos^2 \phi) \chi_{zxx}] \\
&= \Gamma_{sP}^{\text{MR}} [R_p^{M+} \sin \theta_0 \chi_{zxx}] \\
&= \Gamma_{sP}^{\text{MR}} r_{sP}^{\text{MR},(001)}.
\end{aligned}$$

where

$$r_{sP}^{\text{MR},(001)} = R_p^{M+} \sin \theta_0 \chi_{zxx}. \quad (\text{A.44})$$

If we wish to neglect the effects of the multiple reflections, we follow the exact same procedure but starting with Eq. (A.38),

$$\begin{aligned} \Upsilon_{sP}^{(001)} &= \Gamma_{sP} [N_b^2 \sin \theta_0 (\sin^2 \phi + \cos^2 \phi) \chi_{zxx}] \\ &= \Gamma_{sP} [N_b^2 \sin \theta_0 \chi_{zxx}] \\ &= \Gamma_{sP} r_{sP}^{(001)}, \end{aligned}$$

where

$$r_{sP}^{(001)} = N_b^2 \sin \theta_0 \chi_{zxx}. \quad (\text{A.45})$$

## A.5 $\mathcal{R}_{sS}$

Per Table A.1,  $\mathcal{R}_{sS}$  requires Eqs. (A.6) and (A.10). After some algebra, we obtain that

$$\begin{aligned} \Upsilon_{sS}^{\text{MR}} &= \Gamma_{sS}^{\text{MR}} [ -\sin^3 \phi \chi_{xxx} + 2 \sin^2 \phi \cos \phi \chi_{xxy} - \sin \phi \cos^2 \phi \chi_{xyy} \\ &\quad + \sin^2 \phi \cos \phi \chi_{yxx} - 2 \sin \phi \cos^2 \phi \chi_{yxy} + \cos^3 \phi \chi_{yyy} ]. \end{aligned} \quad (\text{A.46})$$

We take this opportunity to introduce a quantity that will be repeated throughout this section,

$$\Gamma_{sS}^{\text{MR}} = T_s^{v\ell} R_s^{M+} \left( t_s^{v\ell} r_s^{M+} \right)^2. \quad (\text{A.47})$$

If we neglect the multiple reflections, as described in the manuscript, we have that

$$\begin{aligned} \Upsilon_{sS} &= \Gamma_{sS} [ -\sin^3 \phi \chi_{xxx} + 2 \sin^2 \phi \cos \phi \chi_{xxy} - \sin \phi \cos^2 \phi \chi_{xyy} \\ &\quad + \sin^2 \phi \cos \phi \chi_{yxx} - 2 \sin \phi \cos^2 \phi \chi_{yxy} + \cos^3 \phi \chi_{yyy} ], \end{aligned} \quad (\text{A.48})$$

and again we introduce a quantity that will be repeated throughout this section,

$$\Gamma_{sS} = T_s^{v\ell} T_s^{\ell b} \left( t_s^{v\ell} t_s^{\ell b} \right)^2. \quad (\text{A.49})$$

We note that both Eqs. (A.46) and (A.48) are identical save for the different  $\Gamma_{sS}$  terms. Therefore, we can safely derive the equations only once, and then use  $\Gamma_{sS}^{\text{MR}}$  when we wish to include multiple reflections, or  $\Gamma_{sS}$  when we do not.

### A.5.1 For the (111) surface

We take Eqs. (A.46) and (A.13), eliminate the components that do not contribute, and apply the symmetry relations as follows,

$$\begin{aligned} \Upsilon_{sS}^{\text{MR}} &= \Gamma_{sS}^{\text{MR}} [(3 \sin \phi \cos^2 \phi - \sin^3 \phi) \chi_{xxx}] \\ &= \Gamma_{sS}^{\text{MR}} [\chi_{xxx} \sin 3\phi] \\ &= \Gamma_{sS}^{\text{MR}} r_{sS}^{\text{MR},(111)}, \end{aligned}$$

where

$$r_{sS}^{\text{MR},(111)} = \chi_{xxx} \sin 3\phi. \quad (\text{A.50})$$

As mentioned above,

$$r_{sS}^{(111)} = r_{sS}^{\text{MR},(111)}, \quad (\text{A.51})$$

so if we wish to neglect the effects of the multiple reflections, we simply use  $\Gamma_{sS}$  instead of  $\Gamma_{sS}^{\text{MR}}$ .

### A.5.2 For the (110) surface

When considering Eqs. (A.46) and (A.14), we see that there are no nonzero components that contribute. Therefore,

$$\Upsilon_{pS}^{\text{MR},(110)} = \Upsilon_{pS}^{(110)} = 0. \quad (\text{A.52})$$

### A.5.3 For the (001) surface

When considering Eqs. (A.46) and (A.14), we see that there are no nonzero components that contribute. Therefore,

$$\Upsilon_{sS}^{\text{MR},(001)} = \Upsilon_{sS}^{(001)} = 0. \quad (\text{A.53})$$

## Appendix B

# Deriving the SSHG yield without multiple reflections

### Outline

---

B.1 Three layer model for SSHG radiation . . . . .	60
B.1.1 SSHG Yield . . . . .	63

---

### B.1 Three layer model for SSHG radiation

In this section we derive the formulas required for the calculation of the SSHG yield, defined by

$$\mathcal{R} = \frac{I(2\omega)}{I^2(\omega)}, \quad (\text{B.1})$$

with the intensity given by[1]

$$I(\omega) = \begin{cases} \frac{c}{2\pi} n(\omega) |E(\omega)|^2 & (\text{cgs units}) \\ 2\epsilon_0 c n(\omega) |E(\omega)|^2 & (\text{MKS units}) \end{cases}, \quad (\text{B.2})$$

where  $n(\omega) = \sqrt{\epsilon(\omega)}$  is the index of refraction with  $\epsilon(\omega)$  the dielectric function,  $\epsilon_0$  is the vacuum permittivity, and  $c$  the speed of light in vacuum. We use Ref. [4] as a starting point for this work, as the derivation of the three layer model is direct. In this scheme, we represent the surface by three regions or layers. The first layer is the vacuum region (denoted by  $v$ ) with a dielectric function  $\epsilon_v(\omega) = 1$  from where the fundamental electric field  $\mathbf{E}_v(\omega)$  impinges on the material. The second layer is a thin layer (denoted by  $\ell$ ) of thickness  $d$  characterized by a dielectric function  $\epsilon_\ell(\omega)$ . It is in this layer where the second harmonic generation takes place. The third layer is the bulk region denoted by  $b$  and characterized by  $\epsilon_b(\omega)$ . Both the vacuum layer and the bulk layer are semi-infinite (see Fig. B.1).

To model the electromagnetic response of the three layer model we follow Ref. [4], and assume a polarization sheet of the form

$$\mathbf{P}(\mathbf{r}, t) = \mathcal{P} e^{i\kappa \cdot \mathbf{R}} e^{-i\omega t} \delta(z - z_\beta) + \text{c.c.}, \quad (\text{B.3})$$

where  $\mathcal{P}$  is the nonlinear polarization (given below),  $\mathbf{R} = (x, y)$ ,  $\kappa$  is the component of the wave vector  $\nu_\beta$  parallel to the surface, and  $z_\beta$  is the position of the sheet within medium  $\beta$  (see Fig. B.1). It is shown in Ref. [5] that the solution of the Maxwell equations for the radiated fields  $E_{\beta,p\pm}$  and  $E_{\beta,s}$ , at points  $z \neq 0$ , with  $\mathbf{P}(\mathbf{r}, t)$  acting as a source can be written as

$$(E_{\beta,p\pm}, E_{\beta,s}) = \left( \frac{\gamma i \tilde{\omega}^2}{\tilde{w}_\beta} \hat{\mathbf{p}}_{\beta\pm} \cdot \mathcal{P}, \frac{\gamma i \tilde{\omega}^2}{\tilde{w}_\beta} \hat{\mathbf{s}} \cdot \mathcal{P} \right), \quad (\text{B.4})$$

where  $\gamma = 2\pi$  in cgs units and  $\gamma = 1/2\epsilon_0$  in MKS units.  $E_{\beta,p\pm}$  represents the electric field for  $p$ -polarization propagating downward ( $-$ ) or upward ( $+$ ), and  $E_{\beta,s}$  that for  $s$ -polarization, both in medium  $\beta$ . Since for  $s$ -polarization the field is parallel to the surface there is no need to distinguish the upward or downward direction of propagation as it is needed for the  $p$ -polarized fields. Also,  $\tilde{\omega} = \omega/c$ , and  $\hat{\mathbf{s}}$  and  $\hat{\mathbf{p}}_{\beta\pm}$  are the unitary vectors for the  $s$  and  $p$  polarization of the radiated field, respectively. The  $\pm$  notation refers to upward (+) or downward (-) direction of propagation within medium  $\beta$ , as shown in Fig. B.1. Thus,

$$\hat{\mathbf{p}}_{\beta\pm}(\omega) = \frac{\kappa(\omega) \hat{\mathbf{z}} \mp \tilde{w}_\beta(\omega) \hat{\boldsymbol{\kappa}}}{\tilde{w}_\beta n_\beta(\omega)} = \frac{\sin \theta_0 \hat{\mathbf{z}} \mp w_\beta(\omega) \hat{\boldsymbol{\kappa}}}{n_\beta(\omega)}, \quad (\text{B.5})$$

where  $\kappa(\omega) = |\kappa(\omega)| = \tilde{\omega} \sin \theta_0$ ,  $n_\beta(\omega) = \sqrt{\epsilon_\beta(\omega)}$  is the index of refraction of medium  $\beta$ , and  $z$  is the direction perpendicular to the surface that points towards the vacuum. Lastly,  $\tilde{w}_\beta(\omega) = \tilde{\omega} w_\beta$ , where

$$w_\beta(\omega) = (\epsilon_\beta(\omega) - \sin^2 \theta_0)^{1/2}, \quad (\text{B.6})$$

with  $\theta_0$  the angle of incidence of  $\mathbf{E}_v(\omega)$ . We choose the plane of incidence along the  $\kappa z$  plane, so

$$\hat{\boldsymbol{\kappa}} = \cos \phi \hat{\mathbf{x}} + \sin \phi \hat{\mathbf{y}}, \quad (\text{B.7})$$

and

$$\hat{\mathbf{s}} = -\sin \phi \hat{\mathbf{x}} + \cos \phi \hat{\mathbf{y}}, \quad (\text{B.8})$$

where  $\phi$  is the azimuthal angle with respect to the  $x$  axis.

In the three layer model, the nonlinear polarization responsible for the SHG is immersed in the thin  $\beta = \ell$  layer, and is given by

$$\mathcal{P}_{\ell,i}(2\omega) = \begin{cases} \chi_{ijk}(-2\omega; \omega, \omega) E_{\ell,j}(\omega) E_{\ell,k}(\omega) & \text{(cgs units)} \\ \epsilon_0 \chi_{ijk}(-2\omega; \omega, \omega) E_{\ell,j}(\omega) E_{\ell,k}(\omega) & \text{(MKS units)} \end{cases}, \quad (\text{B.9})$$

where the tensor  $\chi(-2\omega; \omega, \omega)$  is the surface nonlinear dipolar susceptibility and the Cartesian indices  $i, j, k$  are summed over if repeated. We remark that the thickness of the layer  $\ell$  is considered to be much smaller than the wavelength of the fundamental field, thus multiple reflections of both the fundamental and the SH can be neglected. Also,  $\chi_{ijk}(-2\omega; \omega, \omega) = \chi_{ikj}(-2\omega; \omega, \omega)$  is the

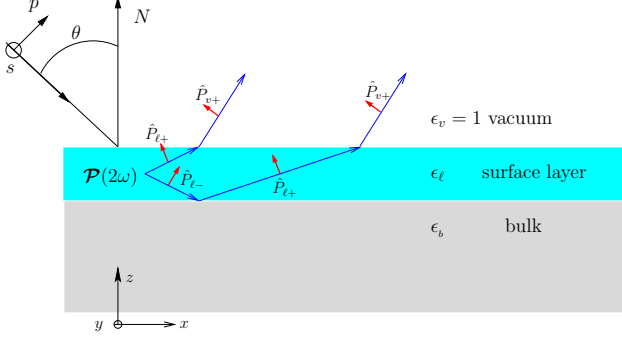


Figure B.1: Sketch of the three layer model for SHG. Vacuum is on top with  $\epsilon_v = 1$ , the layer with nonlinear polarization  $\mathcal{P}(2\omega)$  is characterized with  $\epsilon_\ell(\omega)$  and the bulk with  $\epsilon_b(\omega)$ . In the dipolar approximation the bulk does not radiate SHG. The thin arrows are along the direction of propagation, and the unit vectors for  $p$ -polarization are denoted with thick arrows (capital letters denote SH components). The unit vector for  $s$ -polarization points along  $-y$  (out of the page).

intrinsic permutation symmetry due to the fact that SHG is degenerate in  $E_{\ell,j}(\omega)$  and  $E_{\ell,k}(\omega)$ . For ease of notation, we drop the frequency argument from  $\chi(-2\omega; \omega, \omega)$  and we simply write  $\chi$  from now on. As it was done in Ref. [4], in presenting the results Eq. (B.4)-(B.8) we have taken the polarization sheet (Eq. (B.3)) to be oscillating at some frequency  $\omega$ . However, in the following we find it convenient to use  $\omega$  exclusively to denote the fundamental frequency and  $\kappa$  to denote the component of the incident wave vector parallel to the surface. Then the nonlinear generated polarization is oscillating at  $\Omega = 2\omega$  and will be characterized by a wave vector parallel to the surface  $\mathbf{K} = 2\kappa$ . We can carry over Eqs. (B.3)-(B.8) simply by replacing the lowercase symbols  $(\omega, \tilde{\omega}, \kappa, n_\beta, \tilde{w}_\beta, w_\beta, \hat{\mathbf{p}}_{\beta\pm}, \hat{\mathbf{s}})$  with uppercase symbols  $(\Omega, \tilde{\Omega}, \mathbf{K}, N_\beta, \tilde{W}_\beta, W_\beta, \hat{\mathbf{P}}_{\beta\pm}, \hat{\mathbf{S}})$ , all evaluated at  $2\omega$ . We always have that  $\hat{\mathbf{S}} = \hat{\mathbf{s}}$ .

To describe the propagation of the SH field, we see from Fig. B.1, that it is refracted at the layer-vacuum interface ( $\ell v$ ), and reflected from the layer-bulk ( $\ell b$ ) and layer-vacuum ( $\ell v$ ) interfaces, thus we define

$$\mathbf{T}^{\ell v} = \hat{\mathbf{s}} T_s^{\ell v} \hat{\mathbf{s}} + \hat{\mathbf{P}}_{v+} T_p^{\ell v} \hat{\mathbf{P}}_{\ell+}, \quad (\text{B.10})$$

as the tensor for transmission from the  $\ell v$  interface,

$$\mathbf{R}^{\ell b} = \hat{\mathbf{s}} R_s^{\ell b} \hat{\mathbf{s}} + \hat{\mathbf{P}}_{\ell+} R_p^{\ell b} \hat{\mathbf{P}}_{\ell-}, \quad (\text{B.11})$$

as the tensor of reflection from the  $\ell b$  interface, and

$$\mathbf{R}^{\ell v} = \hat{\mathbf{s}} R_s^{\ell v} \hat{\mathbf{s}} + \hat{\mathbf{P}}_{\ell-} R_p^{\ell v} \hat{\mathbf{P}}_{\ell+}, \quad (\text{B.12})$$

as that from the  $\ell v$  interface. The Fresnel factors in uppercase letters,  $T_{s,p}^{ij}$  and  $R_{s,p}^{ij}$ , are evaluated

at  $2\omega$  from the following well known formulas,[4]

$$t_s^{ij}(\omega) = \frac{2w_i(\omega)}{w_i(\omega) + w_j(\omega)}, \quad (\text{B.13})$$

$$t_p^{ij}(\omega) = \frac{2w_i(\omega)\sqrt{\epsilon_i(\omega)\epsilon_j(\omega)}}{w_i(\omega)\epsilon_j(\omega) + w_j(\omega)\epsilon_i(\omega)}, \quad (\text{B.14})$$

$$r_s^{ij}(\omega) = \frac{w_i(\omega) - w_j(\omega)}{w_i(\omega) + w_j(\omega)}, \quad (\text{B.15})$$

$$r_p^{ij}(\omega) = \frac{w_i(\omega)\epsilon_j(\omega) - w_j(\omega)\epsilon_i(\omega)}{w_i(\omega)\epsilon_j(\omega) + w_j(\omega)\epsilon_i(\omega)}. \quad (\text{B.16})$$

From these expressions one can show that,

$$\begin{aligned} 1 + r_s^{\ell b} &= t_s^{\ell b} \\ 1 + r_p^{\ell b} &= \frac{n_b}{n_\ell} t_p^{\ell b} \\ 1 - r_p^{\ell b} &= \frac{n_\ell}{n_b} \frac{w_b}{w_\ell} t_p^{\ell b} \\ t_{s,p}^{\ell v} &= \frac{w_\ell}{w_v} t_{s,p}^{v\ell}. \end{aligned} \quad (\text{B.17})$$

### B.1.1 SSHG Yield

We obtain the total  $2\omega$  radiated field by using Eqs. (B.10), (B.11), and (B.12),

$$\mathbf{E}(2\omega) = E_s(2\omega) \left( \mathbf{T}^{\ell v} + \mathbf{T}^{\ell v} \cdot \mathbf{R}^{\ell b} \right) \cdot \hat{\mathbf{s}} + E_{p+}(2\omega) \mathbf{T}^{\ell v} \cdot \hat{\mathbf{P}}_{\ell+} + E_{p-}(2\omega) \mathbf{T}^{\ell v} \cdot \mathbf{R}^{\ell b} \cdot \hat{\mathbf{P}}_{\ell-}.$$

The first term is the transmitted  $s$ -polarized field, the second one is the reflected and then transmitted  $s$ -polarized field and the third and fourth terms are the equivalent fields for  $p$ -polarization. The transmission is from the layer into vacuum, and the reflection between the layer and the bulk. After some simple algebra, we obtain

$$\mathbf{E}_\ell(2\omega) = \frac{\gamma i \tilde{\Omega}}{W_\ell} \mathbf{H}_\ell \cdot \mathcal{P}_\ell(2\omega), \quad (\text{B.18})$$

where,

$$\mathbf{H}_\ell = \hat{\mathbf{s}} T_s^{\ell v} \left( 1 + R_s^{\ell b} \right) \hat{\mathbf{s}} + \hat{\mathbf{P}}_{v+} T_p^{\ell v} \left( \hat{\mathbf{P}}_{\ell+} + R_p^{\ell b} \hat{\mathbf{P}}_{\ell-} \right). \quad (\text{B.19})$$

The magnitude of the radiated SH field is given by  $E(2\omega) = \hat{\mathbf{e}}^F \cdot \mathbf{E}_\ell(2\omega)$ , where  $\hat{\mathbf{e}}^F$  is the unit vector of the final polarization, with  $F = S, P$ , and then,  $\hat{\mathbf{e}}^S = \hat{\mathbf{s}}$  and  $\hat{\mathbf{e}}^P = \hat{\mathbf{P}}_{v+}$ . We expand the second term in parenthesis of Eq. (B.19) as

$$\begin{aligned} \hat{\mathbf{P}}_{\ell+} + R_p^{\ell b} \hat{\mathbf{P}}_{\ell-} &= \frac{\sin \theta_0 \hat{\mathbf{z}} - W_\ell \hat{\boldsymbol{\kappa}}}{N_\ell} + R_p^{\ell b} \frac{\sin \theta_0 \hat{\mathbf{z}} + W_\ell \hat{\boldsymbol{\kappa}}}{N_\ell} \\ &= \frac{1}{N_\ell} \left( \sin \theta_0 (1 + R_p^{\ell b}) \hat{\mathbf{z}} - W_\ell (1 - R_p^{\ell b}) \hat{\boldsymbol{\kappa}} \right) \\ &= \frac{T_p^{\ell b}}{N_\ell^2 N_b} \left( N_b^2 \sin \theta_0 \hat{\mathbf{z}} - N_\ell^2 W_b \hat{\boldsymbol{\kappa}} \right), \end{aligned}$$

and rewrite Eq. (B.18) as

$$E(2\omega) = \frac{2\gamma i\omega}{cW_\ell} \hat{\mathbf{e}}^F \cdot \mathbf{H}_\ell \cdot \mathcal{P}_\ell(2\omega) = \frac{2\gamma i\omega}{cW_v} \mathbf{e}_\ell^{2\omega,F} \cdot \mathcal{P}_\ell(2\omega), \quad (\text{B.20})$$

where

$$\mathbf{e}_\ell^{2\omega,F} = \hat{\mathbf{e}}^F \cdot \left[ \hat{\mathbf{s}} T_s^{v\ell} T_s^{\ell b} \hat{\mathbf{s}} + \hat{\mathbf{P}}_{v+} \frac{T_p^{v\ell} T_p^{\ell b}}{N_\ell^2 N_b} (N_b^2 \sin \theta_0 \hat{\mathbf{z}} - N_\ell^2 W_b \hat{\boldsymbol{\kappa}}) \right]. \quad (\text{B.21})$$

In the three layer model the nonlinear polarization is located in layer  $\ell$ , thus, we evaluate the fundamental field required in Eq. (B.9) in this layer as well. We write

$$\mathbf{E}_\ell(\omega) = E_0 \left( \hat{\mathbf{s}} t_s^{v\ell} (1 + r_s^{\ell b}) \hat{\mathbf{s}} + \hat{\mathbf{p}}_{\ell-} t_p^{v\ell} \hat{\mathbf{p}}_{v-} + \hat{\mathbf{p}}_{\ell+} t_p^{v\ell} r_p^{\ell b} \hat{\mathbf{p}}_{v-} \right) \cdot \hat{\mathbf{e}}^{\text{in}} = E_0 \mathbf{e}_\ell^\omega, \quad (\text{B.22})$$

and following the steps that lead to Eq. (B.21), we find that

$$\mathbf{e}_\ell^{\omega,i} = \left[ \hat{\mathbf{s}} t_s^{v\ell} t_s^{\ell b} \hat{\mathbf{s}} + \frac{t_p^{v\ell} t_p^{\ell b}}{n_\ell^2 n_b} (n_b^2 \sin \theta_0 \hat{\mathbf{z}} + n_\ell^2 w_b \hat{\boldsymbol{\kappa}}) \hat{\mathbf{p}}_{v-} \right] \cdot \hat{\mathbf{e}}^i. \quad (\text{B.23})$$

We pause here to reduce this result to the case where the nonlinear polarization  $\mathbf{P}(2\omega)$  radiates from vacuum instead from the layer  $\ell$ . For such case we simply take  $\epsilon_\ell(2\omega) = 1$  and  $\ell = v$  ( $T_{s,p}^{\ell v} = 1$ ), to get

$$\mathbf{e}_v^{2\omega} = \hat{\mathbf{e}}^F \cdot \left[ \hat{\mathbf{s}} T_s^{vb} \hat{\mathbf{s}} + \hat{\mathbf{P}}_{v+} \frac{T_p^{vb}}{\sqrt{\epsilon_b(2\omega)}} (\epsilon_b(2\omega) \sin \theta_0 \hat{\mathbf{z}} - W_b \hat{\boldsymbol{\kappa}}) \right], \quad (\text{B.24})$$

which agrees with Eq. (3.10) of Ref. [4].

In the 3-layer model the SH polarization  $\mathcal{P}(2\omega)$  is located in layer  $\ell$ , where we evaluate the fundamental field required in Eq. (1.9). We write

$$\begin{aligned} \mathbf{E}_\ell(\omega) &= E_0 \left( \hat{\mathbf{s}} t_s^{v\ell} (1 + r_s^{\ell b}) \hat{\mathbf{s}} + \hat{\mathbf{p}}_{\ell-} t_p^{v\ell} \hat{\mathbf{p}}_{v-} + \hat{\mathbf{p}}_{\ell+} t_p^{v\ell} r_p^{\ell b} \hat{\mathbf{p}}_{v-} \right) \cdot \hat{\mathbf{e}}^i \\ &= E_0 \mathbf{e}_\ell^\omega, \end{aligned} \quad (\text{B.25})$$

where  $\hat{\mathbf{e}}^i$  is the  $s$  ( $\hat{\mathbf{s}}$ ) or  $p$  ( $\hat{\mathbf{p}}_{v-}$ ) incoming polarization of the fundamental electric field. This field is composed of the transmitted field and its first reflection from the  $\ell b$  interface for  $s$  and  $p$  polarizations. The fundamental field, once inside the layer  $\ell$  will be reflected multiple times at the  $\ell v$  and  $\ell b$  interfaces. However, each reflection will diminish the intensity of the fundamental field. As the SSHG yield scales with the square of this field, the contribution of the subsequent reflections after the one considered in Eq. (B.25) can be safely neglected. From Eq. (1.14) we find that

$$\mathbf{e}_\ell^\omega = \left[ \hat{\mathbf{s}} t_s^{v\ell} t_s^{\ell b} \hat{\mathbf{s}} + \frac{t_p^{v\ell} t_p^{\ell b}}{n_\ell^2 n_b} (n_b^2 \sin \theta_0 \hat{\mathbf{z}} + n_\ell^2 w_b \hat{\boldsymbol{\kappa}}) \hat{\mathbf{p}}_{v-} \right] \cdot \hat{\mathbf{e}}^{\text{in}}. \quad (\text{B.26})$$

To connect with the work in Ref. [4], we evaluate the fields in the bulk instead of the layer  $\ell$  and simply take  $n_\ell = n_b$  ( $t_{s,p}^{\ell b} = 1$ ), to obtain

$$\mathbf{e}_b^\omega = \left[ \hat{\mathbf{s}} t_s^{vb} \hat{\mathbf{s}} + \frac{t_p^{vb}}{n_b} (\sin \theta_0 \hat{\mathbf{z}} + w_b \hat{\boldsymbol{\kappa}}) \hat{\mathbf{p}}_{v-} \right] \cdot \hat{\mathbf{e}}^{\text{in}}, \quad (\text{B.27})$$

that is in agreement with Eq. (3.5) of Ref. [4].

Replacing  $\mathbf{E}(\omega) \rightarrow E_0 \mathbf{e}_\ell^{\omega,i}$ , in Eq. (B.9), we obtain that

$$\mathcal{P}_\ell(2\omega) = \begin{cases} E_0^2 \chi : \mathbf{e}_\ell^{\omega,i} \mathbf{e}_\ell^{\omega,i} & (\text{cgs units}) \\ \epsilon_0 E_0^2 \chi : \mathbf{e}_\ell^{\omega,i} \mathbf{e}_\ell^{\omega,i} & (\text{MKS units}) \end{cases}, \quad (\text{B.28})$$

where  $\mathbf{e}_\ell^{\omega,i}$  is given by Eq. (B.23), and thus Eq. (B.20) reduces to ( $W_v = \cos \theta_0$ )

$$E(2\omega) = \frac{2\eta i\omega}{c \cos \theta_0} \mathbf{e}_\ell^{2\omega,F} \cdot \chi : \mathbf{e}_\ell^{\omega,i} \mathbf{e}_\ell^{\omega,i}, \quad (\text{B.29})$$

where  $\eta = 2\pi$  for cgs units and  $\eta = 1/2$  for MKS units. For ease of notation, we define

$$\Upsilon_{iF} \equiv \mathbf{e}_\ell^{2\omega,F} \cdot \chi : \mathbf{e}_\ell^{\omega,i} \mathbf{e}_\ell^{\omega,i}. \quad (\text{B.30})$$

From Eqs. (B.1), (B.2), and (B.29) we obtain that

$$\mathcal{R}_{iF} = \frac{\eta \omega^2}{c^3 \cos^2 \theta_0} \left| \frac{1}{n_\ell} \Upsilon_{iF} \right|^2, \quad (\text{B.31})$$

as the SSHG yield, where  $\eta = 32\pi^3$  for cgs units and  $\eta = 1/(2\epsilon_0)$  in MKS units. Since  $\chi$  is a surface second order nonlinear susceptibility, in the MKS unit system is given in  $\text{m}^2/\text{V}$ , and thus  $\mathcal{R}_{iF}$  is given in  $\text{m}^2/\text{W}$ .

It is worth mentioning that we can easily recover the results from Ref. [4], which are in turn equivalent to those in Ref. [10]. We simply take  $\mathbf{e}_\ell^{2\omega} \rightarrow \mathbf{e}_v^{2\omega}$ ,  $\mathbf{e}_\ell^\omega \rightarrow \mathbf{e}_b^\omega$ , and we have

$$\mathcal{R}_{iF}(2\omega) = \frac{\eta \omega^2}{c^3 \cos^2 \theta_0} \left| \mathbf{e}_v^{2\omega} \cdot \chi : \mathbf{e}_b^\omega \mathbf{e}_b^\omega \right|^2. \quad (\text{B.32})$$

This is the SSHG yield of a nonlinear polarization sheet radiating from the vacuum region above the surface, with the fundamental field evaluated below the surface in the bulk of the material characterized by  $\epsilon_b(\omega)$ .

# Appendix C

## Some limiting cases of interest

### Outline

---

C.1	The two layer model . . . . .	66
C.2	Taking $\mathcal{P}(2\omega)$ and the fundamental fields in the bulk . . . . .	67
C.3	Taking $\mathcal{P}(2\omega)$ and the fundamental fields in the vacuum . . . . .	69
C.4	Taking $\mathcal{P}(2\omega)$ in $\ell$ and the fundamental fields in the bulk . . . . .	71

---

In this section, we derive the expressions for  $\mathcal{R}_{pP}$  for different limiting cases. We evaluate  $\mathcal{P}(2\omega)$  and the fundamental fields in different regions. It is worth noting that the first case, the three layer model, can be reduced to any of the other cases by simply considering where we want to evaluate the  $1\omega$  and  $2\omega$  terms.

### C.1 The two layer model

In order to reduce above result to that of Ref. [4] and [10], we now consider that  $\mathcal{P}(2\omega)$  is evaluated in the vacuum region, while the fundamental fields are evaluated in the bulk region. To do this, we take the  $2\omega$  radiations factors for vacuum by taking  $\ell = v$ , thus  $\epsilon_\ell(2\omega) = 1$ ,  $T_p^{\ell v} = 1$ ,  $T_p^{\ell b} = T_p^{vb}$ , and the fundamental field inside medium  $b$  by taking  $\ell = b$ , thus  $\epsilon_\ell(\omega) = \epsilon_b(\omega)$ ,  $t_p^{v\ell} = t_p^{vb}$ , and  $t_p^{\ell b} = 1$ . With these choices

$$\mathbf{e}_v^{2\omega} \cdot \boldsymbol{\chi} : \mathbf{e}_b^\omega \mathbf{e}_b^\omega \equiv \Gamma_{pP}^{vb} r_{pP}^{vb},$$

where,

$$\begin{aligned} r_{pP}^{vb} &= \epsilon_b(2\omega) \sin \theta_0 \left( \sin^2 \theta_0 \chi_{zzz} + k_b^2 \chi_{zxx} \right) \\ &\quad - k_b K_b \left( 2 \sin \theta_0 \chi_{xxz} + k_b \chi_{xxx} \cos(3\phi) \right), \end{aligned}$$

and

$$\Gamma_{pP}^{vb} = \frac{T_p^{vb} (t_p^{vb})^2}{\epsilon_b(\omega) \sqrt{\epsilon_b(2\omega)}}.$$

## C.2 Taking $\mathcal{P}(2\omega)$ and the fundamental fields in the bulk

To consider the  $2\omega$  fields in the bulk, we start with Eq. (B.19) but substitute  $\ell \rightarrow b$ , thus

$$\mathbf{H}_b = \hat{\mathbf{s}} T_s^{bv} \left( 1 + R_s^{bb} \right) \hat{\mathbf{s}} + \hat{\mathbf{P}}_{v+} T_p^{bv} \left( \hat{\mathbf{P}}_{b+} + R_p^{bb} \hat{\mathbf{P}}_{b-} \right).$$

$R_p^{bb}$  and  $R_s^{bb}$  are zero, so we are left with

$$\begin{aligned} \mathbf{H}_b &= \hat{\mathbf{s}} T_s^{bv} \hat{\mathbf{s}} + \hat{\mathbf{P}}_{v+} T_p^{bv} \hat{\mathbf{P}}_{b+} \\ &= \frac{K_b}{K_v} \left( \hat{\mathbf{s}} T_s^{vb} \hat{\mathbf{s}} + \hat{\mathbf{P}}_{v+} T_p^{vb} \hat{\mathbf{P}}_{b+} \right) \\ &= \frac{K_b}{K_v} \left[ \hat{\mathbf{s}} T_s^{vb} \hat{\mathbf{s}} + \hat{\mathbf{P}}_{v+} \frac{T_p^{vb}}{\sqrt{\epsilon_b(2\omega)}} (\sin \theta_0 \hat{\mathbf{z}} - K_b \cos \phi \hat{\mathbf{x}} - K_b \sin \phi \hat{\mathbf{y}}) \right], \end{aligned}$$

and we define

$$\mathbf{e}_b^{2\omega} = \frac{K_b}{K_v} \hat{\mathbf{e}}^{\text{out}} \cdot \left[ \hat{\mathbf{s}} T_s^{vb} \hat{\mathbf{s}} + \hat{\mathbf{P}}_{v+} \frac{T_p^{vb}}{\sqrt{\epsilon_b(2\omega)}} (\sin \theta_0 \hat{\mathbf{z}} - K_b \cos \phi \hat{\mathbf{x}} - K_b \sin \phi \hat{\mathbf{y}}) \right].$$

For  $\mathcal{R}_{pP}$ , we require  $\hat{\mathbf{e}}^{\text{out}} = \hat{\mathbf{P}}_{v+}$ , so we have that

$$\mathbf{e}_b^{2\omega} = \frac{K_b}{K_v} \frac{T_p^{vb}}{\sqrt{\epsilon_b(2\omega)}} (\sin \theta_0 \hat{\mathbf{z}} - K_b \cos \phi \hat{\mathbf{x}} - K_b \sin \phi \hat{\mathbf{y}}).$$

The  $1\omega$  fields will still be evaluated inside the bulk, so we have

$$\mathbf{e}_b^\omega = \left[ \hat{\mathbf{s}} t_s^{vb} \hat{\mathbf{s}} + \frac{t_p^{vb}}{\sqrt{\epsilon_b(\omega)}} (\sin \theta_0 \hat{\mathbf{z}} + k_b \cos \phi \hat{\mathbf{x}} + k_b \sin \phi \hat{\mathbf{y}}) \hat{\mathbf{p}}_{v-} \right] \cdot \hat{\mathbf{e}}^{\text{in}},$$

and for our particular case of  $\hat{\mathbf{e}}^{\text{in}} = \hat{\mathbf{p}}_{v-}$ ,

$$\mathbf{e}_b^\omega = \frac{t_p^{vb}}{\sqrt{\epsilon_b(\omega)}} (\sin \theta_0 \hat{\mathbf{z}} + k_b \cos \phi \hat{\mathbf{x}} + k_b \sin \phi \hat{\mathbf{y}}),$$

and

$$\begin{aligned} \mathbf{e}_b^\omega \mathbf{e}_b^\omega &= \frac{(t_p^{vb})^2}{\epsilon_b(\omega)} (\sin \theta_0 \hat{\mathbf{z}} + k_b \cos \phi \hat{\mathbf{x}} + k_b \sin \phi \hat{\mathbf{y}})^2 \\ &= \frac{(t_p^{vb})^2}{\epsilon_b(\omega)} \left( \sin^2 \theta_0 \hat{\mathbf{z}} \hat{\mathbf{z}} + k_b^2 \cos^2 \phi \hat{\mathbf{x}} \hat{\mathbf{x}} + k_b^2 \sin^2 \phi \hat{\mathbf{y}} \hat{\mathbf{y}} \right. \\ &\quad \left. + 2k_b \sin \theta_0 \cos \phi \hat{\mathbf{z}} \hat{\mathbf{x}} + 2k_b \sin \theta_0 \sin \phi \hat{\mathbf{z}} \hat{\mathbf{y}} + 2k_b^2 \sin \phi \cos \phi \hat{\mathbf{x}} \hat{\mathbf{y}} \right) \end{aligned}$$

So lastly, we have that

$$\begin{aligned}
\mathbf{e}_b^{2\omega} \cdot \boldsymbol{\chi} : \mathbf{e}_b^\omega \mathbf{e}_b^\omega &= \frac{K_b}{K_v} \frac{T_p^{vb} (t_p^{vb})^2}{\epsilon_b(\omega) \sqrt{\epsilon_b(2\omega)}} \left( \sin^3 \theta_0 \chi_{zzz} \right. \\
&\quad + k_b^2 \sin \theta_0 \cos^2 \phi \chi_{zxx} \\
&\quad + k_b^2 \sin \theta_0 \sin^2 \phi \chi_{zyy} \\
&\quad + 2k_b \sin^2 \theta_0 \cos \phi \chi_{zzx} \\
&\quad + 2k_b \sin^2 \theta_0 \sin \phi \chi_{zzy} \\
&\quad + 2k_b^2 \sin \theta_0 \sin \phi \cos \phi \chi_{zxy} \\
&\quad - K_b \sin^2 \theta_0 \cos \phi \chi_{xzz} \\
&\quad - k_b^2 K_b \cos^3 \phi \chi_{xxx} \\
&\quad - k_b^2 K_b \sin^2 \phi \cos \phi \chi_{xyy} \\
&\quad - 2k_b K_b \sin \theta_0 \cos^2 \phi \chi_{xzx} \\
&\quad - 2k_b K_b \sin \theta_0 \sin \phi \cos \phi \chi_{xzy} \\
&\quad - 2k_b^2 K_b \sin \phi \cos^2 \phi \chi_{xxy} \\
&\quad - K_b \sin^2 \theta_0 \sin \phi \chi_{yzz} \\
&\quad - k_b^2 K_b \sin \phi \cos^2 \phi \chi_{yxz} \\
&\quad - k_b^2 K_b \sin^3 \phi \chi_{yyy} \\
&\quad - 2k_b K_b \sin \theta_0 \sin \phi \cos \phi \chi_{yzx} \\
&\quad - 2k_b K_b \sin \theta_0 \sin^2 \phi \chi_{yzy} \\
&\quad \left. - 2k_b^2 K_b \sin^2 \phi \cos \phi \chi_{yxy} \right),
\end{aligned}$$

and we can eliminate many terms since  $\chi_{zzx} = \chi_{zzy} = \chi_{zxy} = \chi_{xzz} = \chi_{xzy} = \chi_{xxy} = \chi_{yzz} = \chi_{yxz} = \chi_{yyy} = \chi_{yzx} = 0$ , and substituting the equivalent components of  $\boldsymbol{\chi}$ ,

$$\begin{aligned}
&= \frac{K_b}{K_v} \Gamma_{pP}^b \left( \sin^3 \theta_0 \chi_{zzz} \right. \\
&\quad + k_b^2 \sin \theta_0 \cos^2 \phi \chi_{zxx} \\
&\quad + k_b^2 \sin \theta_0 \sin^2 \phi \chi_{zxx} \\
&\quad - 2k_b K_b \sin \theta_0 \cos^2 \phi \chi_{xxz} \\
&\quad - 2k_b K_b \sin \theta_0 \sin^2 \phi \chi_{xxz} \\
&\quad - k_b^2 K_b \cos^3 \phi \chi_{xxx} \\
&\quad + k_b^2 K_b \sin^2 \phi \cos \phi \chi_{xxx} \\
&\quad \left. + 2k_b^2 K_b \sin^2 \phi \cos \phi \chi_{xxx} \right),
\end{aligned}$$

and reducing,

$$\begin{aligned}
&= \frac{K_b}{K_v} \Gamma_{pP}^b (\sin^3 \theta_0 \chi_{zzz} \\
&\quad + k_b^2 \sin \theta_0 (\sin^2 \phi + \cos^2 \phi) \chi_{zxx} \\
&\quad - 2k_b K_b \sin \theta_0 (\sin^2 \phi + \cos^2 \phi) \chi_{xxz} \\
&\quad + k_b^2 K_b (3 \sin^2 \phi \cos \phi - \cos^3 \phi) \chi_{xxx}) \\
&= \frac{K_b}{K_v} \Gamma_{pP}^b (\sin^3 \theta_0 \chi_{zzz} + k_b^2 \sin \theta_0 \chi_{zxx} - 2k_b K_b \sin \theta_0 \chi_{xxz} - k_b^2 K_b \chi_{xxx} \cos 3\phi),
\end{aligned}$$

where,

$$\Gamma_{pP}^b = \frac{T_p^{vb} (t_p^{vb})^2}{\epsilon_b(\omega) \sqrt{\epsilon_b(2\omega)}}.$$

We find the equivalent expression for  $\mathcal{R}$  evaluated inside the bulk as

$$R(2\omega) = \frac{32\pi^3 \omega^2}{c^3 K_b^2} |\mathbf{e}_b^{2\omega} \cdot \boldsymbol{\chi} : \mathbf{e}_b^\omega \mathbf{e}_b^\omega|^2,$$

and we can remove the  $K_b/K_v$  factor completely and reduce to the standard form of

$$R(2\omega) = \frac{32\pi^3 \omega^2}{c^3 \cos^2 \theta_0} |\mathbf{e}_b^{2\omega} \cdot \boldsymbol{\chi} : \mathbf{e}_b^\omega \mathbf{e}_b^\omega|^2.$$

### C.3 Taking $\mathcal{P}(2\omega)$ and the fundamental fields in the vacuum

To consider the  $1\omega$  fields in the vacuum, we start with Eq. (B.22) but substitute  $\ell \rightarrow v$ , thus

$$\mathbf{E}_v(\omega) = E_0 \left[ \hat{\mathbf{s}} t_s^{vv} (1 + r_s^{vb}) \hat{\mathbf{s}} + \hat{\mathbf{p}}_v - t_p^{vv} \hat{\mathbf{p}}_{v-} + \hat{\mathbf{p}}_v + t_p^{vv} r_p^{vb} \hat{\mathbf{p}}_{v-} \right] \cdot \hat{\mathbf{e}}^{\text{in}},$$

$t_p^{vv}$  and  $t_s^{vv}$  are one, so we are left with

$$\begin{aligned}
\mathbf{e}_v^\omega &= \left[ \hat{\mathbf{s}} (1 + r_s^{vb}) \hat{\mathbf{s}} + \hat{\mathbf{p}}_v - \hat{\mathbf{p}}_{v-} + \hat{\mathbf{p}}_v + r_p^{vb} \hat{\mathbf{p}}_{v-} \right] \cdot \hat{\mathbf{e}}^{\text{in}} \\
&= \left[ \hat{\mathbf{s}} (t_s^{vb}) \hat{\mathbf{s}} + (\hat{\mathbf{p}}_{v-} + \hat{\mathbf{p}}_v + r_p^{vb}) \hat{\mathbf{p}}_{v-} \right] \cdot \hat{\mathbf{e}}^{\text{in}} \\
&= \left[ \hat{\mathbf{s}} (t_s^{vb}) \hat{\mathbf{s}} + \frac{1}{\sqrt{\epsilon_v(\omega)}} (k_v (1 - r_p^{vb}) \hat{\boldsymbol{\kappa}} + \sin \theta_0 (1 + r_p^{vb}) \hat{\mathbf{z}}) \hat{\mathbf{p}}_{v-} \right] \\
&= \left[ \hat{\mathbf{s}} (t_s^{vb}) \hat{\mathbf{s}} + \left( \frac{k_b}{\sqrt{\epsilon_b(\omega)}} t_p^{vb} \hat{\boldsymbol{\kappa}} + \sqrt{\epsilon_b(\omega)} \sin \theta_0 t_p^{vb} \hat{\mathbf{z}} \right) \hat{\mathbf{p}}_{v-} \right] \cdot \hat{\mathbf{e}}^{\text{in}} \\
&= \left[ \hat{\mathbf{s}} (t_s^{vb}) \hat{\mathbf{s}} + \frac{t_p^{vb}}{\sqrt{\epsilon_b(\omega)}} (k_b \cos \phi \hat{\mathbf{x}} + k_b \sin \phi \hat{\mathbf{y}} + \epsilon_b(\omega) \sin \theta_0 \hat{\mathbf{z}}) \hat{\mathbf{p}}_{v-} \right] \cdot \hat{\mathbf{e}}^{\text{in}}.
\end{aligned}$$

For  $\mathcal{R}_{pP}$  we require that  $\hat{\mathbf{e}}^{\text{in}} = \hat{\mathbf{p}}_{v-}$ , so

$$\mathbf{e}_v^\omega = \frac{t_p^{vb}}{\sqrt{\epsilon_b(\omega)}} (k_b \cos \phi \hat{\mathbf{x}} + k_b \sin \phi \hat{\mathbf{y}} + \epsilon_b(\omega) \sin \theta_0 \hat{\mathbf{z}}),$$

and

$$\begin{aligned}\mathbf{e}_v^\omega \mathbf{e}_v^\omega = & \left( \frac{t_p^{vb}}{\sqrt{\epsilon_b(\omega)}} \right)^2 [k_b^2 \cos^2 \phi \hat{\mathbf{x}} \hat{\mathbf{x}} \\ & + k_b^2 \sin^2 \phi \hat{\mathbf{y}} \hat{\mathbf{y}} \\ & + \epsilon_b^2(\omega) \sin^2 \theta_0 \hat{\mathbf{z}} \hat{\mathbf{z}} \\ & + 2k_b^2 \sin \phi \cos \phi \hat{\mathbf{x}} \hat{\mathbf{y}} \\ & + 2\epsilon_b(\omega) k_b \sin \theta_0 \sin \phi \hat{\mathbf{y}} \hat{\mathbf{z}} \\ & + 2\epsilon_b(\omega) k_b \sin \theta_0 \cos \phi \hat{\mathbf{x}} \hat{\mathbf{z}}].\end{aligned}$$

We also require the  $2\omega$  fields evaluated in the vacuum, so

$$\mathbf{e}_v^{2\omega} = \hat{\mathbf{e}}^{\text{out}} \cdot \left[ \hat{\mathbf{s}} T_s^{vb} \hat{\mathbf{s}} + \hat{\mathbf{P}}_{v+} \frac{T_p^{vb}}{\sqrt{\epsilon_b(2\omega)}} (\epsilon_b(2\omega) \sin \theta_0 \hat{\mathbf{z}} - K_b \hat{\mathbf{k}}) \right], \quad (\text{C.1})$$

and with  $\hat{\mathbf{e}}^{\text{out}} = \hat{\mathbf{P}}_{v+}$  we have

$$\mathbf{e}_v^{2\omega} = \frac{T_p^{vb}}{\sqrt{\epsilon_b(2\omega)}} (\epsilon_b(2\omega) \sin \theta_0 \hat{\mathbf{z}} - K_b \cos \phi \hat{\mathbf{x}} - K_b \sin \phi \hat{\mathbf{y}}). \quad (\text{C.2})$$

So lastly, we have that

$$\begin{aligned}\mathbf{e}_v^{2\omega} \cdot \boldsymbol{\chi} : \mathbf{e}_v^\omega \mathbf{e}_v^\omega = & \frac{T_p^{vb}}{\sqrt{\epsilon_b(2\omega)}} \left( \frac{t_p^{vb}}{\sqrt{\epsilon_b(\omega)}} \right)^2 [\epsilon_b(2\omega) k_b^2 \sin \theta_0 \cos^2 \phi \chi_{zxx} \\ & + \epsilon_b(2\omega) k_b^2 \sin \theta_0 \sin^2 \phi \chi_{zyy} \\ & + \epsilon_b^2(\omega) \epsilon_b(2\omega) \sin^3 \theta_0 \chi_{zzz} \\ & + 2\epsilon_b(2\omega) k_b^2 \sin \theta_0 \sin \phi \cos \phi \chi_{zxy} \\ & + 2\epsilon_b(\omega) \epsilon_b(2\omega) k_b \sin^2 \theta_0 \sin \phi \chi_{zyz} \\ & + 2\epsilon_b(\omega) \epsilon_b(2\omega) k_b \sin^2 \theta_0 \cos \phi \chi_{zxz} \\ & - k_b^2 K_b \cos^3 \phi \chi_{xxx} \\ & - k_b^2 K_b \sin^2 \phi \cos \phi \chi_{xyy} \\ & - \epsilon_b^2(\omega) K_b \sin^2 \theta_0 \cos \phi \chi_{xzz} \\ & - 2k_b^2 K_b \sin \phi \cos^2 \phi \chi_{xxy} \\ & - 2\epsilon_b(\omega) k_b K_b \sin \theta_0 \sin \phi \cos \phi \chi_{xyz} \\ & - 2\epsilon_b(\omega) k_b K_b \sin \theta_0 \cos^2 \phi \chi_{xxz} \\ & - k_b^2 K_b \sin \phi \cos^2 \phi \chi_{yxx} \\ & - k_b^2 K_b \sin^3 \phi \chi_{yyy} \\ & - \epsilon_b^2(\omega) K_b \sin^2 \theta_0 \sin \phi \chi_{yzz} \\ & - 2k_b^2 K_b \sin^2 \phi \cos \phi \chi_{yxy} \\ & - 2\epsilon_b(\omega) k_b K_b \sin \theta_0 \sin^2 \phi \chi_{yyz} \\ & - 2\epsilon_b(\omega) k_b K_b \sin \theta_0 \sin \phi \cos \phi \chi_{yxz}],\end{aligned}$$

and after eliminating components,

$$\begin{aligned}
&= \Gamma_{pP}^v [\epsilon_b^2(\omega) \epsilon_b(2\omega) \sin^3 \theta_0 \chi_{zzz} \\
&\quad + \epsilon_b(2\omega) k_b^2 \sin \theta_0 \cos^2 \phi \chi_{zxx} \\
&\quad + \epsilon_b(2\omega) k_b^2 \sin \theta_0 \sin^2 \phi \chi_{zxz} \\
&\quad - 2\epsilon_b(\omega) k_b K_b \sin \theta_0 \cos^2 \phi \chi_{xxz} \\
&\quad - 2\epsilon_b(\omega) k_b K_b \sin \theta_0 \sin^2 \phi \chi_{xxz} \\
&\quad + 3k_b^2 K_b \sin^2 \phi \cos \phi \chi_{xxx} \\
&\quad - k_b^2 K_b \cos^3 \phi \chi_{xxx}] \\
&= \Gamma_{pP}^v [\epsilon_b^2(\omega) \epsilon_b(2\omega) \sin^3 \theta_0 \chi_{zzz} + \epsilon_b(2\omega) k_b^2 \sin \theta_0 \chi_{zxz} \\
&\quad - 2\epsilon_b(\omega) k_b K_b \sin \theta_0 \chi_{xxz} - k_b^2 K_b \chi_{xxx} \cos 3\phi],
\end{aligned}$$

where

$$\Gamma_{pP}^v = \frac{T_p^{vb} (t_p^{vb})^2}{\epsilon_b(\omega) \sqrt{\epsilon_b(2\omega)}}.$$

#### C.4 Taking $\mathcal{P}(2\omega)$ in $\ell$ and the fundamental fields in the bulk

For this scenario with  $\hat{\mathbf{e}}^{\text{in}} = \hat{\mathbf{p}}_{v-}$  and  $\hat{\mathbf{e}}^{\text{out}} = \hat{\mathbf{P}}_{v+}$  we have,

$$\mathbf{e}_\ell^{2\omega} = \frac{T_p^{v\ell} T_p^{\ell b}}{\epsilon_\ell(2\omega) \sqrt{\epsilon_b(2\omega)}} (\epsilon_b(2\omega) \sin \theta_0 \hat{\mathbf{z}} - \epsilon_\ell(2\omega) K_b \cos \phi \hat{\mathbf{x}} - \epsilon_\ell(2\omega) K_b \sin \phi \hat{\mathbf{y}}),$$

and

$$\begin{aligned}
\mathbf{e}_b^\omega \mathbf{e}_b^\omega &= \frac{(t_p^{vb})^2}{\epsilon_b(\omega)} (\sin^2 \theta_0 \hat{\mathbf{z}} \hat{\mathbf{z}} + k_b^2 \cos^2 \phi \hat{\mathbf{x}} \hat{\mathbf{x}} + k_b^2 \sin^2 \phi \hat{\mathbf{y}} \hat{\mathbf{y}} \\
&\quad + 2k_b \sin \theta_0 \cos \phi \hat{\mathbf{z}} \hat{\mathbf{x}} + 2k_b \sin \theta_0 \sin \phi \hat{\mathbf{z}} \hat{\mathbf{y}} + 2k_b^2 \sin \phi \cos \phi \hat{\mathbf{x}} \hat{\mathbf{y}}).
\end{aligned}$$

Thus,

$$\mathbf{e}_\ell^{2\omega} \cdot \boldsymbol{\chi} : \mathbf{e}_b^\omega \mathbf{e}_b^\omega = \frac{T_p^{v\ell} T_p^{\ell b} (t_p^{vb})^2}{\epsilon_\ell(2\omega) \epsilon_b(\omega) \sqrt{\epsilon_b(2\omega)}} \left[ + \epsilon_b(2\omega) \sin^3 \theta_0 \chi_{zzz} \right.$$

$$+ \epsilon_b(2\omega) k_b^2 \sin \theta_0 \cos^2 \phi \chi_{zxx}$$

$$+ \epsilon_b(2\omega) k_b^2 \sin \theta_0 \sin^2 \phi \chi_{zyy}$$

$$+ 2\epsilon_b(2\omega) k_b \sin^2 \theta_0 \cos \phi \chi_{zzx}$$

$$+ 2\epsilon_b(2\omega) k_b \sin^2 \theta_0 \sin \phi \chi_{zzy}$$

$$+ 2\epsilon_b(2\omega) k_b^2 \sin \theta_0 \sin \phi \cos \phi \chi_{zxy}$$

$$- \epsilon_\ell(2\omega) \sin^2 \theta_0 K_b \cos \phi \chi_{xzz}$$

$$- \epsilon_\ell(2\omega) k_b^2 K_b \cos^3 \phi \chi_{xxx}$$

$$- \epsilon_\ell(2\omega) k_b^2 K_b \sin^2 \phi \cos \phi \chi_{xyy}$$

$$- 2\epsilon_\ell(2\omega) k_b K_b \sin \theta_0 \cos^2 \phi \chi_{xzx}$$

$$- 2\epsilon_\ell(2\omega) k_b K_b \sin \theta_0 \sin \phi \cos \phi \chi_{xzy}$$

$$- 2\epsilon_\ell(2\omega) k_b^2 K_b \sin \phi \cos^2 \phi \chi_{xxy}$$

$$- \epsilon_\ell(2\omega) K_b \sin^2 \theta_0 \sin \phi \chi_{yzz}$$

$$- \epsilon_\ell(2\omega) k_b^2 K_b \cos^2 \phi \sin \phi \chi_{yxx}$$

$$- \epsilon_\ell(2\omega) k_b^2 K_b \sin^3 \phi \chi_{yyy}$$

$$- 2\epsilon_\ell(2\omega) k_b K_b \sin \theta_0 \cos \phi \sin \phi \chi_{yzx}$$

$$- 2\epsilon_\ell(2\omega) k_b K_b \sin \theta_0 \sin^2 \phi \chi_{yzy}$$

$$\left. - 2\epsilon_\ell(2\omega) k_b^2 K_b \sin^2 \phi \cos \phi \chi_{yxy} \right].$$

We eliminate and replace components,

$$\mathbf{e}_\ell^{2\omega} \cdot \boldsymbol{\chi} : \mathbf{e}_b^\omega \mathbf{e}_b^\omega = \Gamma_{pP}^{\ell b} \left[ + \epsilon_b(2\omega) \sin^3 \theta_0 \chi_{zzz} \right.$$

$$+ \epsilon_b(2\omega) k_b^2 \sin \theta_0 \cos^2 \phi \chi_{zxx}$$

$$+ \epsilon_b(2\omega) k_b^2 \sin \theta_0 \sin^2 \phi \chi_{zxx}$$

$$- 2\epsilon_\ell(2\omega) k_b K_b \sin \theta_0 \cos^2 \phi \chi_{xxz}$$

$$- 2\epsilon_\ell(2\omega) k_b K_b \sin \theta_0 \sin^2 \phi \chi_{xxz}$$

$$- \epsilon_\ell(2\omega) k_b^2 K_b \cos^3 \phi \chi_{xxx}$$

$$+ \epsilon_\ell(2\omega) k_b^2 K_b \sin^2 \phi \cos \phi \chi_{xxx}$$

$$\left. + 2\epsilon_\ell(2\omega) k_b^2 K_b \sin^2 \phi \cos \phi \chi_{xxx} \right],$$

so lastly

$$\mathbf{e}_\ell^{2\omega} \cdot \boldsymbol{\chi} : \mathbf{e}_b^\omega \mathbf{e}_b^\omega = \Gamma_{pP}^{\ell b} \left[ \epsilon_b(2\omega) \sin^3 \theta_0 \chi_{zzz} + \epsilon_b(2\omega) k_b^2 \sin \theta_0 \chi_{zxx} \right.$$

$$\left. - 2\epsilon_\ell(2\omega) k_b K_b \sin \theta_0 \chi_{xxz} - \epsilon_\ell(2\omega) k_b^2 K_b \chi_{xxx} \cos 3\phi \right],$$

where

$$\Gamma_{pP}^{\ell b} = \frac{T_p^{v\ell} T_p^{\ell b} (t_p^{vb})^2}{\epsilon_\ell(2\omega) \epsilon_b(\omega) \sqrt{\epsilon_b(2\omega)}}.$$

## Appendix D

# The two layer model for SHG radiation from Sipe, Moss, and van Driel

### Outline

---

D.1	$\mathcal{R}_{pP}$	75
D.2	$\mathcal{R}_{pS}$	77
D.3	$\mathcal{R}_{sP}$	78
D.4	Summary	79

---

In this treatment we follow the work of Ref. [10]. They define the following for all polarizations;

$$\begin{aligned} f_s &= \frac{\kappa}{n\tilde{\omega}} = \frac{\kappa}{\sqrt{\epsilon(\omega)}\tilde{\omega}}, \\ f_c &= \frac{w}{n\tilde{\omega}} = \frac{w}{\sqrt{\epsilon(\omega)}\tilde{\omega}}, \\ f_s^2 + f_c^2 &= 1, \end{aligned} \tag{D.1}$$

where

$$\kappa = \tilde{\omega} \sin \theta, \tag{D.2}$$

$$w_0 = \sqrt{\tilde{\omega} - \kappa^2} = \tilde{\omega} \cos \theta, \tag{D.2}$$

$$w = \sqrt{\tilde{\omega}\epsilon(\omega) - \kappa^2} = \tilde{\omega}k_z(\omega). \tag{D.3}$$

From this point on, all capital letters and symbols indicate evaluation at  $2\omega$ . Common to all three polarization cases studied here, we require the nonzero components for the (111) face for crystals

with  $C_{3v}$  symmetry,

$$\begin{aligned}\delta_{11} &= \chi^{xxx} = -\chi^{xyy} = -\chi^{yyx}, \\ \delta_{15} &= \chi^{xxz} = \chi^{yyz}, \\ \delta_{31} &= \chi^{zxx} = \chi^{zyy}, \\ \delta_{33} &= \chi^{zzz}.\end{aligned}\tag{D.4}$$

Lastly, the remaining quantities that will be needed for all three cases are

$$\begin{aligned}A_p &= \frac{4\pi\tilde{\Omega}\sqrt{\epsilon(2\omega)}}{W_0\epsilon(2\omega) + W}, \\ A_s &= \frac{4\pi\tilde{\Omega}}{W_0 + W}.\end{aligned}\tag{D.5}$$

## D.1 $\mathcal{R}_{pP}$

For the (111) face ( $m = 3$ ), we have

$$\frac{E^{(2\omega)}(\parallel, \parallel)}{E_p^2 A_p} = a_{\parallel, \parallel} + c_{\parallel, \parallel}^{(3)} \cos 3\phi.\tag{D.6}$$

We extract these coefficients from Table V, noting that  $\Gamma = \gamma = 0$  as we are only interested in the surface contribution,

$$\begin{aligned}a_{\parallel, \parallel} &= i\tilde{\Omega}F_s\epsilon(2\omega)\delta_{31} + i\tilde{\Omega}\epsilon(2\omega)F_sf_s^2(\delta_{33} - \delta_{31}) - 2i\tilde{\Omega}f_sf_cF_c\delta_{15}, \\ c_{\parallel, \parallel}^{(3)} &= -i\tilde{\Omega}F_cf_c^2\delta_{11}.\end{aligned}$$

We substitute these in Eq. (D.6),

$$\begin{aligned}\frac{E^{(2\omega)}(\parallel, \parallel)}{E_p^2 A_p} &= i\tilde{\Omega}F_s\epsilon(2\omega)\delta_{31} + i\tilde{\Omega}\epsilon(2\omega)F_sf_s^2(\delta_{33} - \delta_{31}) \\ &\quad - 2i\tilde{\Omega}f_sf_cF_c\delta_{15} - i\tilde{\Omega}F_cf_c^2\delta_{11} \cos 3\phi\end{aligned}$$

and reduce (omitting the  $(\parallel, \parallel)$  notation),

$$\begin{aligned}\frac{E^{(2\omega)}}{E_p^2} &= A_p i\tilde{\Omega} [F_s\epsilon(2\omega)(\delta_{31} + f_s^2(\delta_{33} - \delta_{31})) - f_cF_c(2f_s\delta_{15} + f_c\delta_{11} \cos 3\phi)] \\ &= A_p i\tilde{\Omega} [F_s\epsilon(2\omega)(f_s^2\delta_{33} + (1 - f_s^2)\delta_{31}) - f_cF_c(2f_s\delta_{15} + f_c\delta_{11} \cos 3\phi)] \\ &= A_p i\tilde{\Omega} [F_s\epsilon(2\omega)(f_s^2\delta_{33} + f_c^2\delta_{31}) - f_cF_c(2f_s\delta_{15} + f_c\delta_{11} \cos 3\phi)].\end{aligned}$$

As every term has an  $f_i^2 F_i$ , we can factor out the common

$$\frac{1}{\tilde{\omega}^2 \tilde{\Omega} \epsilon(\omega) \sqrt{\epsilon(2\omega)}}$$

factor after substituting the appropriate terms from Eq. (D.1),

$$\begin{aligned}
\frac{E^{(2\omega)}}{E_p^2} &= \frac{A_p i}{\epsilon(\omega) \sqrt{\epsilon(2\omega)} \tilde{\omega}^2} [K\epsilon(2\omega)(\kappa^2 \delta_{33} + w^2 \delta_{31}) - wW(2\kappa \delta_{15} + w \delta_{11} \cos 3\phi)] \\
&= \frac{A_p i \tilde{\Omega}}{\epsilon(\omega) \sqrt{\epsilon(2\omega)}} [\sin \theta \epsilon(2\omega) (\sin^2 \theta \delta_{33} + k_z^2(\omega) \delta_{31}) \\
&\quad - k_z(\omega) k_z(2\omega) (2 \sin \theta \delta_{15} + k_z(\omega) \delta_{11} \cos 3\phi)] \\
&= \frac{A_p i \tilde{\Omega}}{\epsilon(\omega) \sqrt{\epsilon(2\omega)}} [\sin \theta \epsilon(2\omega) (\sin^2 \theta \chi^{zzz} + k_z^2(\omega) \chi^{xxx}) \\
&\quad - k_z(\omega) k_z(2\omega) (2 \sin \theta \chi^{xxz} + k_z(\omega) \chi^{xxx} \cos 3\phi)].
\end{aligned}$$

We substitute Eq. (D.5) to complete the expression,

$$\begin{aligned}
\frac{E^{(2\omega)}}{E_p^2} &= \frac{4i\pi\tilde{\Omega}^2}{\epsilon(\omega)(W_0\epsilon(2\omega) + W)} [\dots] \\
&= \frac{4i\pi\tilde{\Omega}}{\epsilon(\omega)(\epsilon(2\omega) \cos \theta + k_z(2\omega))} [\dots] \\
&= \frac{4i\pi\tilde{\omega}}{\cos \theta} \frac{1}{\epsilon(\omega)} \frac{2 \cos \theta}{\epsilon(2\omega) \cos \theta + k_z(2\omega)} [\dots].
\end{aligned}$$

However, our interest lies in  $\mathcal{R}_{pP}$  which is calculated as

$$\mathcal{R}_{pP} = \frac{I_p(2\omega)}{I_p^2(\omega)} = \frac{2\pi}{c} \left| \frac{E^{(2\omega)}(\parallel, \parallel)}{E_p^2} \right|^2,$$

and we can finally complete the expression,

$$\begin{aligned}
\mathcal{R}_{pP} &= \frac{2\pi}{c} \left| \frac{4i\pi\tilde{\omega}}{\cos \theta} \frac{1}{\epsilon(\omega)} \frac{2 \cos \theta}{\epsilon(2\omega) \cos \theta + k_z(2\omega)} r_{pP} \right|^2 \\
&= \frac{32\pi^3 \tilde{\omega}^2}{c \cos^2 \theta} |t_p(\omega) T_p(2\omega) r_{pP}|^2 \\
&= \frac{32\pi^3 \omega^2}{c^3 \cos^2 \theta} |t_p(\omega) T_p(2\omega) r_{pP}|^2,
\end{aligned} \tag{D.7}$$

where

$$\begin{aligned}
t_p(\omega) &= \frac{1}{\epsilon(\omega)}, \\
T_p(2\omega) &= \frac{2 \cos \theta}{\epsilon(2\omega) \cos \theta + k_z(2\omega)}, \\
r_{pP} &= \sin \theta \epsilon(2\omega) (\sin^2 \theta \chi^{zzz} + k_z^2(\omega) \chi^{xxx}) \\
&\quad - k_z(\omega) k_z(2\omega) (2 \sin \theta \chi^{xxz} + k_z(\omega) \chi^{xxx} \cos 3\phi).
\end{aligned}$$

## D.2 $\mathcal{R}_{pS}$

We follow the same procedure as above. For the (111) face ( $m = 3$ ),

$$\frac{E^{(2\omega)}(\parallel, \perp)}{E_p^2 A_s} = b_{\parallel, \perp}^{(3)} \sin 3\phi, \quad (\text{D.8})$$

and we extract the relevant coefficient from Table V with  $\Gamma = \gamma = 0$ ,

$$b_{\parallel, \perp}^{(3)} = i\tilde{\Omega} f_c^2 \delta_{11}.$$

Substituting this coefficient and Eq. (D.5) into Eq. (D.8),

$$\begin{aligned} \frac{E^{(2\omega)}(\parallel, \perp)}{E_p^2} &= A_s i\tilde{\Omega} f_c^2 \delta_{11} \sin 3\phi \\ &= \frac{A_s i\tilde{\Omega}}{\tilde{\omega}^2 \epsilon(\omega)} w^2 \delta_{11} \sin 3\phi \\ &= \frac{A_s i\tilde{\Omega}}{\epsilon(\omega)} k_z^2(\omega) \delta_{11} \sin 3\phi \\ &= \frac{A_s i\tilde{\Omega}}{\epsilon(\omega)} k_z^2(\omega) \chi^{xxx} \sin 3\phi \\ &= \frac{4i\pi\tilde{\Omega}^2}{W_0 + W} \frac{1}{\epsilon(\omega)} k_z^2(\omega) \chi^{xxx} \sin 3\phi \\ &= 4i\pi\tilde{\Omega} \frac{1}{\epsilon(\omega) \cos \theta + k_z(2\omega)} k_z^2(\omega) \chi^{xxx} \sin 3\phi \\ &= \frac{4i\pi\omega}{c \cos \theta} \frac{1}{\epsilon(\omega) \cos \theta + k_z(2\omega)} k_z^2(\omega) \chi^{xxx} \sin 3\phi \end{aligned}$$

As before, we must calculate

$$\mathcal{R}_{pS} = \frac{2\pi}{c} \left| \frac{E^{(2\omega)}(\parallel, \perp)}{E_s^2} \right|^2,$$

to obtain the final expression,

$$\begin{aligned} \mathcal{R}_{pS} &= \frac{2\pi}{c} \left| \frac{4i\pi\omega}{c \cos \theta} \frac{1}{\epsilon(\omega) \cos \theta + k_z(2\omega)} k_z^2(\omega) \chi^{xxx} \sin 3\phi \right|^2 \\ &= \frac{32\pi^3 \omega^2}{c^3 \cos^2 \theta} \left| \frac{1}{\epsilon(\omega) \cos \theta + k_z(2\omega)} k_z^2(\omega) \chi^{xxx} \sin 3\phi \right|^2 \\ &= \frac{32\pi^3 \omega^2}{c^3 \cos^2 \theta} |t_p(\omega) T_s(2\omega) k_z^2(\omega) r_{pS}|^2, \end{aligned} \quad (\text{D.9})$$

where

$$\begin{aligned} t_p(\omega) &= \frac{1}{\epsilon(\omega)}, \\ T_s(2\omega) &= \frac{2 \cos \theta}{\cos \theta + k_z(2\omega)}, \\ r_{pS} &= k_z^2(\omega) \chi^{xxx} \sin 3\phi. \end{aligned}$$

### D.3 $\mathcal{R}_{sP}$

We follow the same procedure as above for the final polarization case. For the (111) face ( $m = 3$ ),

$$\frac{E^{(2\omega)}(\perp, \parallel)}{E_s^2 A_p} = a_{\perp, \parallel} + c_{\perp, \parallel}^{(3)} \cos 3\phi, \quad (\text{D.10})$$

and we extract the relevant coefficients from Table V with  $\Gamma = \gamma = 0$ ,

$$\begin{aligned} a_{\perp, \parallel} &= i\tilde{\Omega}F_s\epsilon(2\omega)\delta_{31}, \\ c_{\perp, \parallel}^{(3)} &= i\tilde{\Omega}F_c\delta_{11}. \end{aligned}$$

Substituting this coefficient and Eq. (D.5) into Eq. (D.10),

$$\begin{aligned} \frac{E^{(2\omega)}(\perp, \parallel)}{E_s^2} &= A_p(i\tilde{\Omega}F_s\epsilon(2\omega)\delta_{31} + i\tilde{\Omega}F_c\delta_{11}\cos 3\phi) \\ &= A_p i\tilde{\Omega}(F_s\epsilon(2\omega)\delta_{31} + F_c\delta_{11}\cos 3\phi) \\ &= \frac{A_p i\tilde{\Omega}}{\sqrt{\epsilon(2\omega)}}(\sin\theta\epsilon(2\omega)\delta_{31} + k_z(2\omega)\delta_{11}\cos 3\phi) \\ &= \frac{A_p i\tilde{\Omega}}{\sqrt{\epsilon(2\omega)}}(\sin\theta\epsilon(2\omega)\chi^{zxx} + k_z(2\omega)\chi^{xxx}\cos 3\phi) \\ &= \frac{4i\pi\tilde{\Omega}^2}{W_0\epsilon(2\omega) + W}(\sin\theta\epsilon(2\omega)\chi^{zxx} + k_z(2\omega)\chi^{xxx}\cos 3\phi) \\ &= \frac{4i\pi\tilde{\Omega}}{\epsilon(2\omega)\cos\theta + k_z(2\omega)}(\sin\theta\epsilon(2\omega)\chi^{zxx} + k_z(2\omega)\chi^{xxx}\cos 3\phi) \\ &= \frac{4i\pi\omega}{c\cos\theta} \frac{2\cos\theta}{\epsilon(2\omega)\cos\theta + k_z(2\omega)}(\sin\theta\epsilon(2\omega)\chi^{zxx} + k_z(2\omega)\chi^{xxx}\cos 3\phi). \end{aligned}$$

And we finally obtain  $\mathcal{R}_{sP}$ ,

$$\begin{aligned} \mathcal{R}_{sP} &= \frac{2\pi}{c} \left| \frac{E^{(2\omega)}(\perp, \parallel)}{E_s^2} \right|^2 \\ &= \frac{2\pi}{c} \left| \frac{4i\pi\omega}{c\cos\theta} \frac{2\cos\theta}{\epsilon(2\omega)\cos\theta + k_z(2\omega)}(\sin\theta\epsilon(2\omega)\chi^{zxx} + k_z(2\omega)\chi^{xxx}\cos 3\phi) \right|^2 \\ &= \frac{32\pi^3\omega^2}{c^3\cos^2\theta} \left| \frac{2\cos\theta}{\epsilon(2\omega)\cos\theta + k_z(2\omega)}(\sin\theta\epsilon(2\omega)\chi^{zxx} + k_z(2\omega)\chi^{xxx}\cos 3\phi) \right|^2 \\ &= \frac{32\pi^3\omega^2}{c^3\cos^2\theta} |t_s(\omega)T_p(2\omega)r_{sP}|^2, \end{aligned} \quad (\text{D.11})$$

where

$$\begin{aligned} t_s(\omega) &= 1, \\ T_p(2\omega) &= \frac{2\cos\theta}{\epsilon(2\omega)\cos\theta + k_z(2\omega)}, \\ r_{sP} &= \sin\theta\epsilon(2\omega)\chi^{zxx} + k_z(2\omega)\chi^{xxx}\cos 3\phi. \end{aligned}$$

$iF$	$t_i(\omega)$	$T_F(2\omega)$	$r_{iF}$
$pP$	$\frac{1}{\epsilon(\omega)}$	$\frac{2 \cos \theta}{\epsilon(2\omega) \cos \theta + k_z(2\omega)}$	$\sin \theta \epsilon(2\omega) (\sin^2 \theta \chi^{zzz} + k_z^2(\omega) \chi^{zxx})$ $-k_z(\omega) k_z(2\omega) (2 \sin \theta \chi^{xxz}$ $+ k_z(\omega) \chi^{xxx} \cos 3\phi)$ $+$
$pS$	$\frac{1}{\epsilon(\omega)}$	$\frac{2 \cos \theta}{\cos \theta + k_z(2\omega)}$	$k_z^2(\omega) \chi^{xxx} \sin 3\phi$
$sP$	1	$\frac{2 \cos \theta}{\epsilon(2\omega) \cos \theta + k_z(2\omega)}$	$\sin \theta \epsilon(2\omega) \chi^{zxx} + k_z(2\omega) \chi^{xxx} \cos 3\phi$

Table D.1: The necessary factors for Eq. (D.12) for each polarization case.

## D.4 Summary

We unify the final expressions for the SHG yield, Eqs. (D.7), (D.9), and (D.11), as

$$\mathcal{R}_{iF} = \frac{32\pi^3 \omega^2}{c^3 \cos^2 \theta} |t_i(\omega) T_F(2\omega) r_{iF}|^2. \quad (\text{D.12})$$

The necessary factors are summarized in Table D.1.

# Bibliography

- [1] Robert W. Boyd. *Nonlinear Optics*. AP, New York, 2007.
- [2] Richard L. Sutherland. *Handbook of Nonlinear Optics*. CRC Press, April 2003.
- [3] Michele Cini. Simple model of electric-dipole second-harmonic generation from interfaces. *Phys. Rev. B*, 43(6):4792–4802, February 1991.
- [4] V. Mizrahi and J. E. Sipe. Phenomenological treatment of surface second-harmonic generation. *J. Opt. Soc. Am. B*, 5(3):660–667, 1988.
- [5] J. E. Sipe. New Green-function formalism for surface optics. *Journal of the Optical Society of America B*, 4(4):481–489, 1987.
- [6] B. S. Mendoza, F. Nastos, N. Arzate, and J. Sipe. Layer-by-layer analysis of the linear optical response of clean and hydrogenated si(100) surfaces. *Phys. Rev. B*, 74(7):075318, 2006.
- [7] N. Tancogne-Dejean, C. Giorgetti, and V. Véniard. Optical properties of surfaces with supercell *ab initio* calculations: Local-field effects. *Phys. Rev. B*, 92(24):245308, July 2015.
- [8] C. Hogan, R. Del Sole, and G. Onida. Optical properties of real surfaces from microscopic calculations of the dielectric function of finite atomic slabs. *Phys. Rev. B*, 68(3):035405, 2003.
- [9] C. Castillo, B. S. Mendoza, W. G. Schmidt, P. H. Hahn, and F. Bechstedt. Layer-by-layer analysis of surface reflectance anisotropy in semiconductors. *Phys. Rev. B*, 68(4):041310, 2003.
- [10] J. E. Sipe, D. J. Moss, and H. M. van Driel. Phenomenological theory of optical second- and third-harmonic generation from cubic centrosymmetric crystals. *Phys. Rev. B*, 35(3):1129–1141, January 1987.
- [11] S. V. Popov, Y. P. Svirko, and N. I. Zheludev. *Susceptibility tensors for nonlinear optics*. CRC Press, 1995.
- [12] U. Höfer. Nonlinear optical investigations of the dynamics of hydrogen interaction with silicon surfaces. *Appl. Phys. A*, 63(6):533–547, December 1996.
- [13] S. Bergfeld, B. Braunschweig, and W. Daum. Nonlinear Optical Spectroscopy of Suboxides at Oxidized Si(111) Interfaces. *Phys. Rev. Lett.*, 93(9):097402, August 2004.
- [14] J. E. Mejía, B. S. Mendoza, M. Palummo, G. Onida, R. Del Sole, S. Bergfeld, and W. Daum. Surface second-harmonic generation from si (111)(1x1) h: Theory versus experiment. *Phys. Rev. B*, 66(19):195329, 2002.

- [15] S. A. Mitchell, M. Mehendale, D. M. Villeneuve, and R. Boukherroub. Second harmonic generation spectroscopy of chemically modified Si(1 1 1) surfaces. *Surf. Sci.*, 488(3):367–378, August 2001.
- [16] X. Gonze, B. Amadon, P. . M. Anglade, J. . M. Beuken, F. Bottin, P. Boulanger, F. Bruneval, D. Caliste, R. Caracas, M. Cote, T. Deutsch, L. Genovese, Ph. Ghosez, M. Giantomassi, S. Goedecker, D. R. Hamann, P. Hermet, F. Jollet, G. Jomard, S. Leroux, M. Mancini, S. Mazevert, M. J. T. Oliveira, G. Onida, Y. Pouillon, T. Rangel, G. . M. Rignanese, D. Sangalli, R. Shaltaf, M. Torrent, M. J. Verstraete, G. Zerah, and J. W. Zwanziger. ABINIT: First-principles approach to material and nanosystem properties. *Comput. Phys. Commun.*, 180(12):2582–2615, December 2009.
- [17] The ABINIT code is a common project of the Université Catholique de Louvain, Corning Incorporated, and other contributors (URL <http://www.abinit.org>).
- [18] N. Troullier and J. L. Martins. Efficient pseudopotentials for plane-wave calculations. *Phys. Rev. B*, 43(3):1993–2006, January 1991.
- [19] L. Kleinman and D. M. Bylander. Efficacious form for model pseudopotentials. *Phys. Rev. Lett.*, 48(20):1425–1428, 1982.
- [20] V. Olevano, L. Reining, and F. Sottile. <http://dp-code.org>.
- [21] L. Caramella, C. Hogan, G. Onida, and R. Del Sole. High-resolution electron energy loss spectra of reconstructed si(100) surfaces: First-principles study. *Phys. Rev. B*, 79:155447, Apr 2009.
- [22] For bulk calculations schemes of the SH susceptibility tensor beyond the independent particle approximation, see Refs. [33, 32, 31, 49, 50, 51, 52, 53].
- [23] F. Nastos, B. Olejnik, K. Schwarz, and J. E. Sipe. Scissors implementation within length-gauge formulations of the frequency-dependent nonlinear optical response of semiconductors. *Phys. Rev. B*, 72(4):045223, 2005.
- [24] Valérie Véniant, E. Luppi, and H. Hübener. unpublished.
- [25] The half-slab layer extends to the middle of the vacuum region between consecutive (front-back or back-front) surfaces of the repeated super cell scheme.
- [26] M. Rohlfing, P. Krüger, and J. Pollmann. Efficient scheme for GW quasiparticle band-structure calculations with applications to bulk si and to the si(001)-(2x1) surface. *Phys. Rev. B*, 52(3):1905–1917, July 1995.
- [27] P. García-González and R. W. Godby. GW self-energy calculations for surfaces and interfaces. *Comput. Phys. Commun.*, 137(1):108–122, June 2001.
- [28] Eleonora Luppi, Hans-Christian Weissker, Sandro Bottaro, Sottile Francesco, Valérie Véniant, Lucia Reining, and Giovanni Onida. Accuracy of the pseudopotential approximation in *ab initio* theoretical spectroscopies. *Phys. Rev. B*, 78:245124, 2008.

- [29] R. Asahi, W. Mannstadt, and A. J. Freeman. Screened-exchange lda methods for films and superlattices with applications to the si(100)2x1 surface and inasoinbs superlattices. *Phys. Rev. B*, 62:2552, 2000.
- [30] J. Cabellos, B. Mendoza, M. Escobar, F. Nastos, and J. Sipe. Effects of nonlocality on second-harmonic generation in bulk semiconductors. *Phys. Rev. B*, 80(15):155205, 2009.
- [31] E. Luppi, H. Hübener, and V. Véniard. Ab initio second-order nonlinear optics in solids: Second-harmonic generation spectroscopy from time-dependent density-functional theory. *Phys. Rev. B*, 82:235201, 2010.
- [32] R. Leitsmann, W. Schmidt, P. Hahn, and F. Bechstedt. Second-harmonic polarizability including electron-hole attraction from band-structure theory. *Phys. Rev. B*, 71(19):195209, 2005.
- [33] B. Adolph and F. Bechstedt. Influence of crystal structure and quasiparticle effects on second-harmonic generation: Silicon carbide polytypes. *Phys. Rev. B*, 62:1706, 2000.
- [34] S. M. Anderson, N. Tancogne-Dejean, B. S. Mendoza, and V. Véniard. Theory of surface second-harmonic generation for semiconductors including effects of nonlocal operators. *Phys. Rev. B*, 91(7):075302, February 2015.
- [35] Nicolas Tancogne-Dejean. *Ab initio description of second-harmonic generation from crystal surfaces*. PhD thesis, Ecole polytechnique, September 2015.
- [36] J. R. Power, J. D. O'Mahony, S. Chandola, and J. F. McGilp. Resonant optical second harmonic generation at the steps of vicinal si(001). *Phys. Rev. Lett.*, 75(6):1138–1141, August 1995.
- [37] E. Kaxiras and J. D. Joannopoulos. Hydrogenation of semiconductor surfaces: Si and Ge (111). *Phys. Rev. B*, 37(15):8842–8848, May 1988.
- [38] F. Jona, W. A. Thompson, and P. M. Marcus. Experimental determination of the atomic structure of a H-terminated Si111 surface. *Phys. Rev. B*, 52(11):8226–8230, September 1995.
- [39] D. R. Alfonso, C. Noguez, D. A. Drabold, and S. E. Ulloa. First-principles studies of hydrogenated Si(111)-7x7. *Phys. Rev. B*, 54(11):8028–8032, September 1996.
- [40] F. Cargnani, C. Gatti, E. May, and D. Narducci. Geometrical reconstructions and electronic relaxations of silicon surfaces. I. An electron density topological study of H-covered and clean Si(111)(1×1) surfaces. *J. Chem. Phys.*, 112(2):887–899, January 2000.
- [41] R. C. Weast, M. J. Astle, and W. H. Beyer. *CRC handbook of chemistry and physics*, volume 69. CRC press Boca Raton, FL, 1988.
- [42] Y. Li and G. Galli. Electronic and spectroscopic properties of the hydrogen-terminated Si(111) surface from ab initio calculations. *Phys. Rev. B*, 82(4):045321, July 2010.
- [43] P. Yu and M. Cardona. *Fundamentals of Semiconductors: Physics and Materials Properties*. Springer Science & Business Media, third edition, March 2005.

- [44] S. M. Anderson, N. Tancogne-Dejean, B. S. Mendoza, and V. Véniard. Improved *ab initio* calculation of surface second-harmonic generation from si(111)(1×1)h. *Physical Review B*, May 2016. *Submitted*.
- [45] J. I. Dadap, Z. Xu, X. F. Hu, M. C. Downer, N. M. Russell, J. G. Ekerdt, and O. A. Aktsipetrov. Second-harmonic spectroscopy of a Si (001) surface during calibrated variations in temperature and hydrogen coverage. *Phys. Rev. B*, 56(20):13367, 1997.
- [46] M. Palummo, G. Onida, R. Del Sole, and B. S. Mendoza. Ab initio optical properties of Si(100). *Phys. Rev. B*, 60(4):2522–2527, July 1999.
- [47] K. Gaál-Nagy, A. Incze, G. Onida, Y. Borensztein, N. Witkowski, O. Pluchery, F. Fuchs, F. Bechstedt, and R. Del Sole. Optical spectra and microscopic structure of the oxidized Si(100) surface: Combined *in situ* optical experiments and first principles calculations. *Phys. Rev. B*, 79(4):045312, January 2009.
- [48] The size of the excitonic Hamiltonian scales as  $(N_k^3 \times N_v \times N_c)^2$ , where  $N_k$  is the total number of  $\mathbf{k}$ -points, and  $N_v$  and  $N_c$  are the number of valence and conduction states, respectively. For these values, the size of the Hamiltonian for the Si(111)(1×1):H surface of this article would be over 1 petabyte, which far exceeds conventional computing capabilities.
- [49] E. Luppi, H. Hübener, and V. Véniard. Communications: Ab initio second-order nonlinear optics in solids. *J. Chem. Phys.*, 132(24):241104, 2010.
- [50] H. Hübener, E. Luppi, and V. Véniard. Ab initio calculation of many-body effects on the second-harmonic generation spectra of hexagonal sic polytypes. *Phys. Rev. B*, 83:115205, 2011.
- [51] Mads L. Trolle, Gotthard Seifert, and Thomas G. Pedersen. Theory of excitonic second-harmonic generation in monolayer MoS<sub>2</sub>. *Phys. Rev. B*, 89(23):235410, June 2014.
- [52] C. Attaccalite and M. Grüning. Nonlinear optics from an ab initio approach by means of the dynamical berry phase: Application to second- and third-harmonic generation in semiconductors. *Phys. Rev. B*, 88:235113, 2013.
- [53] M. Grüning and C. Attaccalite. Second harmonic generation in *h*-bn and mos<sub>2</sub> monolayers: Role of electron-hole interaction. *Phys. Rev. B*, 89:081102, 2014.